NBS-3253

ABSTRACT

A COMPUTER-INTERFACED SCANNING STOPPED-FLOW SYSTEM AND ITS APPLICATION TO THE KINETICS OF AIR-SENSITIVE REACTIONS

By

Nicholas Papadakis

A double-beam, vacuum tight, thermostated stopped-flow apparatus has been constructed and computer interfaced. A specially designed all quartz mixing and observation cell, equipped with a double mixer and two optical path lengths has been used. The syringes were made out of heavy-walled precision bore tubing. Steel plungers with adjustable Teflon tips were machined to fit them. Metal flags mounted on the stopping plunger provide useful timing pulses by interrupting two light beams which are detected by photo-transistors. The entire apparatus was constructed such that the solutions contact only Pyrex, quartz and Teflon. A thermostat bath which surrounds the flow system allows for temperature dependent studies and helps to establish thermal equilibrium between the solutions and the system in order to eliminate thermal artifacts. After dispersion

with a rapid-scan monochromator, light beams are transmitted via quartz fiber optics to the flow cell and reference cell and then to a pair of photomultipliers. Sample and reference photocurrents are converted to absorbance by means of operational amplifiers. The absorbance is sampled and digitized at a nominal 20.4 KHz rate which is controlled by the rotation of the monochromator mirror with the aid of a phase-locked loop circuit. Parallel digital transmission is utilized to send the absorbance signal and the required control signals to (and from) a remote PDP8-I computer, with line-drivers and receivers in a "party-line" structure. A versatile real-time averaging scheme is used to store complete time-dependent spectra with enhanced signal-to-noise ratio at long times. Any spectrum or combination of spectra can be examined on a CRT display terminal. Time cuts can be displayed at any desired wavelength and then punched onto computer cards for rigorous data analysis with a CDC-6500 computer. The system has been tested extensively by studying a number of well characterized chemical reactions and its performance characteristics are excellent.

The effect of the cation complexing agents dicyclohexyl-18-crown-6 ("Crown") and 4,7,13,16,21,24-hexaoxa-1,10-diazabicyclic (8,8,8) hexacosane ("2,2,2 Crypt") upon the rate of protonation of potassium-anthracenide (K^+,$An^{\cdot-}$) with ethanol (EtOH) in tetrahydrofuran (THF) was examined with the stopped-flow system. In the absence of complexing agent,

pseudo-parallel first and second order reactions were observed, in agreement with the results of other investigators. The contribution of the second order component was controlled by the addition of various amounts of the complexing agents to the $K^+,An^{\cdot-}$ solution prior to reaction. The results obtained, showed conclusively that two contact ion pairs ($K^+,An^{\cdot-}$) are required for the second order process. The alcohol dependence of the pseudo-first order rate constant (without complexing agent) as computed from the data at low concentration of $K^+,An^{\cdot-}$ ($\sim 5 \times 10^{-5}$ M), was found to be second order. When "Crown" (C) or "2,2,2 Crypt" (CR) was added to the solution of $K^+,An^{\cdot-}$, a very slow pseudo-first order process was observed together with the regular protonation of $K^+,An^{\cdot-}$. This slow step was attributed to the protonation of the species $K^+C,An^{\cdot-}$ and $K^+CR,An^{\cdot-}$. The corresponding rate constant was larger for $K^+C,An^{\cdot-}$ than for $K^+CR,An^{\cdot-}$ at all the alcohol concentrations used. This was expected from the presumed difference in charge localization caused by the structures of the "Crown" and "2,2,2 Crypt" complexes.

A COMPUTER-INTERFACED SCANNING STOPPED-FLOW SYSTEM AND ITS APPLICATION TO THE KINETICS OF AIR-SENSITIVE REACTIONS

By

Nicholas Papadakis

A DISSERTATION

Submitted to
Michigan State University
in partial fulfillment of the requirements
for the degree of

DOCTOR OF PHILOSOPHY
Department of Chemistry

1974

To

Euridici and My Parents

ACKNOWLEDGMENTS

The author wishes to express his special gratitude to Professor James L. Dye for his guidance, assistance and encouragement throughout the course of this work.

He would also like to thank Mr. Richard B. Coolen for his collaboration in the construction and interfacing of the stopped-flow apparatus and Mr. James Avery for his assistance in the development of the hardware and software. Thanks go to professor C. G. Enke for his valuable suggestions on the interface and to Mr. R. E. Teets for his help with the display software. The helpful suggestions and criticisms of Professor S. R. Crouch who served as my second reader are appreciated.

The author also wishes to acknowledge the help of J. M. Ceraso, M. T. Lok, L. D. Long, E. Mei, and F. J. Tehan. The cooperation of the MSU glass shop and the Chemistry Department machine shop is acknowledged. Financial support from the Atomic Energy Commission is also acknowledged.

Last, but not least, many thanks go to my wife, Euridici, for her understanding and patience which made attainment of this goal possible.

TABLE OF CONTENTS

Page

LIST OF TABLES

LIST OF FIGURES

I. INTRODUCTION

Utilization of the stopped-flow method for the study of chemical reactions has been well established[1]. The coupling of a stopped-flow apparatus with a rapid scanning spectrometer has produced a very versatile instrument, developed primarily for the study of chemical reactions which involve short-lived intermediates[2,3]. Scanning of the appropriate spectral region can provide information about the number and types of intermediate species present as well as the kinetics of the formation and decay of these species. For studies with very reactive air-sensitive systems, the stopped-flow apparatus must be evacuable and constructed such that only quartz, Pyrex and Teflon come into contact with the reacting solutions.

The advantages of on-line laboratory computers for high speed data acquisition, rapid data handling or data processing have been demonstrated for a variety of instruments in a great number of applications[4,5,6,94]. In a well programmed interactive computer system, the computer can execute a variety of tedius processing operations under the continuous guidance of the experimenter. Thus, the experimenter can impose his experienced judgment and make important decisions during the data acquisition and analysis. For routine applications, where the boundary

conditions are well defined, a high degree of automation is usually desirable[52]. However, for research and development projects, when the information obtained may be unpredictable, it is important that the experimenter communicates with the computer and establishes the best procedure for data acquisition and processing, such that the information necessary for characterizing the system under study can be obtained.

The purpose of the present research was to:

(1) Develop a rapid scanning, variable temperature, vacuum tight stopped-flow system for kinetics studies with air-sensitive systems. Two optical path lengths were desirable for the apparatus in order to be able to carry out studies over a wide concentration range.

(2) Interface the stopped-flow system to a remote PDP-8I computer and write a sophisticated set of computer routines to collect, average, modify and output the kinetics data. These routines had to fully utilize the scanning ability of the instrument and provide sufficient interaction between computer and experimenter that important decisions could be made during the actual experiment.

(3) Extensively test and calibrate the entire system, utilizing well-studied chemical reactions.

(4) Apply the system to the study of:

(a) The dissociation of sodium anion (Na^-) in ethylenediamine (EDA). The results of this work could help us to better understand the nature of metal-amine solutions.

(b) The effect of the complexing agents dicyclohexyl-18-Crown-6 ("Crown") and 4,7,13,16,21,24-hexaoxa-1,10-diazabicyclic (8,8,8) hexacosane ("2,2,2 Crypt") on the protonation of potassium anthracenide with ethanol in tetrahydrofuran. This would further elucidate the important role of ion-pairs in the protonation of aromatic radical anions.

Because of the complexity and the size of the project, the construction and interfacing of the stopped-flow apparatus was carried out in collaboration with Mr. Richard B. Coolen, who demonstrated the applicability of the instrument to the study of transients in enzyme kinetics. His Ph.D. thesis should be consulted for additional information.

II. HISTORICAL

Since a large amount of work has been done on each of the subjects included in this work, it is not feasible to give a detailed historical development. Instead, only the necessary information is given to establish a connection between past work and our studies.

This section is divided into four main parts. In the first two parts recent studies on the protonation of aromatic radical anions and the reaction of sodium-ethylenediamine solutions with water are presented. The development of the stopped-flow method to a very important tool for kinetics studies follows in the third part. Finally, a brief presentation on the use of on-line computers for data acquisition and analysis is given in the fourth part.

II.1. Protonation of aromatic radical anions in ethereal solvents

Various techniques have been used to produce aromatic radical anions in solution and to study their properties and reactions[7,8]. The stopped-flow method has been used by several investigators for the study of the protonation of such anions in ethereal solvents[9-15].

II.1.1. The work of Minnich and Long

A scanning stopped-flow apparatus[2] was employed by Minnich and Long for their kinetics studies. The radical

anions were produced by reduction of the parent hydrocarbons with alkali-metals.

Minnich studied the reactions of the radical anions of anthracene (An) and terphenyl (Te) with various alcohols (ROH) and water in tetrahydrofuran (THF) and dimethoxyethane (DME).

The reactions of potassium-anthracenide (K^+,$An^{\cdot-}$) with ethanol (EtOH), methanol (MeOH), t-butanol (t-BuOH), i-propanol (i-PrOH) and water (H_2O) in THF, were reported to be second order in the anion and about half-order in ROH[7,9]. The concentration of An was kept nearly the same in many experiments and the ROH concentration was varied within limited ranges. No dependence of the reaction rates upon the alkoxide (RO^-) concentration was found.

For the reactions in DME, similar results were observed, but with lower pseudo-second order rate constants.

In THF, the reactions of sodium-anthracenide (Na^+, $An^{\cdot-}$) with EtOH were similar to those with K^+,$An^{\cdot-}$ in the same solvent. However, the reaction with H_2O did not give consistent results; namely a pseudo-second order decay was observed in one experiment but a mixed pseudo-first and -second order decay was found in the other one.

In DME, the reactions of Na^+,$An^{\cdot-}$ with EtOH or H_2O, were found to be slower by a factor of 10 than those of K^+,$An^{\cdot-}$, and moreover the decay of Na^+,$An^{\cdot-}$ was first order.

The reaction of potassium-terphenylide with EtOH in THF appeared to be first order in each reactant.

The above results were consistent with the proposed

general mechanism:

$$M^+,Ar^{\cdot-} + M^+,Ar^{\cdot-} \underset{k_-'}{\overset{k_+'}{\rightleftharpoons}} (M^+,Ar^{\cdot-})_2 \qquad 1a$$

$$(M^+,Ar^{\cdot-})_2 + ROH \xrightarrow{k_1} M^+ArH^- + M^+,RO^- + Ar \qquad 1b$$

$$M^+ArH^- + ROH \xrightarrow[fast]{k_2} ArH_2 + M^+,RO^- \qquad 1c$$

$$M^+,Ar^{\cdot-} + ROH \xrightarrow{k_3} ArH^{\cdot} + M^+,RO^- \qquad 1d$$

$$M^+,Ar^{\cdot-} + ArH^{\cdot} \xrightarrow[fast]{k_4} M^+ArH^- + Ar \qquad 1e$$

The following general rate law was derived, assuming a steady state concentration for the species $(M^+,Ar^{\cdot-})_2$:

$$-\frac{d[M^+,Ar^{\cdot-}]}{dt} = \frac{2k_+'}{1+(k_-'/k_1[ROH])}[M^+,An^{\cdot-}]^2 + k_3[ROH][K^+,An^{\cdot-}]$$

Under conditions which favor ion-pair formation, the second order process dominates (equations 1a, b, c), but where ion-pairing is not favored, the first order process is observed (equations 1d, e, c).

At about the same time, Bank and Bockrath reported[11] a pseudo-first order rate law for the protonation of Na- Napthalenide with H_2O in THF. Also, Levin, et al.[13] had observed a second order decay for sodium-perylenide in its reaction with various alcohols in THF. They also found the reaction to be inverse first

order in the perylene (Pe) concentration, which was consistent with the protonation of the ion-paired perylene dianion ($Pe^{=},2Na^{+}$) as the intermediate species.

In order to further investigate the second order behavior in the protonation reactions, Long and Ceraso extended Minnich's work. The reaction of $K^{+},An^{\cdot-}$ with EtOH in THF was studied over a wide concentration range of EtOH and An[8,10]. At low EtOH concentrations (<0.01 M) the rate was found to depend upon the ratio [EtOH]/[An], consistent with the formation and subsequent protonation of the anthracene dianion ($An^{=},2M^{+}$). The pseudo-second order rate constant increased with EtOH concentration, but became essentially independent of An concentration at higher concentrations of EtOH. Above an EtOH concentration of ~0.1 M, a first order contribution to the decay became apparent. All the above observations were consistent with the following proposed dianion and ion-cluster mechanism:

$$2(K^{+},An^{\cdot-}) \overset{K_Q}{\rightleftharpoons} (K^{+},An^{\cdot-})_2 \underset{k''_-}{\overset{k''_+}{\rightleftharpoons}} 2K^{+},An^{=} + An \qquad 2a$$

$$2K^{+},An^{=} + ROH \overset{k_1}{\rightarrow} K^{+}AnH^{-} + K^{+},RO^{-} \qquad 2b$$

$$(K^{+},An^{\cdot-})_2 + ROH \overset{k_2}{\rightarrow} K^{+}AnH^{-} + K^{+},RO^{-} + An \qquad 2c$$

$$K^{+}AnH^{-} + ROH \overset{fast}{\rightarrow} AnH_2 + K^{+},RO^{-} \qquad 2d$$

$$K^+,An^{\cdot-} + ROH \xrightarrow{k_3} AnH^{\cdot} + K^+,RO^- \qquad 2e$$

$$K^+,An^{\cdot-} + AnH^{\cdot} \xrightarrow{fast} K^+AnH^- + An \qquad 2f$$

which leads to the general rate law:

$$-\frac{d[K^+,An^{\cdot-}]}{dt} = \left[\frac{2k''K_Q}{1+\frac{k''}{k_1}\frac{[An]}{[ROH]}} + 2k_2K_Q[ROH]\right](K^+,An^{\cdot-})^2$$

$$+ k_3[ROH][K^+,An^{\cdot-}] \qquad 2g$$

provided that a steady-state concentration of the dianion is obtained.

At high values of [ROH], the second term dominates in the second order component and the decay becomes pseudo-second order in $[K^+,An^{\cdot-}]$ and first order in [ROH], after correction for the first order (in$[K^+,An^{\cdot-}]$) protonation. At low [ROH], the second term becomes less important and the rate expression reverts to that of the dianion mechanism.

An alternative mechanism introduced by Minnich et al.[10] was the cation solvation mechanism. According to this mechanism, potassium ion is solvated by ROH as follows:

$$K^+ + ROH \overset{K_s}{\rightleftharpoons} K^+{\cdot}ROH \qquad 3a$$

or

$$An^{\cdot-},K^+ + ROH \overset{K_s}{\rightleftharpoons} An^{\cdot-},K^+{\cdot}ROH \qquad 3b$$

Substitution of K^+ROH for the THF-solvated cation in the contact ion pair with $An^{\cdot-}$ could increase the charge localization on the radical anion in the vicinity of the cation. Whether this leads to an increased rate of formation of the dianion or to a concerted protonation of the quadruple ion-cluster is difficult to assess, because rate expressions derived by using either assumption fit the experimental data as well as equation (2g). However, the apparent insensitivity to the nature of the proton donor suggests that a cation-solvation mechanism may be responsible for the breakdown of the dianion mechanism at high concentrations of the proton donor.

The important role played by contact ion pairing in the protonation of aromatic radical anions was further tested by Long and Ceraso. They added "Crown" to a solution of $K^+,An^{\cdot-}$ in THF prior to protonation[8]. The "Crown" had been proven to be a good complexing agent for alkali metal cations[16]. They observed a dramatic effect on the protonation rate. When ["Crown"] >> $[K^+,An^{\cdot-}]$ only a slow first order protonation remained, while when ["Crown"] < $[K^+,An^{\cdot-}]$, a fast initial decay followed by a much slower first order decay was observed. Although the studies with "Crown" were only preliminary, it was noticed that the first order protonation of the solvent (and/or "Crown") separated ion pairs (in THF) was ~100 times slower than the similar reaction of the contact ion pairs (in THF).

II.1.2. The results of Bank and Bockrath

Bank and Bockrath produced sodium naphthalenide (Na^+, $Nap^{\cdot-}$) in THF by reduction of naphthalene (Nap) with metallic sodium and studied its reaction with H_2O[11]. They found that the reaction followed a pseudo-first order rate law similar to the one reported by Paul, Lipkin and Weissman[69], namely:

$$Nap^{\cdot-} + H_2O \xrightarrow{k_1} NapH^{\cdot} + OH^- \qquad 4a$$

$$NapH^{\cdot} + Nap^{\cdot-} \xrightarrow{k_2} NapH^- + Nap \qquad 4b$$

$$NapH^- + H_2O \xrightarrow{k_3} NapH_2 + OH^- \qquad 4c$$

If a steady-state concentration is assumed for $[NapH^{\cdot}]$, the following pseudo-first order rate law is derived:

$$-\frac{d[Nap^{\cdot-}]}{dt} = 2k_1'[Nap^{\cdot-}]; \text{ with } k_1' = k_1[H_2O] \qquad 5$$

At 20° C they computed: $k_1 = 0.01 \times 10^4\ M^{-1}\ sec^{-1}$.

They also studied the protonation of $Na^+,An^{\cdot-}$ with H_2O in THF, DME and mixtures of these solvents[12]. In this case the following reaction was used to produce $Na^+,An^{\cdot-}$:

$$Na^+,Nap^{\cdot-} + An \rightleftarrows Na^+,An^{\cdot-} + Nap \qquad 6$$

Of course appropriate assumptions were made to justify

subsequent protonation of $Na^+,An^{\cdot-}$ without significant interference from the other species present in solution. The reaction of $Na^+,An^{\cdot-}$ with H_2O in THF was reported to be similar to the same reaction of $Na^+,Nap^{\cdot-}$, but ~200 times slower. The stopped-flow method was employed in all of their kinetics work.

The above results do not agree well with the observations of Szwarc in DME and Minnich et al. in THF.

II.1.3. The work of Szwarc and co-workers

Rainis, Tung and Szwarc[14,15], have studied the effect of cation, alcohol and solvent on the protonation of aromatic radical anions by the stopped-flow method. Solutions of the aromatic anions were prepared by reacting the parent hydrocarbon with the appropriate alkali metal. In most of their experiments the corresponding alkali metal salt of tetraphenylborate was added in excess to the $M^+,Ar^{\cdot-}$ solution, in order to repress the dissociation of $M^+,Ar^{\cdot-}$ ion pairs into the less reactive free $Ar^{\cdot-}$ ions.

The following results were reported: The protonation of $Li^+,An^{\cdot-}$ was first order in $[Li^+,An^{\cdot-}]$ regardless of solvent or alcohol used. The protonation of $Na^+,An^{\cdot-}$ by MeOH in DME was also first order in $[Na^+,An^{\cdot-}]$, while a simultaneous first and second order reaction was observed in THF. With the less reactive t-BuOH, the first and second order reactions contribute simultaneously to the protonation in DME, but only the second order reaction was observed in THF.

Finally, in the protonation of the least reactive $K^+,An^{\cdot-}$ by MeOH, contributions from both first and second order reactions were seen in both solvents, while only the second order dependence was observed when t-BuOH was used.

The reaction with $Li^+,An^{\cdot-}$ was also found to be first order in alcohol, with MeOH being more reactive than t-BuOH and with rates slightly higher in THF than in DME. A second order alcohol dependence became evident in the protonation of $Na^+,An^{\cdot-}$ with MeOH, while in the $K^+,An^{\cdot-}$-MeOH system the alcohol dependence was purely second order. When t-BuOH was used, only first order alcohol dependence was observed. They proposed the following mechanisms in order to explain the alcohol dependence:

$$\text{(A)} \quad M^+,An^{\cdot-} + ROH \overset{k_{pm}}{\rightarrow} AnH^{\cdot} + M^+,RO^- \qquad 7a$$

$$2ROH \overset{K_D}{\rightleftarrows} (ROH)_2 \qquad 7b$$

$$M^+,An^{\cdot-} + (ROH)_2 \overset{k_{pd}}{\rightarrow} AnH^{\cdot} + RO^+,M^+,ROH \qquad 7c$$

$$\text{(B)} \quad M^+,An^{\cdot-} + ROH \rightleftarrows An^{\cdot-},M^+(ROH) \qquad 8a$$

$$An^{\cdot-},M^+(ROH) \rightarrow AnH^{\cdot} + RO^-,M^+ \qquad 8b$$

$$An^{\cdot-},M^+(ROH) + ROH \rightarrow AnH^{\cdot} + RO^-,M^+,ROH \qquad 8c$$

It was noted that the first order dependence on t-BuOH

would be expected according to mechanism A because the bulkiness of t-BuOH prevents the reaction (7_b) which introduces the second order dependence.

The following mechanism was suggested for the dianion protonation:

$$2An^{\cdot-},M^+ \overset{K_1}{\rightleftharpoons} (An^{\cdot-},M^+;\ An^{\cdot-},M^+) \overset{k_2}{\underset{k_{-2}}{\rightleftharpoons}}$$

$$(An;\ M^+,An^{=},M^+) \overset{k_3}{\underset{k_{-3}}{\rightleftharpoons}} An + An^{=},2M^+$$

$$k_{p_1} \downarrow [+ROH] \qquad k_{p_2} \downarrow [+ROH] \qquad (9)$$

Protonation Products

The contribution of dianions to the protonation, then depends upon the disproportionation constant $K_{Dispr} = K_1K_2K_3$. The above mechanism is basically identical with the first of the mechanisms proposed by Minnich et al.[10] and there is a very good qualitative and in many cases quantitative agreement between the results reported from the two groups.

In summary, the studies presented have demonstrated the validity of a general mechanism for the protonation of aromatic anions over a very wide range of conditions for one system[10] as well as for several different systems[15]. The pronounced effect of ion pair formation upon the protonation is undeniable. The free ions are the least reactive, while the reactivity of ion pairs increases with their tightness, as was demonstrated by the effect of "Crown" on the protonation of $K^+,An^{\cdot-}$[8].

II.2. Reaction of Sodium-ethylenediamine Solutions With Water

Alkali or alkaline earth metals when dissolved in liquid ammonia, aliphatic amines and certain ethers, form metastable blue solutions with no chemical reaction. These solutions have been the subject of very extensive study since the first characteristic blue color was observed in 1864 by Weyl[17]. The nature of metal-ammonia solutions is still a subject of controversy. However, there is general agreement that the optical absorption band can be attributed to the solvated electron (e^-_{solv}) and its loosely-bound aggregates. The optical spectra of metal-amine solutions are more complicated and their interpretation has been simplified only with the results of the past few years. The species responsible for the IR-band in metal-amine solutions are probably the same as in the metal-ammonia case, while the anionic species M^- has been shown to be responsible for the metal dependent band[18].

II.2.1. The Work of Feldman and Hansen

The first direct observation of the hydrated electron in 1962[19] initiated a great deal of work related to the kinetics of reactions of solvated electrons. The rate constant for the reaction of the hydrated electron (e^-_{aq}) with water

$$e^-_{aq} + H_2O \rightarrow H + OH^-$$

has been found to be 16 M^{-1} sec^{-1}[20].

Dewald[21] and Feldman[22] utilized the stopped-flow technique in trying to measure the rate of reaction of the solvated electron with water in ethylenediamine (EDA).

Feldman extended the work of Dewald et al.[23] and found the following: The reaction of cesium with H_2O in EDA gave a rate constant similar to the one reported before[23], but in many cases showed the presence of a slower pseudo-first order process. Similar results were found for the corresponding reactions of rubidium and potassium. The reaction of sodium with H_2O in EDA was found to be first order in the metal absorbance, but the order in water varied with the H_2O concentration. The lithium-H_2O reactions yielded as many as three pseudo-first-order rate constants.

Hansen[24] used the scanning stopped-flow system introduced by Dye and Feldman[2] but a better data analysis process, utilizing a Varian C-1024 Computer of Average Transients (CAT)[57]. He found that the reaction of sodium with H_2O in EDA was second order in water at $[H_2O]$ greater than 1M, and the decay of the metal band was nearly first order. However, the corresponding reactions of potassium, rubidium and cesium were all apparently first order in $[H_2O]$, but the decay of the metal band was not simply first or second order. All the above results combined with studies with EDA labelled at the α-position with tritium, convinced Hansen[24] that the reactions of alkali metals with H_2O in EDA are faster than and proceed via a different mechanism

from similar reactions in dilute metal-ammonia solutions. The mechanism proposed by Hansen[24] was consistent with the observed rates and the existing models for metal-amine solutions. To describe the sodium abnormality, he suggested the following mechanism:

$$Na^- + H_2O \underset{\text{fast}}{\overset{K_1}{\rightleftharpoons}} Na^-\cdot H^+ + OH^- \qquad 10a$$

$$Na^-\cdot H^+ + H_2O \overset{k_1}{\rightarrow} Na^+ + OH^- + H_2 \qquad 10b$$

which yields:

$$\frac{d[H_2]}{dt} = k_1K_1 \frac{[Na^-][H_2O]^2}{[OH^-]} \qquad 10c$$

if equilibrium is maintained in (10a). The validity of (10c) could be tested by observing the effect of sodium hydroxide (NaOH) on the reaction rate.

II.2.2. The Work of DeBacker:

Using the stopped-flow method, DeBacker studied the effect of NaOH on the reaction of sodium with H_2O in EDA[25]. He did not observe any hydroxide effect upon the reaction rate and found a first order dependence on metal and close to third order dependence on the H_2O concentration. No simple mechanism could account for these observations and a shift of the equilibrium

$$Na^- \rightleftarrows Na^+ + 2e^-_{solv}$$

to the right by the addition of large amounts of H_2O was suggested. Stopped-flow results combined with pulse-radiolysis studies[26] indicated that the reaction

$$Na^- \rightarrow Na^+ + 2^-_{solv}$$

might be the rate determining step in the reaction of sodium with H_2O in EDA.

Summarizing, the complicated nature of metal-amine solutions and their high instability make kinetics studies difficult. However, it is hoped that the current models for metal-amine solutions, combined with results such as those presented here, will help us to better understand the nature of metal-EDA solutions.

II.3. The Stopped-flow Apparatus

Since the earliest kinetics investigation in 1850[27], a variety of methods have been developed for the study of chemical reactions in solution, and the range now extends to reactions with half-lives as short as 10^{-9} sec[1]. Although the continuous-flow method had been introduced by Hartridge and Roughton in 1923[28], it was in 1940 that Chance[29] introduced the first systematic development of the stopped-flow method. Today the stopped-flow method is widely used because of its simplicity and real time data presentation[1,2,30-36]. The method is, however generally

limited to reactions with half-lives of about a millisecond or longer.

II.3.1. First Systematic Development by Chance and Gibson

In the continuous-flow method, the two reactants are mixed and the resulting solution flows at a constant velocity through an observation tube of uniform geometry. The progress of the reaction can then be monitored by measuring some property of the system at various points along the observation tube. At constant flow velocity the extent of reaction will remain constant at any fixed distance from the point of mixing. Thus a method of rapid detection is not essential. Of course the efficiency of mixing determines the time resolution of such an apparatus. Also, the continuous-flow method requires large volumes (liters) of solutions to obtain one rate curve. In the stopped-flow method, the reactants are forced through a mixing chamber into an observation area and the flow is then abruptly stopped. At the time of stopping, the mixture is only a few milliseconds old, and the remaining progress of the reaction is monitored. In this case we need a detection system with very rapid response because the extent of reaction changes according to the corresponding rate constant.

By 1940 adequately rapid methods of observation were available to permit the first systematic development and application of a stopped-flow apparatus.

Chance[29] worked mainly on the development of an

accelerated-flow apparatus, which could also be used for stopped-flow measurements after the flow had been stopped. He gives a detailed analysis of all the factors influencing the performance of the apparatus as well as kinetics data which illustrate its applicability. Chance's apparatus utilized two tuberculin type pushing syringes, screwed into a polystyrene mixer at the end of which the glass observation tube was sealed. Many mixers of various types were made and tested for mixing efficiency. A rotary potentiometer attached by a chain to the sliding pushing block was used to measure the flow velocity. An appropriately stabilized tungsten filament lamp was used with the necessary filters for wavelength selection. The light passing through the observation tube was detected by a photocell for absorption measurements. The output was amplified and fed into a cathode ray oscilloscope where the record of the kinetics curve was displayed and photographed. This apparatus was used for accelerated-flow measurements with times from 0.2 to 10 milliseconds and for stopped-flow measurements with times greater than 30 milliseconds and up to 60 seconds (30 msec was the time required for the solutions to leave the mixing chamber and stop at the observation point = dead time). Very efficient mixing was reported with no cavitation phenomena. Even though this stopped-flow apparatus had a large dead volume, it had a major advantage over the continuous-flow method; namely, the much smaller volumes of reactants required for a set

of measurements. In 1951[37] Chance introduced a new stopped-flow apparatus with a dead time of ∿20 milliseconds.

The stopped-flow method owes its wide adoption to the stopping device introduced by Gibson[38]. A small piston at the end of the observation tube is pushed along by the reaction mixture, and is suddenly stopped by coming against a seat or an external stop. This simple arrangement was found to be extremely effective, with stopping times of 1-2 msec, resulting in dead times of ∿3-5 msec. The apparatus used by Gibson[33] has been the prototype of most of the stopped-flow systems now in existence.

II.3.2. Commercially Available Instruments

II.3.2.1. Durrum-Gibson Stopped Flow Spectrophotometer

The instrument initially developed by Gibson[33] has been manufactured by Durrum Instrument Corp. since 1966[40]. A large number of improvements and options have been added to the originally manufactured instrument and have made it an easy to operate, versatile and reliable apparatus. The entire block containing the reservoir syringes and the flow system can be thermostated by circulating a constant temperature liquid through the appropriate channels. Some problems with studies at other than ambient temperatures have been reported[42]. The horizontal position of the flow system can cause bubble problems; studies regarding this problem together with cavitation artifacts have been carried out in a

similar apparatus and in the flow rate range of 5-10 m/sec[39]. Even though it has been used for studies with air-sensitive systems[11,14], its applicability to very reactive unstable chemical systems is questionable. The instrument has been used widely in biochemical studies, where two of the offered options (Fluorescence measurements[40], and multi-mixing system[41]) are very useful.

II.3.2.2. Aminco-Morrow Stopped-flow Apparatus

Developed by J. I. Morrow[36] and manufactured by American Instruments Company since 1971[43], this apparatus employs a solution delivering arrangement (which connects the reservoir and drive syringes) which minimizes bubble problems and allows solutions to be easily changed. The reacting solutions contact only KEL-F, Teflon and quartz, and the observation cell offers two path lengths for following absorption changes of the reacting mixture. (However, no performance data for the short path length have been published).

From the reported performance characteristics the apparatus seems to be very good for biochemical applications, but its applicability to very reactive, air-sensitive systems is also questionable.

II.3.3. Scanning Stopped-flow System of Dye and Feldman

Rapid scanning spectroscopy is a technique in which a selected region of the electromagnetic spectrum is scanned on a time scale ranging from several seconds down to a few

microseconds. The advantages to be gained from such a technique (especially for the study of chemical reactions which involve short-lived intermediates) have led to the development of several rapid scanning spectrometers[44-47].

Earlier studies of the kinetics of electron attachment reactions in ethylenediamine by the stopped-flow method convinced Dye and Feldman that due to the complexity of metal-amine solutions (overlapping of various absorption bands) a rapid scanning spectrometer was necessary in order to obtain clean kinetics data[2]. They used a Perkin-Elmer model 108 rapid scan monochromator coupled with a home built stopped-flow apparatus. The entire flow system was evacuable and all the manipulations could be carried out in the absence of air. Thermostated burettes were used for making dilutions into a thermostated storage vessel. The pushing syringes could also be thermostated by circulating a constant temperature liquid through the appropriate plastic jackets. The entire flow system was vertical in order to eliminate bubbles. The mixing chamber and observation cell was constructed from precision bore heavy walled capillary by a very elaborate procedure[2,22], and was shown to perform satisfactorily.

The scanning monochromator could in principle (with the appropriate prism) scan a selected spectral region between 0.2 and 10 μm, with from 3 to 150 scans per second. External controls permitted selection both of the interval

to be scanned and the center of scan. The spectral scan was produced by a modified double pass Littrow system with a rotating tilted mirror. The light after leaving the monochromator impinged on a beam splitter from a Bausch & Lomb Spectronic 505 spectrometer. The parallel beams from the splitter were focussed with spherical mirrors onto the center of the flow cell and a reference cell and then were directed to two photomultiplier tubes. The anode currents, which were balanced as well as possible over the region of interest, were then input to a logarithmic amplifier circuit. This circuit gave an output voltage which was directly proportional to the logarithm of the ratio of the current from the reference phototube to that from the sample, and hence to the absorbance of the sample.

During a run, all pertinent data were stored on magnetic tape by utilizing an Ampex SP-300 FM direct recorder/reproducer. A synchronization signal from the monochromator was also stored in one of the recorder channels. The recorded information was played back into a Tektronix type 564 storage oscilloscope with the time base triggered by the channel which contained the synchronization signal (which indicated the beginning of each revolution). The data on the scope were then photographed, using a Polaroid camera, and the resulting transparencies were magnified with a photographic enlarger and traced on graph paper. The greased glass syringes and stopcocks of the flow system introduced many difficulties because of the slow attack upon the silicone

grease by the metal-amine solutions. This problem was solved later[7,24,25] by using syringe plungers with Teflon tips, Fisher-porter "solv-seal" joints and various types of valves with Teflon stopcocks. Also the data analysis procedure was modified by introducing the use of a Varian C-1024 Computer of Average Transients (CAT)[24]. In this way, the data could be read from the tape recorder onto graph paper in analog form for display purpose, and onto computer cards in digital form for the purpose of rigorous analysis. This system has been used successfully for various kinetics studies[7,8,24,25].

II.3.4. Thermostated Stopped-flow System of Dewald and Brooks

In order to increase the temperature range over which reactions could be studied by the stopped-flow technique, Allen et al.[48] had constructed a stainless steel apparatus, capable of operating at -120° C. However, stainless steel is not compatible with a number of reactive systems such as metal-ammonia solutions.

To adapt the flow method for use with very reactive chemical systems at low temperatures, Dewald and Brooks constructed an all-Pyrex thermostated system capable of operating from -40° C to above room temperature[34]. The system could be evacuated and all the manipulations were carried out in vacuum and at low temperatures. The entire flow system as well as the storage vessels were surrounded by a Plexiglass thermostated bath. Three-way

greased stopcocks were used to connect the pushing syringes to the mixing chamber and reactant reservoirs. Three-turn spirals of 2 mm tubing were used to connect the mixing chamber with the stopcocks. These spirals were found to be necessary to prevent breakage of the glass when the apparatus was cooled, probably because of the difference in the coefficients of thermal expansion of the metal frame (on which the entire glass assembly was mounted) and the glass. Light wires (Bausch & Lomb 321306) were used to transmit the light through the bath fluid to the observation tube and then to the photo-tube. The system has been used successfully in the study of electron attachment reactions in liquid ammonia solutions at $\sim -35°$ C[49].

In summary, the stopped-flow technique has been used for kinetics studies with a variety of systems. A great number of instruments have been constructed and successfully used. The coupling of such an apparatus with a rapid scanning spectrometer has produced a very efficient system, which has proven to be of great importance for the study of reactions involving transient intermediates.

II.4. Computer-assisted Data Analysis

It appears that it was in the middle 1960's when scientists first realized that computer handling of experimental data would soon be an absolute necessity, because of the large amounts of raw data being generated by modern instrumental techniques. The earliest solutions to these

problems involved the construction of off-line (data processing with no real-time requirements) data acquisition (in digital or analog form) and data-logging hardware[50].

Even though the off-line computer-assisted data analysis was much better than prior methods, it still was frustrating for the researcher who could turn out mountains of data in minutes, but then had to wait as long as a few days to analyze the results of these experiments. It then became obvious that a more direct line of communication between the experiment and the computer was necessary. The earliest extensive use of on-line (direct coupling of computer and instrument) computers was in the field of nuclear chemistry[51]. These first types of laboratory computer applications were passive - no significant computer control of the experiment. Today active on-line computer systems (the computer is involved to some significant extent in the control of the experiment) can be found in many chemistry laboratories, especially the ones for analytical applications.

Of course, calculation problems in theoretical chemistry as well as in reaction kinetics and spectroscopy, may still require off-line computers with large core memory, but the data acquisition can be carried out much more efficiently with on-line laboratory computers. The number of published applications of small laboratory computers is increasing very rapidly. Small dedicated systems (one instrument per computer) for a variety of instruments[4,6,53,94] up to complex satellite systems (large computer, 48K; several small

computers; extensive periphery)[5] have been reported to be used in chemical and biochemical laboratories. It is in clinical routine analyses that automation has almost reached the ultimate; the operator just starts the system and provides the appropriate samples[52].

Recent advances in integrated circuit technology have made it possible to manufacture minicomputer systems which possess tremendous real-time data acquisition and control capabilities[54]. Unfortunately the task of connecting or interfacing the computer to a particular instrument or to a set of instruments is still a problem. One might consider it irrelevant whether a card reader, a magnetic tape or an analytical instrument (commonly via an Analog-to-Digital converter) were connected to the computer. However, whereas conventional devices such as card readers and magnetic tapes transmit data to the computer according to the needs of the appropriate program, the data from an analytical instrument must be taken by the computer at times which are determined by the on-line experiment (real-time data acquisition). A day-by-day increasing number of basic commercially available elements, make the interfacing barrier surmountable[54].

III. EXPERIMENTAL

III.1. General Techniques

III.1.1. Glassware Cleaning

All glassware was first cleaned with an HF cleaning solution (33% HNO_3, 5% HF, 2% acid soluble detergent, 60% water) followed by thorough rinsing with distilled water. The item was then filled with boiling aqua regia, which was allowed to remain in it for at least 10 hours. After rinsing six times with distilled water and six times with conductance water, the glassware was dried in an oven (110° C) overnight.

All the parts of the stopped-flow apparatus were cleaned in the same way before assembling the system. Prior to each run, the entire system was washed by allowing boiling aqua regia to remain in it for ∿5 hours and then rinsing it with distilled and conductance water until no change of pH of the water could be detected. The system was dried by evacuation. All the glassware destined to be used in the kinetics experiments as well as the stopped-flow apparatus was again rinsed after the above cleaning procedure, as described in Section III.2.3.

III.1.2. Vacuum Techniques

All of our work was carried out with standard high vacuum techniques. The vacuum lines were evacuated by using dual-stage mechanical pumps and two stage oil diffusion pumps, with Dow Corning 704 diffusion pump fluid. Liquid nitrogen cooled traps were positioned between the vacuum line and the diffusion pump. Pressure measurements were made with a Veeco RG75P glass ionization tube and a Veeco RGLL6 or a Granville-Phillips 260-001 gauge controller. Greaseless Teflon valves (Fisher-Porter, Delmar, Kontes and Rotaflo types) some of which were specially modified for high vacuum work[55], were extensively used.

III.1.3. Metal Purification

Alkali metals were purchased as follows:

Na : J. T. Baker Co. (99.99%)

K : J. T. Baker Co. (99.99%)

The metals were distilled several times prior to actual use.

The technique used for preparing and storing small quantities of these metals in small tubes has been given elsewhere[18].

III.2. Solvent Purification and Solution Preparation

III.2.1. Tetrahydrofuran (THF)

"Distilled in Glass" type THF was purchased from Burdick and Jackson. About 3 liters of THF were poured into a large

glass vessel containing ∿10 grams of purified grade CaH_2 (from Fisher scientific company). The vessel was then cooled with an ice bath and the solvent was thoroughly degassed by pumping through a liquid nitrogen cooled trap. A Teflon-coated magnet in the vessel was used to stir the mixture for several days and then the degassing procedure was repeated. The THF was then vacuum distilled into a flask containing ∿6 grams of benzophenone (Eastman-Kodak Company) and an excess of sodium-potassium alloy (1:3). A dry-ice isopropanol bath was used to help the distillation, while the vessel with THF over CaH_2 was kept at room temperature. The excess of Na-K alloy was necessary in order to make sure that only the non-volatile benzophenone ketyl and not benzophenone was left. The formation of benzophenone ketyl resulted in a dark purple solution. Because of its reactivity with water, the benzophenone ketyl served both as a drying agent and as an indicator of dryness. This purple solution was stable for months at room temperature. The solvent used for the experiments was vacuum distilled from such purple solutions.

III.2.2. Ethylenediamine (EDA)

EDA of 99% stated purity was obtained as a gift from the Dow Chemical Co. After a freeze purification step[25], the solvent was transferred under vacuum into small bottles (∿300 ml at a time) through a medium porosity glass frit There EDA was degassed by successive freeze-pump-thaw cycles

until the pressure change between two successive cycles was $\leq 2 \times 10^{-6}$ torr. The solvent was then transferred in the same way as above, into vessels containing Na-K alloy (1:3), which were kept in a dry-ice isopropanol bath. A very dark blue solution was formed as soon as the solvent was brought to room temperature. After keeping the solvent over the alloy for $\sim$1 week, the desired amounts of EDA were vacuum distilled into the appropriate bottles for preparing the required solutions.

III.2.3. Pre-rinsing Techniques

All the vessels destined to be used for solution preparation as well as the solvent bottles were pre-rinsed with a solution of potassium-anthracenide in THF[8]. The bottles used in the study of the reaction of Na^- in EDA were further dried by distilling liquid ammonia from a storage vessel into them 3 or 4 times[24,25]. The vessels were then pumped to $\leq 2 \times 10^{-6}$ torr and used as required.

Before all the runs (except the first one with Na-EDA solutions) the stopped-flow apparatus was evacuated (pressure $\leq 1 \times 10^{-4}$ torr) and then rinsed with a dilute solution of K-anthracenide in THF ($[K^+, An^{\cdot-}] \sim 10^{-4}$M) as follows: The entire flow system as well as the storage vessels and the thermostated burettes were filled with the rinsing solution and allowed to sit for $\sim$20 minutes. After that, the system was rinsed thoroughly with THF and pumped to $p \leq 1 \times 10^{-4}$ torr, through liquid nitrogen cooled traps,

before being used. This rinsing proved to be very helpful, because we did not detect any decomposition of our solutions while filling the system.

III.2.4. Solutions of Sodium in Ethylenediamine

Solutions of Na in EDA were prepared in vessels similar to the ones used for the K^+,An^- solutions (Figure 1a), but without the glass frit and the side arm for the anthracene. Sodium was distilled into the bottles through the appropriate side arm (after the bottle had been pumped to $\sim 5 \times 10^{-6}$ torr), then EDA was vacuum distilled into the non-metal side of the vessel using a dry-ice isopropanol bath. After bringing the vessel to room temperature, a small amount of EDA was transferred over the metal and a dark blue solution was formed. This blue solution was then mixed with the rest of the solvent without any detectable decomposition. This step was repeated until it was judged that the absorption of the solution was appropriate for our kinetics studies. Solutions made in this way were stable at room temperatures for ~ 12 hours.

III.2.5. Solution of NH_3 in EDA

Ammonia (Baker Chemical Co.) was distilled onto Na-K alloy yielding a blue solution. After several days of freeze-pump-thaw cycles, it was stored over Na-K alloy at liquid nitrogen temperature. The desired amount of NH_3 was vacuum distilled from the storage vessel into a preweighed

heavy-walled bottle and after its exact weight had been determined, it was distilled into another heavy-walled vessel with a known amount of EDA.

III.2.6. Aromatic Anion Solutions

Solutions of K-anthracenide in THF were prepared in vessels such as those shown in Figure 1a. The procedure was nearly the same as for sodium solutions in EDA. The only difference was that the break-seal containing a known amount of anthracene was broken by a Teflon enclosed magnet and the anthracene was dissolved in THF just before the formation of the blue solution. PAR grade anthracene from Princeton Organics was used without further purification and enclosed in the break-seal as described elsewhere[8]. From the weight of the bottle empty and with solvent, the amount of THF used was determined. Solutions made in this way were stable with no detectable change in absorbance for days at room temperatures.

III.2.7. "2,2,2 Crypt", "Crown" and Alcohol Solutions

Zone-refined "2,2,2 Crypt"[56] and "Crown" from E. I. duPont de Nemours & Co. were used without further purification. Weighed amounts of "Crown" (or "2,2,2 Crypt") were put into preweighed glass tubes which had a break-seal on one end and a 5 mm Fisher-Porter joint on the other. The tubes were then connected to the vacuum line via the 5 mm joints and pumped to $\sim 5 \times 10^{-6}$ torr. After that, anhydrous ammonia was condensed onto them and distilled away several times to

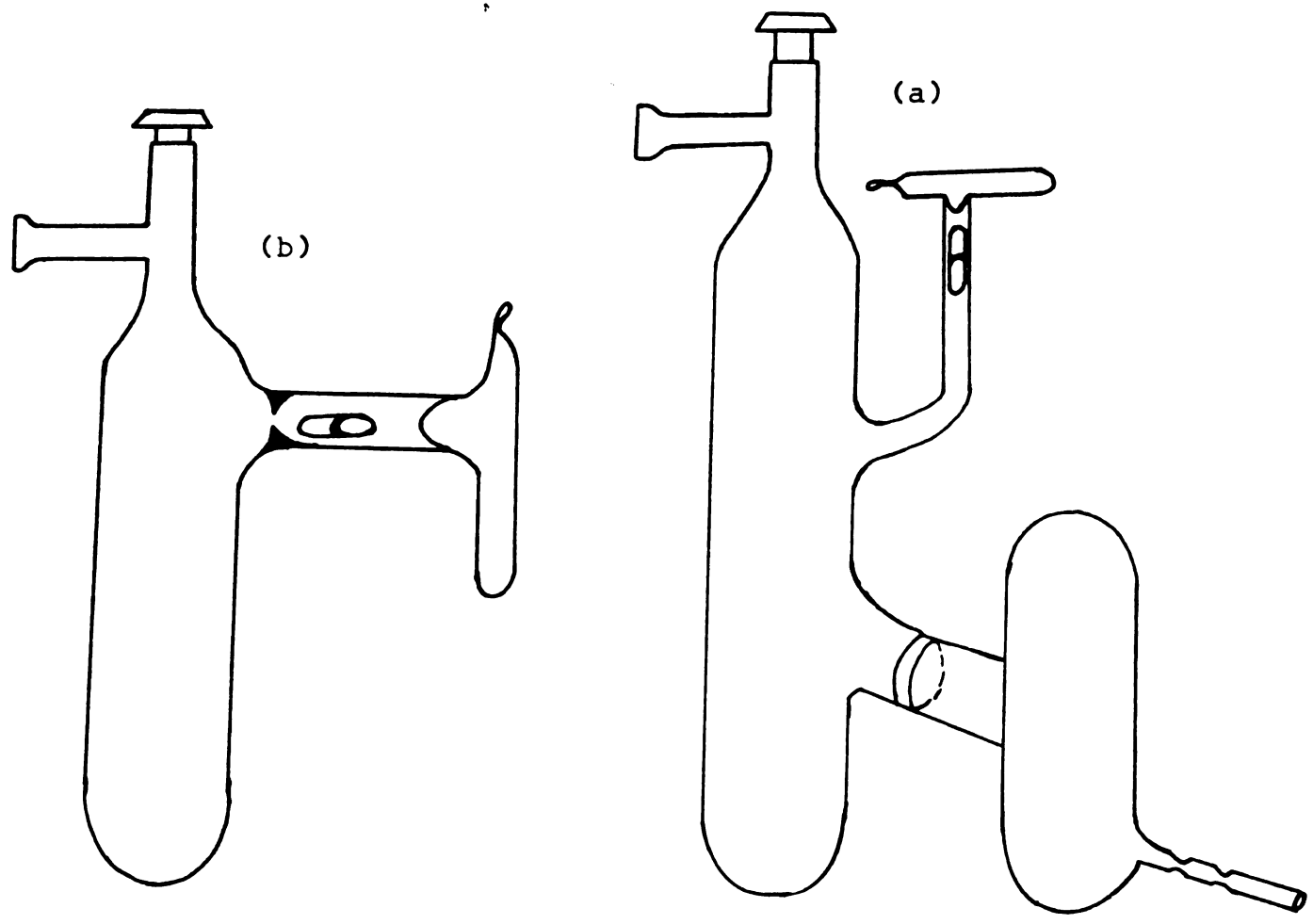

Figure 1. Vessels used for the preparation of: (a) K^+,An^- solutions, (b) all other solutions.

complete the drying process. Pumping was continued for ∿2 days after the NH_3 condensation, and then the tubes were sealed off under vacuum, weighed and attached to the appropriate bottles (Figure 1b).

Spectral grade ethanol (Gold Shield grade from Commercial Solvents Corporation) was further purified by distillation over a sodium mirror followed by degassing through freeze-pump-thaw cycles[8]. Pure alcohol was then distilled into a preweighed glass tube with a breakseal in one end. This tube had been dried by condensing anhydrous NH_3 into it several times, followed by pumping for ∿2 days. The alcohol was then frozen in the tube with liquid nitrogen, pumped to ∿2 x 10^{-5} torr, sealed off, weighed and connected to the solution make up bottle (Figure 1b).

After rinsing (Section III.2.3), solvent distillation and solution preparation were carried out as described elsewhere[8].

All the solutions were pressurized with ∿0.5 atm of appropriately purified helium gas[8], before being connected to the stopped-flow apparatus.

IV. THE STOPPED-FLOW APPARATUS

IV.1. Introduction

Since the initial measurement of the rate of reaction of the solvated electron (e^-_{solv}) with water in ethylenediamine[23], Dye and co-workers have continued to work on the development and improvement of stopped-flow systems for work with very reactive air-sensitive solutions. Three major improvements were, the incorporation of a scanning monochromator which permits the entire spectrum to be examined during reaction[2], the development of all-quartz mixing and observation chambers by the use of an air-brasive drilling unit[24], and the acquisition of data with an FM tape recorder for subsequent analysis by computer[24,25,57]. However, the kinetics studies were still limited by the necessity to work at or near room temperature and by analog storage of the data. Also another major disadvantage was the inability to analyze data rapidly during a particular experiment so that important decisions could be made and conditions modified if required.

A major effort has been made during the last three years to develop a variable temperature, vacuum-tight, stopped-flow system which is on-line with a remote PDP-8I computer. An appropriately planned averaging scheme could increase substantially the signal-to-noise ratio, especially in the "tail" of a reaction and thus increase the sensitivity of

the instrument. At the same time, two easily interchangeable path lengths were desirable for the stopped-flow apparatus, such that a much wider concentration range could be studied. Finally, the system had to be constructed not only for use with reactive systems but also for the study of transient state enzyme-kinetics[58].

IV.2. Flow System Design

A schematic diagram of the system is shown in Figure 2.

IV.2.1. General Description

Because of the nature of the solutions, the flow apparatus had to be constructed such that only quartz, Pyrex and Teflon come into contact with the reacting systems, and the entire system could be evacuated. Also temperature insensitive seals had to be made, to permit variable temperature studies. This introduces a major problem because the Teflon seals had to be adjustable in order to maintain a vacuum at temperatures below about 10° C. Since temperature artifacts are common with flow systems[59,42] the thermostat bath was constructed to include the entire flow apparatus in order to keep the reacting solutions at the same temperature as the flow system. A reference cell which could be filled easily with any solution was necessary since we wished to utilize double-beam operation.

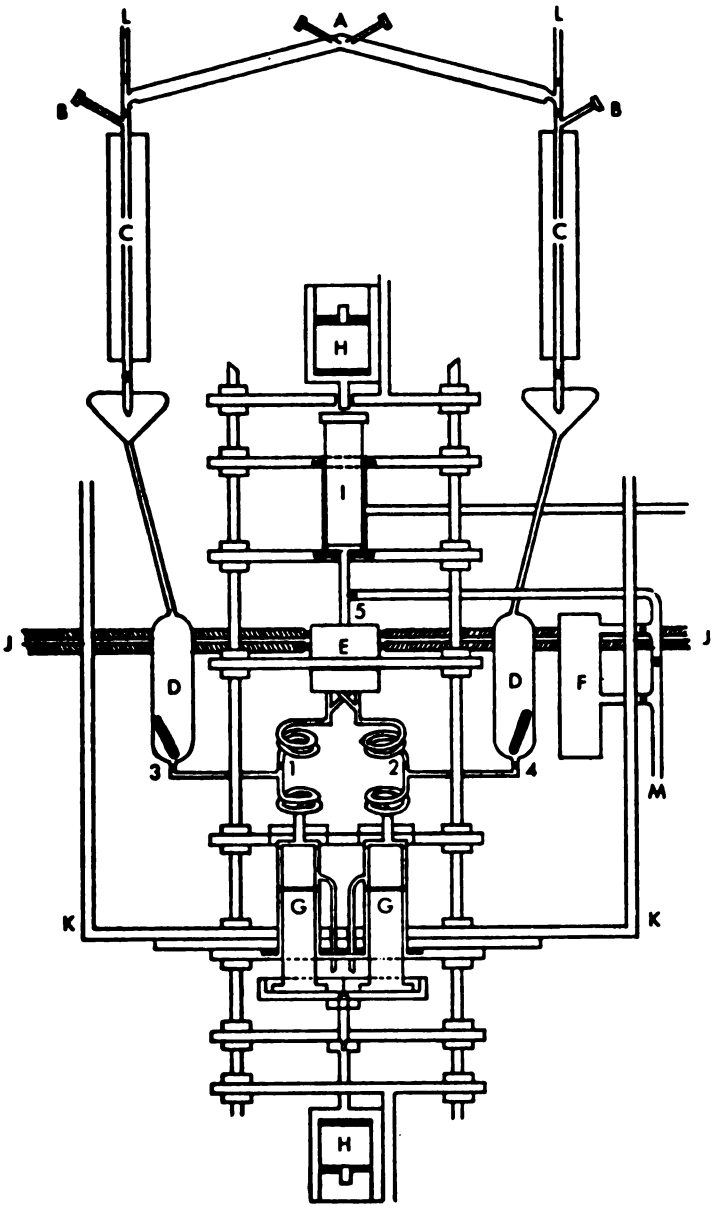

Figure 2. Schematic diagram of the thermostated stopped-flow apparatus. A - Joints for rinsing solutions, B - Joints for reactants, C - thermostated burettes, D - reactant reservoirs, E - mixing and observation cell, F - reference cell, G - pushing syringes, H - pneumatic pistons, I - stopping syringe, J - quartz light fibers, K - thermostat bath, L - to vacuum, M - to vacuum and "waste", 1, 2, 3, 4, 5-flow valves.

IV.2.2. Flow Cell and Reference Cell

IV.2.2.1. Drilling of Quartz

The earlier mixing cells were constructed from Plexiglas, and the observation tube with the in-coming lines was sealed to it by using epoxy resin[21]. Since this mixing chamber was attacked by the solutions, an all Pyrex mixing and observation cell was constructed by a very elaborate technique[2,22]. Also, all quartz cells were made by the same technique[22], but their cost was very high. Hansen[24] describes a better way to construct quartz cells which utilizes Airbrasive drilling of heavy-walled 1 mm i.d. quartz capillaries. The performance of cells constructed in this way has proven to be very good[7,8,10,25].

In constructing the cells we followed the method described by Hansen, with some modifications, which were necessary because of the complexity of our cells. The starting materials were 7.7 cm lengths of heavy-walled 1 or 2 mm i.d. quartz capillaries (purchased from Engelhard Industries, Inc., Amersil Quartz Division, Hillside, N.J., at the price of $2-3/ft for tubing selected to be close to 1 or 2 mm, or $25/ft for tubes exactly 1.0 mm i.d.). These lengths of capillaries were polished flat on two opposite sides (by Precision Glass Products Co., Oreland, PA). The drilling of the inlets and outlets was accomplished by utilizing an Airbrasive unit (S. S. White Industrial Division, New York, NY, a model C unit was used with No. 1 Airbrasive powder). This instrument

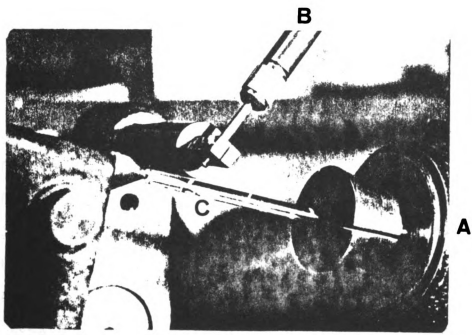

Figure 3. Set-up for the drilling of quartz capillaries. A - indexing head, B - to the airbrasive unit, C - capillary tube.

outputs a high speed stream of nitrogen gas, which contains finely divided aluminum oxide (or another powder) and may be used to drill holes of the desired shape and size (this depends upon the nozzle tip used and the distance of the tip from the item to be drilled[60]). The capillaries were mounted on a horizontal drilling table utilizing an indexing head for very accurate positioning. The drilling set-up is shown in Figure 3.

IV.2.2.2. Cell Construction

IV.2.2.2.1. Drilling

In order to achieve more complete mixing, we wanted to divide the solution into four streams after initial mixing and then mix them again. This had to be accomplished with a very little increase in dead volume. Also we wanted two path lengths for each cell.

To accomplish this, first the capillary for the double mixer was drilled as follows. A 0.5 cm quartz rod was inserted and sealed into the central bore about one cm from one end. Then, using the device described above (Section IV.2.2.1), the four inlet holes were drilled, entering the central bore of the capillary almost tangentially and at an angle of about 105° to it. The capillary was rotated 90° between successive holes, until all four holes had been drilled. To prevent unwanted drilling of the capillary wall opposite the hole being drilled, a piece of polyethylene medical tubing was inserted in the central bore of the capillary tube. By using the

appropriate nozzle tip and positioning it at the proper distance from the tube, we were able to drill holes which were slightly tapered from the outside surface of the capillary to the central bore. The entrance diameters were just under half the bore diameter. At a distance of one cm above these inlets, four similar holes were drilled at an angle of ∿135° to the central bore, and 0.5 cm lower (also 0.5 cm from the inlets) four more holes were drilled at an angle of ∿45° (see Figure 4). To enlarge these holes to an entrance diameter equal to half the bore diameter, we used an appropriate diameter tungsten rod coated with a mixture of water and Airbrasive powder in a drill press.

For the long path length optical cell, another capillary was utilized. On the two flat sides of this capillary two parallel holes were drilled at an angle of ∿135°. The entrance diameters of these holes were equal to the bore diameter and at the desired distance apart (∿1 or ∿2 cm).

IV.2.2.2.2. Glassblowing[61]

The capillaries drilled as above were then cut to the appropriate lengths (Figure 4). The mixer was finished by attaching the vacuum joints (Fisher-Porter 2 mm "solv-seal" quartz joints) and sealing the unwanted holes with appropriately ground quartz rods. The capillary destined to form the long path length cell was then connected to the mixer with the top joint as shown in Figure 4. Finally, the two ends of the long path length were ground such that

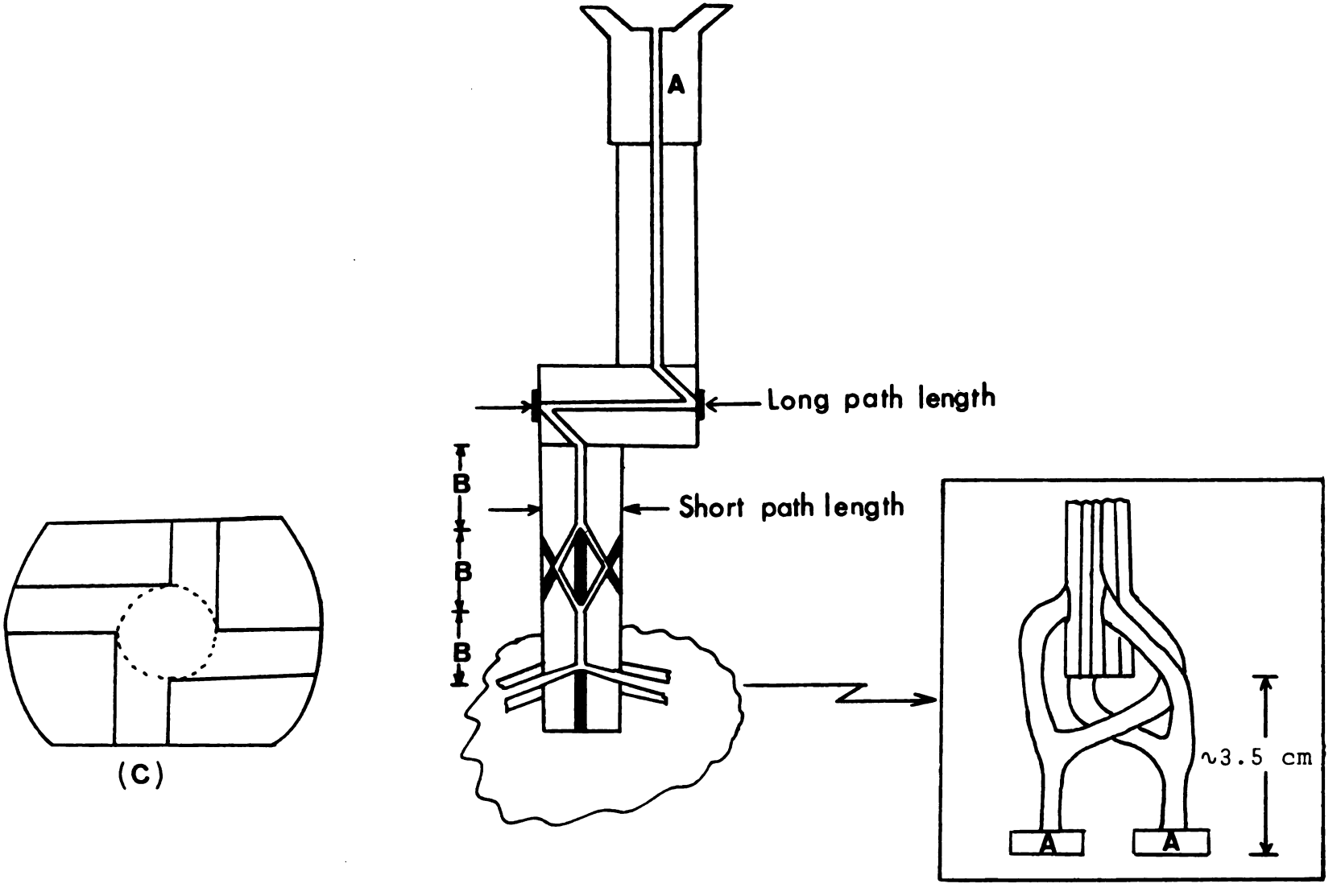

Figure 4. Schematic diagram of the mixing and observation cell. A - Fisher-Porter 2 mm quartz joints, B - ~0.5 cm, C - cross-section of a mixer.

the two parallel holes were just uncovered and then two flat optical windows were sealed on. These windows were cut from transparent fused quartz cover slips of ∿0.2 mm thickness (purchased from Thermal American Fused Quartz, Montvill, N.J.). Also, thicker windows were used, but they had to be ground and polished after being sealed on.

IV.2.2.2.3. Description of the Reference Cell

The reference cell was constructed the same way as the sample cell but, of course, without the mixer (see Figure 5).

We have constructed sample and reference cells from 1 mm (long path length is ∿1 cm) as well as 2 mm capillary tubing (long path length is ∿2 cm). The latter was used more extensively, because it had better optical characteristics with the weak light sources used initially.

IV.2.2.3. Cell Mounting

Individual holders were machined from stock-aluminum for each of the cells. Each holder consists of four separate pieces which fit around the cell, as closely as possible, and are held together by six screws (see, for example, Figure 5). To make sure that the cell did not move inside the holder we wrapped it with Teflon tape. The holder has openings into which the light fibers fit. Each opening has a light window of the appropriate size at the cell end. The light windows are round (1 or 2 mm in diameter) for the long path lengths and rectangular

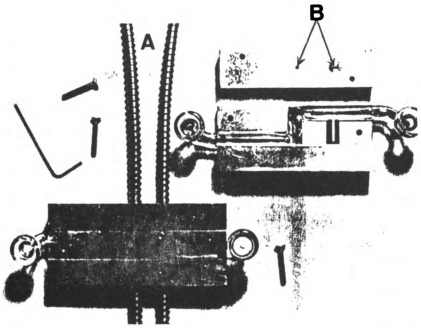

Figure 5. Reference cell and its holder. A - quartz fiber optics, B - observation windows.

(0.5 x 2 or 1 x 2 mm) for the short path lengths. The short path length is located ∿1 mm above the second mixer. With this set-up we have been able to obtain very efficient mixing as well as good light transmission.

IV.2.3. Pushing and Stopping System

IV.2.3.1. Syringe Design

Glass syringes, lubricated with Dow-Corning silicone grease, were used previously[21,22], but caused many problems because the metal solutions attacked the silicone grease[24]. Greaseless plungers were then made by mounting Teflon tips on plungers from Hamilton glass syringes. The tips had been machined appropriately to insure a vacuum tight liquid seal[24]. Uranium glass was used to seal these Hamilton "gas tight" syringes to Pyrex joints. A side arm was introduced later with a new type plunger to eliminate the problem of the high permeability of Teflon to oxygen[7,25]. Even better results were obtained by making special syringes with precision bore tubing[8,25] and similar plungers.

We have modified this last technique in making our syringe and plungers, in order to permit compensation for changes in the dimensions of Teflon with temperature (see Figure 6). The syringes were made out of heavy-walled precision bore tubing (Trubore 8700-765, I.D. = 0.553", ACE Glass Inc., Vineland NJ) and the plungers were machined to fit these syringes. They are vacuum tight down to -30° C (tested), and have solved the recurring problems associated

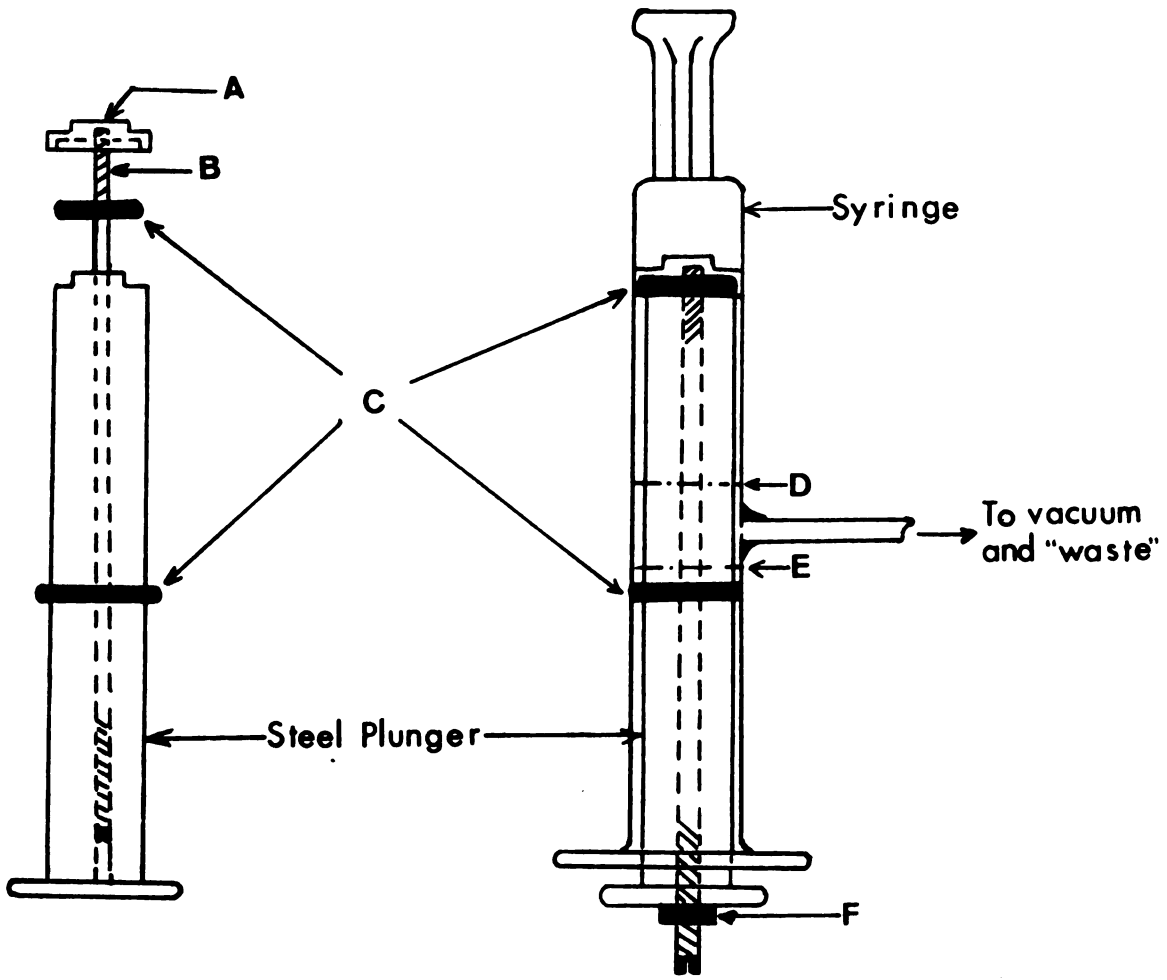

Figure 6. Detailed view of a syringe used in the stopped-flow system. A - Teflon tip, B - threaded rod, C - Viton "O" rings, D - fill position, E - rinse position, F - locking nut.

with leaky syringes. The Teflon seals are forced against the glass walls by Viton "O" rings held under compression. To further insure against leakage, the Teflon wipers can be pulled down by the adjusting threaded rod, thus maintaining a good vacuum seal. By using the side-arm for back pumping, we insure that the section between the Teflon wiper and the second "O" ring is constantly evacuated during the motion of the plungers.

An operation which wastes solution in many stopped-flow systems is that required to rinse the previous solution from the syringe and to introduce a new solution of known composition. We use the back-pumping side-arms of the syringes as exit ports for the purpose of rinsing the system prior to re-filling. Special care was taken in drilling a small hole on the glass wall (utilizing the Airbrasive unit; Section IV.2.2.1) and sealing the side arm, such that the barrel is not distorted and a good seal is maintained, even when the Teflon wiper is lowered to the rinsing position.

IV.2.3.2. Mechanical System and Framework

The flow system was mounted on a framework of suitably machined aluminum plates, which were bolted in place to four threaded rods (3/8"). One of the plates was bolted to a sturdy angle iron table. On the same table were mounted the monochromator, the lamp and the detectors. As can be seen in Figure 2, the flow system is mounted vertically.

This position eliminates bubble formation, but it can cause back diffusion problems as described in a later section.

The plungers of the pushing syringes were bolted to an aluminum block, which has the appropriate holes to allow easy adjustment of the Teflon tips. This block was then connected to a pneumatic piston[62] via a threaded rod passing through an aluminum plate. The plate was used for stopping the plungers when they were lowered to the rinsing position, while small aluminum blocks were inserted between the pushing block and the plate in order to stop the plungers at the filling position.

The pneumatic piston could be operated manually (with a 4-way, 3-position valve[62]) or automatically by utilizing solenoid operated valves[62]. Usually we fill the syringes by using the manually actuated valves and then have the scanning monochromator control signals (beginning of scan pulses) trigger the pushing operation by setting the appropriate logic gate to "1" when we are ready. In this way, we synchronize the scanning monochromator with the stopped-flow apparatus. When fixed wavelength experiments were performed, the pushing was actuated manually (a minor modification could be introduced to allow for automatic pushing when the monochromator is not scanning).

A miniature pneumatic cylinder operated with a manual valve was used to expel the waste solution from the stopping syringe. All of these operations could be easily computer controlled if the manually operated flow valves were replaced

with solenoid operated ones (see Section IV.4.4.3).

The thermostat bath, which surrounds the entire flow system (see Figure 2), was constructed from 3/8" Plexiglas sheets (Plexiglas gives good visibility and insulating characteristics[34]). Three bath walls were permanently sealed to the bottom piece, while the fourth one was mounted on with screws, such that it could be taken off easily. Also, part of another wall could be removed to allow work to be done in the bath. The flow valves were mounted on one of the permanent bath walls and utilized small Plexiglas blocks, which were fit firmly around each valve (with the appropriate length of Teflon tape) and then connected to the wall with screws. This way of mounting has proven to be very efficient and allows for removal of the valves when necessary.

The pushing syringes pass through the bottom Plexiglas piece together with their side-arms. The syringes were mounted on an aluminum plate which was forced against the bath with an "O" ring in order to make a liquid-tight seal. Having the side-arms coming out through the syringe mounting plate allows for easy replacement of the syringes.

Holes were drilled in the Plexiglas walls for the fibers and the waste lines. Dow Corning 3110 RTV encapsulating compound was used as required to make liquid-tight seals.

Two air-driven magnetic stirrers (Arthur H. Thomas Company, 8612-B50) were used in the bath to mix the solutions in the reservoir vessels.

A lab-line Hi-Lo Tempmobile unit was available for circulating the thermostatting fluid. For work at or above room temperature, a water bath was thermostated by circulating a 50:50 mixture of water and antifreeze from the Tempmobile unit through copper coils in the water bath. The water was then circulated through the Plexiglas bath with a centrifugal pump. In this way the temperature of the Plexiglas bath could be controlled to within $\pm 0.1^{\circ}$ C[58].

IV. 2.3.3. Stopping Syringe and Waste Lines

The stopping syringe was similar to the pushing syringes with an adjustable Teflon plunger. An aluminum plate located at the desired distance above the syringe was used to abruptly stop the plunger during an experiment. The stopping plate can be easily moved to a different position; however, we have found that the optimum position is one which allows the plunger to move about 1 cm. This traveling distance allows for maximum flow velocity to be obtained (with moderate air pressures), and gives three successive pushes per filling of the pushing syringes. Two metal flags were mounted on the stopping plunger. These flags interrupt light beams which strike two phototransistors (GEL14B) to give timing pulses from which the flow velocity can be accurately calculated (see Figure 7). These pulses were used to trigger the data collection. We can start collecting data either as soon as the maximum flow velocity has been reached (trigger with the start flag, which had to be

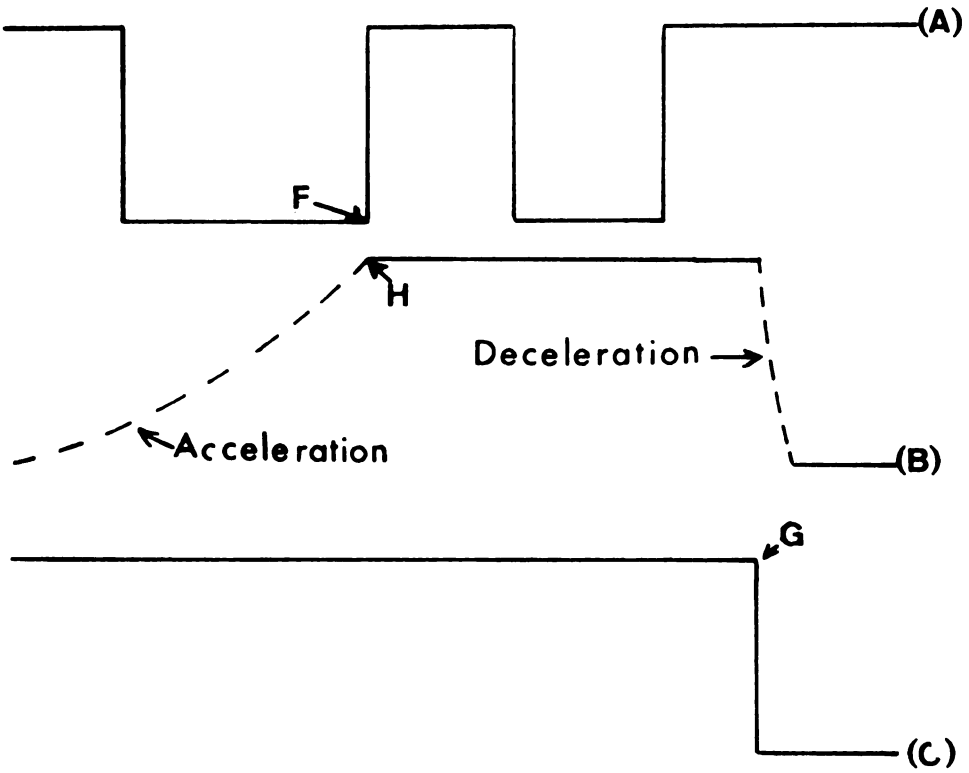

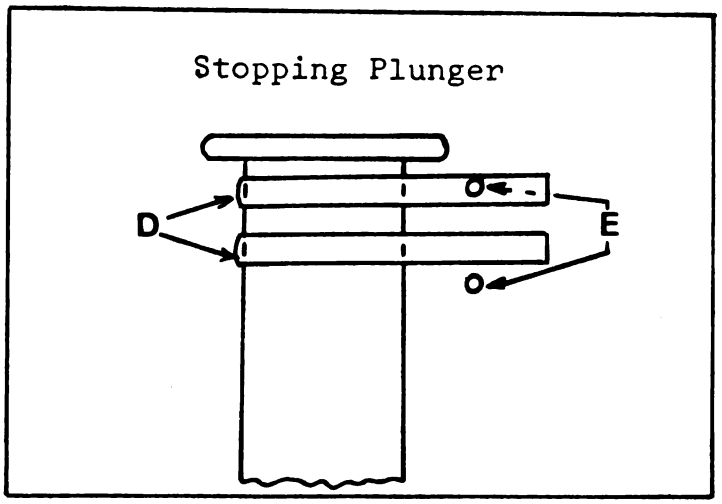

Figure 7. Timing pulses from the flow-flags. A - start flag, B - flow velocity profile, C - stop flag, D - location of the metal flags on the stopping plunger, E - location of the phototransistors, F, G - data collection can be initiated at one of these points, H - constant flow velocity has been reached at this point.

inverted in order to trigger our circuitry), or just a few milliseconds before the stopping occurred (trigger with the stop flag). In this way we always collect some data during flow and thus have a better estimate of the initial absorbance. Also by utilizing these pulses to start and stop a clock, and knowing the exact separation of the two phototransistors as well as the thickness of each metal flag we have been able to compute (within the experimental error) the zero of time; that is, the time when the mixed solutions come to complete rest.

The waste line coming out from the exhaust valve was connected via two valves to the reference cell. In this way we have been able to make a reference solution of the desired composition in the flow system and then fill the reference cell with it. This would be useful when observing the formation of unstable compounds in the presence of large amounts of interfering reagents.

IV.2.3.4. Delivery System

The pushing syringes were connected to the flow control valves (Kontes Teflon valves) via two-turn spirals made out of 2 mm regular wall tubing. These spirals have been found to be necessary for low temperature work[34]. Two flow control valves (1,2 Figure 2) connected the syringes with the mixing and observation cell and two more (3,4 Figure 2) were used in the lines to the storage vessels. Between the valves and the cell, we have inserted two more (3 turn) spirals, which are coupled to the cell with

2 mm Fisher-Porter joints. The same kind of joints have been used in connecting the top of the cell with the exhaust valve (5 Figure 2) and the stopping syringe.

IV.2.4. Solution-handling System

Up to four solution bottles could be mounted on each side of the apparatus (Figure 2). The bottles were connected to the system via 5 mm Fisher-Porter joints and at an angle which allowed for transfer of their entire contents if so required. Each bottle was attached to a 10 ml thermostated burette, such that accurate dilutions could be made. The burettes were connected to the vacuum line at the upper end (via Kontes valves) and to the mixing vessel at the lower end (via Rotaflo adjustable Teflon valves with small dead-volumes).

All four burettes on each side were connected with ∿1 mm tips to a funnel-shaped tube which drained into the storage vessel (∿40 ml vessel).

After the solution bottles were mounted, the system was evacuated (low vacuum for non-air-sensitive systems or high vacuum for unstable solutions). After the necessary vacuum was obtained, the system was isolated from the vacuum line, and solvent was admitted into both storage vessels. Subsequently, the pushing syringes were filled and pushed slowly to fill the system with solvent. Appropriate adjustments were made (light, absorbance circuitry, amplification, etc.) and the solvent background spectrum was collected. Any solvent left in the storage vessels was then removed

(either pushed out or through the side-arms of the syringes), the desired solutions were transferred into the storage vessels, where they were mixed (with a Teflon enclosed magnet) and allowed to reach thermal equilibrium with the bath (~10 minutes, depending upon the temperature difference and the volume of the solutions). The system was then ready for the kinetics experiment to begin.

Commonly, small volumes of the concentrations to be studied were prepared in order to rinse the storage vessels and the syringes before starting the data collection. After the pushing syringes were rinsed and the solutions to be studied were prepared in the storage vessels, the data collection was carried out as follows:

Valves 1 and 2 were closed and valves 3 and 4 were opened. The pushing plungers were then lowered to the filling position and the syringes were filled with the solutions. Valves 3 and 4 were closed, valves 1 and 2 were opened and the "push ready" logic gate was set to "1". The next beginning of the scan pulse from the monochromator activated the pneumatic piston which forced the plungers to move upward. This caused the reactants to flow through the mixing and observation cell to the stopping syringe. The stopping plunger was thus forced to move upward and strike the stopping plate to halt the flow and the advance of the pushing plungers. After the data collection was over valves 1 and 2 were closed, while the pneumatic piston was returned to the hold position. Valve 5 was opened and the

reacted solutions were expelled to the "waste". With valve 5 closed, valves 1 and 2 were re-opened and the pneumatic piston was activated for a second push. A third kinetics record was obtained in the same way before refilling the bottom syringes.

IV.3. Optical System Design

IV.3.1. Overall Characteristics

Quartz fiber optics[63] transfer the dispersed light from the monochromator, through the bath fluid, to the cells and then to the photomultiplier detectors. The use of fibers also helps to overcome problems associated with alignment of the optical components and allowed for a more convenient positioning of the monochromator and the phototubes. At the same time, we eliminated errors resulting from vibration of the cell out of and into the light beam, since, if vibration occurred, the fiber end could move with the cell. As mentioned before, double beam operation and analog conversion of intensities to absorbance were employed in order to permit a wide dynamic range of input intensities, to cancel out lamp intensity and photomultiplier voltage fluctuations and to allow for observation of small absorbance changes over large background contributions. Small Pyrex fibers were used to illuminate the phototransistors (with a miniature bulb) for the timing pulses of the stopping plunger (Section IV.2.2.3).

IV.3.2. Light Sources, Monochromator, Fibers

In the early stages of our work we used either a Tungsten (Quartz Iodine) or a 150-watt Xenon light source (both Bausch & Lomb products). Their low intensities, combined with inefficient matching of their output with the monochromator input, gave low signal-to-noise ratio values. Later, we were able to utilize a 1000-watt Xenon arc lamp with the appropriate optics to match its output to the monochromator input and this improved our results dramatically. This lamp was mounted in a model C-60-50 Universal Lamp housing and powered from a model C-72-50 Universal Lamp power supply (all from Oriel Optics Corporation, Stamford, CT).

A Perkin-Elmer model 108 rapid scanning monochromator[2] was coupled with the system, and allowed us to scan a selected spectral region between 280 and 1050 nm with 3 to 150 scans per second (a new prism to be mounted soon should lower the U.V. limit to ∿220 mm, which is the cut-off wavelength of the fibers). Two kinds of triggering signals are produced by the scanning monochromator. One of them marks the beginning of each revolution (BS-signal) while the other one is related to the rotation angle of the nutating mirror (GT-signal). To generate these signals we utilize a miniature lamp to illuminate the gear which is directly attached to the nutating mirror. This light beam is reflected from a small polished spot on the black (painted) gear and strikes a phototransistor (GEL14B) to give the BS-signal. Another phototransistor, located behind the gear, is used to detect

the light beam as it is interrupted by the gear teeth, and gives the GT-signal (136 teeth on the gear give 136 pulses per revolution). The frequency of the GT-signal is then appropriately multiplied (see Section V.2.3), and the resultant signal is used to trigger the sample-and-hold amplifier and the analog-to-digital converter (ADC). In this way, data points are collected at equal increments of rotational angle of the mirror, and since wavelength is determined by the angle of rotation, corrections are automatically made for slight changes in rotational velocity (due to "play" in the gear train).

The output of the monochromator was coupled to the fibers by use of a metal tube which was mounted on the monochromator cover. The fibers were held in place with small set-screws, while the mounting assembly allowed for adjustments (slotted mounting holes) to be made in optimizing the light intensity on the reference and sample fibers. An attempt to combine four fiber-bundles into a slit-shaped end was aborted because the quartz fibers are very fragile, making their handling almost impossible. Commercially available 2 mm round end, 50 cm long, quartz fibers[63] were used. The present fiber set-up introduces a problem because the sample and reference fibers "see" different regions of the Xenon arc, so that spatial fluctuations are not averaged out. A factory-made beam splitter[63] with a slit shaped end has been ordered and will be attached to the monochromator to minimize this problem.

IV.3.3. .Detectors

The use of either quartz-envelope RCA photomultiplier tubes (RCA 6903, S-13 response; from RCA, Harrison, NJ), or EMI photomultiplier tubes (EMI 9684B, S-1 response; from Gencom Division/Emitronics, Inc., Plainview, NY), allowed us to detect light in any spectral region between 220 and 1050 nm. In order to reduce the dark current of the EMI photomultipliers (PMT's) we used the appropriate magnetic lens assembly (supplied by the manufacturer) and also enclosed them in a specially made, dry-ice cooled, housing. This was a two compartment housing designed so that we could add dry-ice during the experiment without exposing the PMT's to ambient light. Styroform insulation was used in the cooling compartment and a double quartz window was mounted at the two ends of the magnetic lens assembly to avoid condensation on the PMT window when the tubes were kept at low temperatures. Since two fibers are used for each PMT (short and long path length), a sliding bar was mounted between the tubes and the fiber ends, which allowed for isolation of one beam at a time. Provision was also made for calibration filters to be inserted into the sample beam, while a V-shaped vane positioned in front of the reference tube allowed for intensity adjustments. This cooled housing has been used successfully from -70° C up to room temperatures.

The detectors were powered with a regulated power supply from Furst Electronics (model 710-P).

IV.3.4. Absorbance Circuitry

The outputs of the PMT's were the inputs to a logarithmic ratio amplifier, whose circuit diagram is shown in Figure 8. All components used in this circuit are from Philbrick/Nexus research, Dedham, Mass. The output voltage is proportional to the logarithm of the ratio of the reference to the sample intensity. At 27° C and gain 1, the output is actually ∿0.9824 volts per absorbance unit (the variable gain switch allows for gains of 1,2,5,10,20). This voltage was then converted to absolute absorbance by utilizing calibrated neutral density filters (Optical Industries, Inc., Santa Ana, CA) as described in Section IV.5.3. The output of the absorbance circuit was appropriately biased to allow for utilization of the entire range of the data acquisition system (from -5 to +5 volts).

IV.4. Performance Tests

Performance tests have been made with the entire system in a variety of ways, including the study of a number of standard reactions.

IV.4.1. Optical Calibration Data

The wavelength resolution of the instrument depends upon the instrumental settings. An example is given in Figure 9, which shows a portion of a 128 points holmium oxide spectrum collected while scanning at 75 scans per sec (26.66 msec per revolution; 13.33 msec per spectrum).

The effective path lengths of the cell were determined

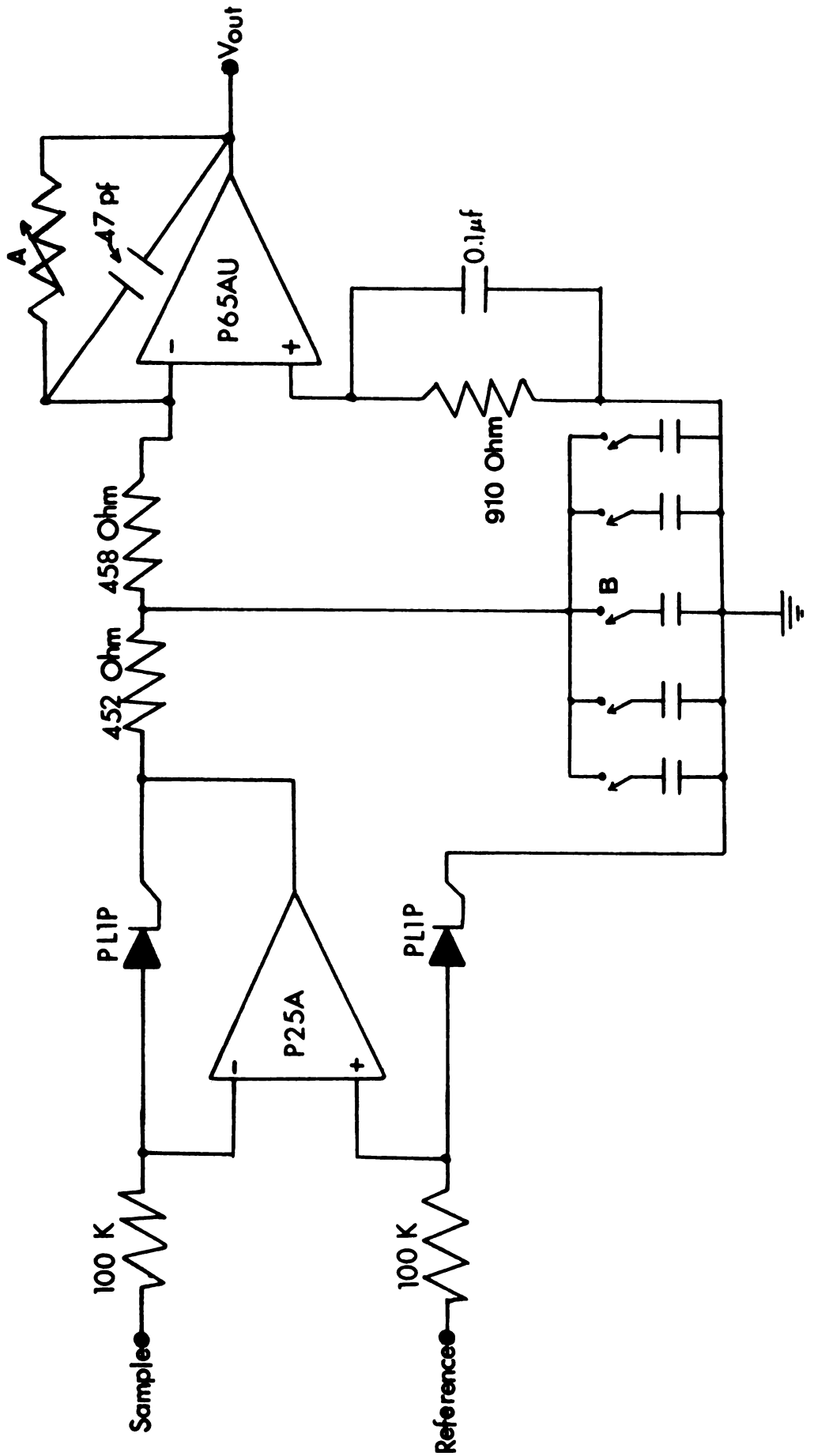

Figure 8. Absorbance circuity. A - variable gain potentiometer, B - high frequency noise filters, (controlled with toggle switches). All the major components are from Philbrick/Nexus Research.

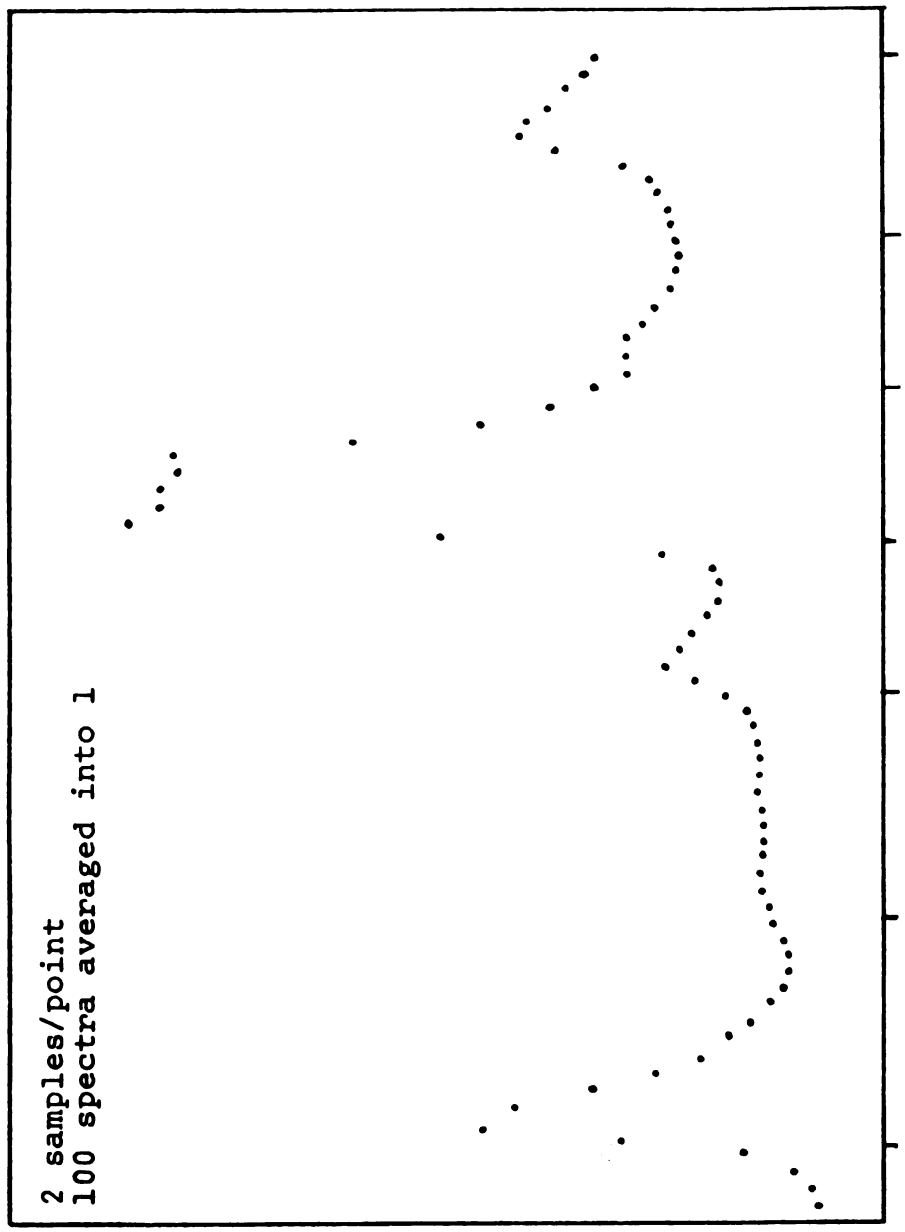

Figure 9. Holmium oxide spectrum recorded while scanning at 75 spectra/sec. Solvent background has not been subtracted.

by utilizing Beer's law tests. For the short path length, freshly prepared aqueous solutions of $KMnO_4$ were used. The solutions were calibrated with a Cary model 15 spectrophotometer by using 1.00±0.01 mm SCC cells, just before being used. In Figure 10, the results obtained with our instrument at 524 nm have been plotted against the corresponding results from the Cary. It can be seen that Beer's law is obeyed for absorbances up to ∿2.0, and that the path length calculated by using least squares for the first 6 points is 1.99±0.02 mm.

Similar tests for the long path length with aqueous solutions of 2,4-dinitrophenolate at 360 nm, gave an effective path length of 1.85 cm[58].

The lack of linearity for absorbances greater than 2.0, could result from non-linear response of the absorbance circuit (it is linear over the range of 10^{-3} to 10^{-9} amps of photocurrent).

Scattered light problems were minimized by positioning the appropriate cut-off filters in the light beam between the lamp and the monochromator (e.g. for the Na^- work a CS 3-66 Corning filter was found to perform satisfactorily, while for the anthracenide work a Pyrex glass filter was used). No light leaks were detected in any of the experiments.

The signal-to-noise ratio depends of course upon the wavelength region examined. With the 1000-watt Xenon arc lamp we have studied total absorbance changes at 330-450 nm, of 0.08 absorbance units on a 0.2-0.6 absorbance units

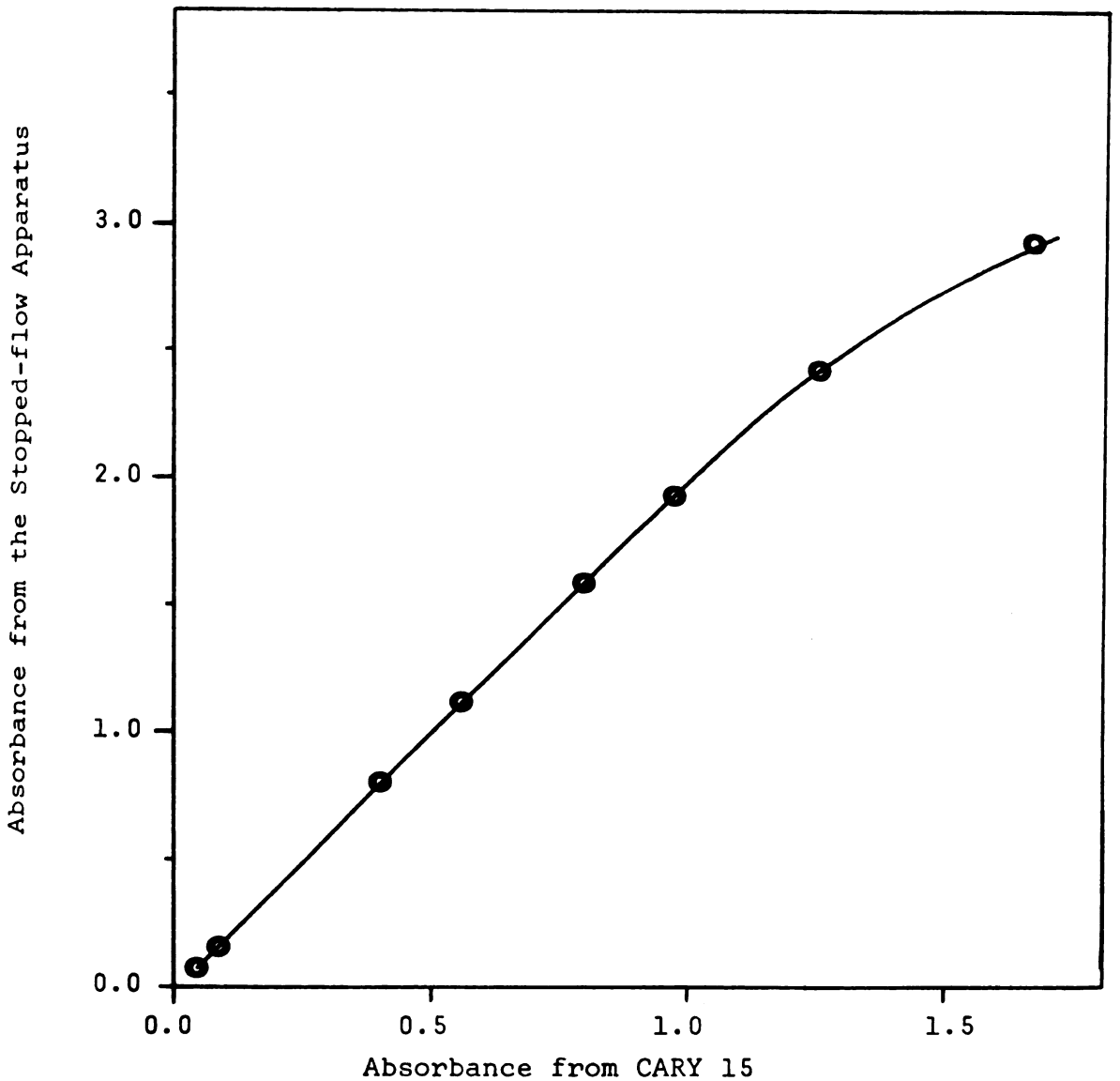

Figure 10. Absorbance from the stopped-flow system vs absorbance from a CARY 15 spectrophotometer for aqueous solutions of $KMnO_4$. The line drawn has a slope of 2.0.

background at 75 spectra/sec[58]. For this case, the r.m.s. noise as estimated from an analog storage oscilloscope was ∿0.002 absorbance units.

Two major sources of noise are limiting at the present time. One arises from vibrations of the scanning mirror and can be removed only by collecting data at fixed wavelengths. However, the second one is associated with the position of the fibers at the exit slit of the monochromator (see Section IV.3.2) and could probably be minimized by using an appropriate beam-splitter. This second source sometimes gave us r.m.s. noise as high as 0.02 absorbance units, for absorbance changes of ∿1.0 units over no background absorbance.

IV.4.2. Flow Calibration Data

Utilizing the flow flags described in Section IV.2.3.3 we were able to compute the flow velocity for each push. We actually measured the flow time; that is the time required for the stopping plunger to travel a given distance (depending upon the separation of the two phototransistors); and then computed the flow velocity. For example in one set of pushes we had (air pressure ∿50 PSI):

(a) Flow time for 25 successive pushes = 76.5±4.3 msec.

(b) Distance to travel (for stopping plunger) within this time = 5 mm.

These resulted in a flow velocity in the stopping syringe: U_{ss} = 0.065±0.003 m sec^{-1}, or a flow velocity in the mixing chamber: U_{mc} = 3.22±0.15 m sec^{-1}. Note that the critical velocity for turbulent flow for water at 20° C in a 2 mm

tube is $\sim$1 m sec^{-1}(1a, pg. 715).

The time between the pulse which started the flow time clock and the next BS-pulse (for scanning experiments) was found to vary from a few msec to the time corresponding to a complete revolution. This time was always measured by the computer with a real time clock(64).

From these measurements and the instrumental stopping time we were able to compute the time which elapsed between the initiation of the data collection and the actual stopping of the solution. In this way, the appropriate time corrections could be made to our data.

Vibrational artifacts appeared to be absent, and cavitation did not occur during flow or upon stopping. Trapped gas bubbles are easily swept out of the system.

IV.4.3. General Performance, Scanning Mode

As mentioned earlier, one source of error results from vibrations of the scanning monochromator. As expected, the size of the error depends upon the scan speed. We have been able to collect scanning data at speeds up to 150 spectra per second (13.34 msec per revolution), with satisfactory signal-to-noise ratios. However, the system operates much better at lower scan speeds and most of our work has been carried out at 75 spectra per second.

The peak positions for successive unaveraged spectra were found to be very reproducible, generally within $\pm$1 core memory location for sharp peaks and over the range covered in

Figure 9. Also the absorbance of calibration filters or solutions did not change between successive scans.

IV.4.3.1. Clean Stoichiometry and Isobestic Point

One of the systems used to test the performance of the instrument, was the production of peroxychromic acid from hydrogen peroxide and acidified solutions of dichromate, according to the reaction: $HCrO_4^- + 2H_2O_2 + H^+ \rightleftarrows CrO_5 + 3H_2O$[65]. Figure 11 shows the results obtained while scanning at 75 spectra/sec from ∿300 to ∿600 nm. At low wavelengths we observe the decay of Cr(VI) while at high wavelengths the growth of the peroxychromic acid gives an increase in absorbance. For this particular experiment we used the following initial concentrations:

$$[HCrO_4^-]^\circ = 0.5 \text{ mM}$$
$$[H_2O_2]^\circ = 4.54 \text{ mM}$$
$$[H^+]^\circ = 10.0 \text{ mM}$$

In Figure 12 we have isolated only a few spectra from the same experiment, and here we can see better the decay at ∿354 nm the growth at ∿600 nm, and the isosbestic point at ∿480 nm. Also in this figure can be seen the effect of the averaging scheme in smoothing the data. Starting from the top (of the decay) each spectrum is the average of 1, 2,4,8,16 (13.3 msec) spectra respectively, and the effect of averaging on the signal-to-noise ratio is profound.

In Figure 13 are shown the time cuts for the first 9 seconds, from the same experiment, at wavelengths which

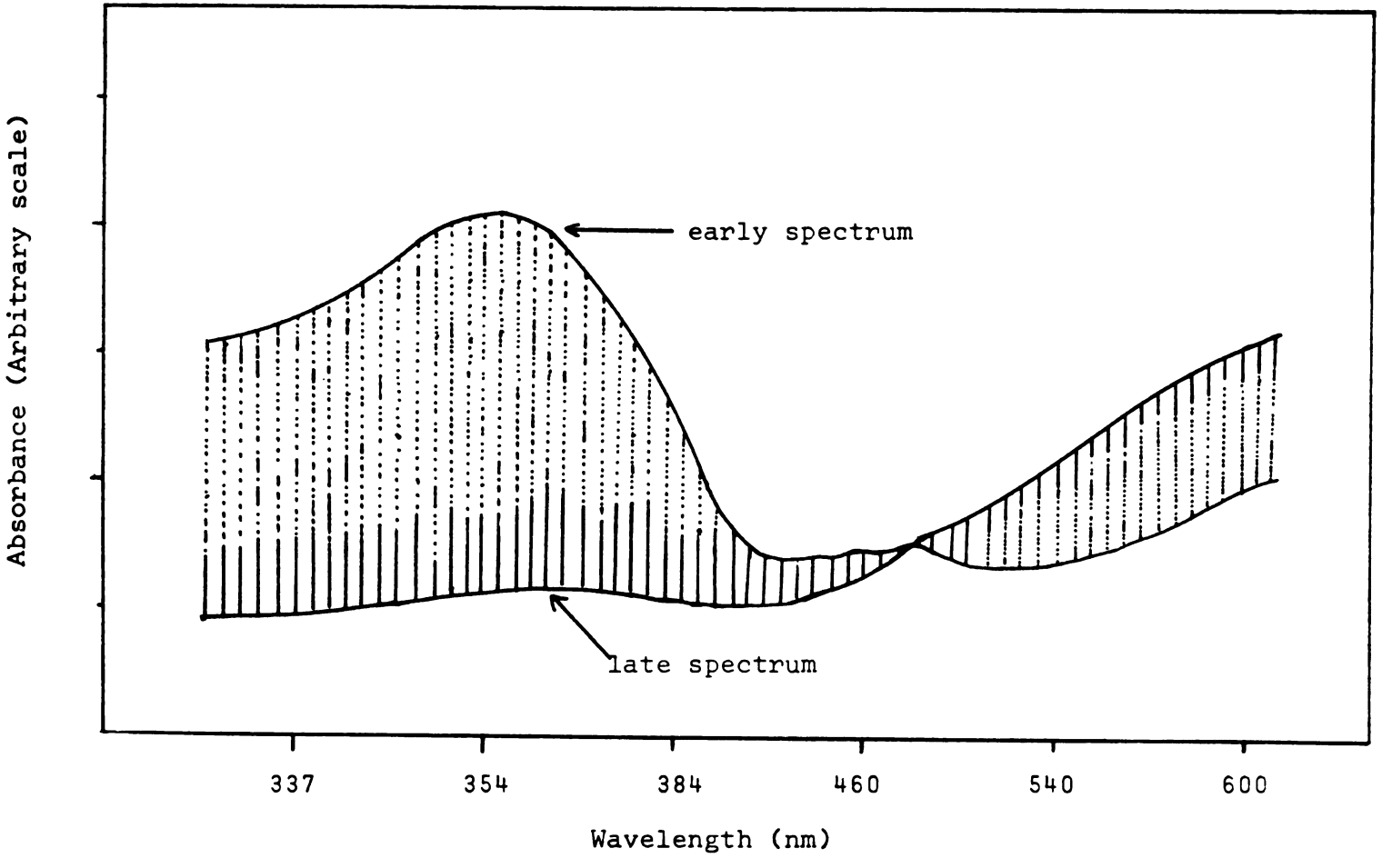

Figure 11. Overall spectral changes for the formation of peroxychromic acid. Solvent background has not been subtracted.

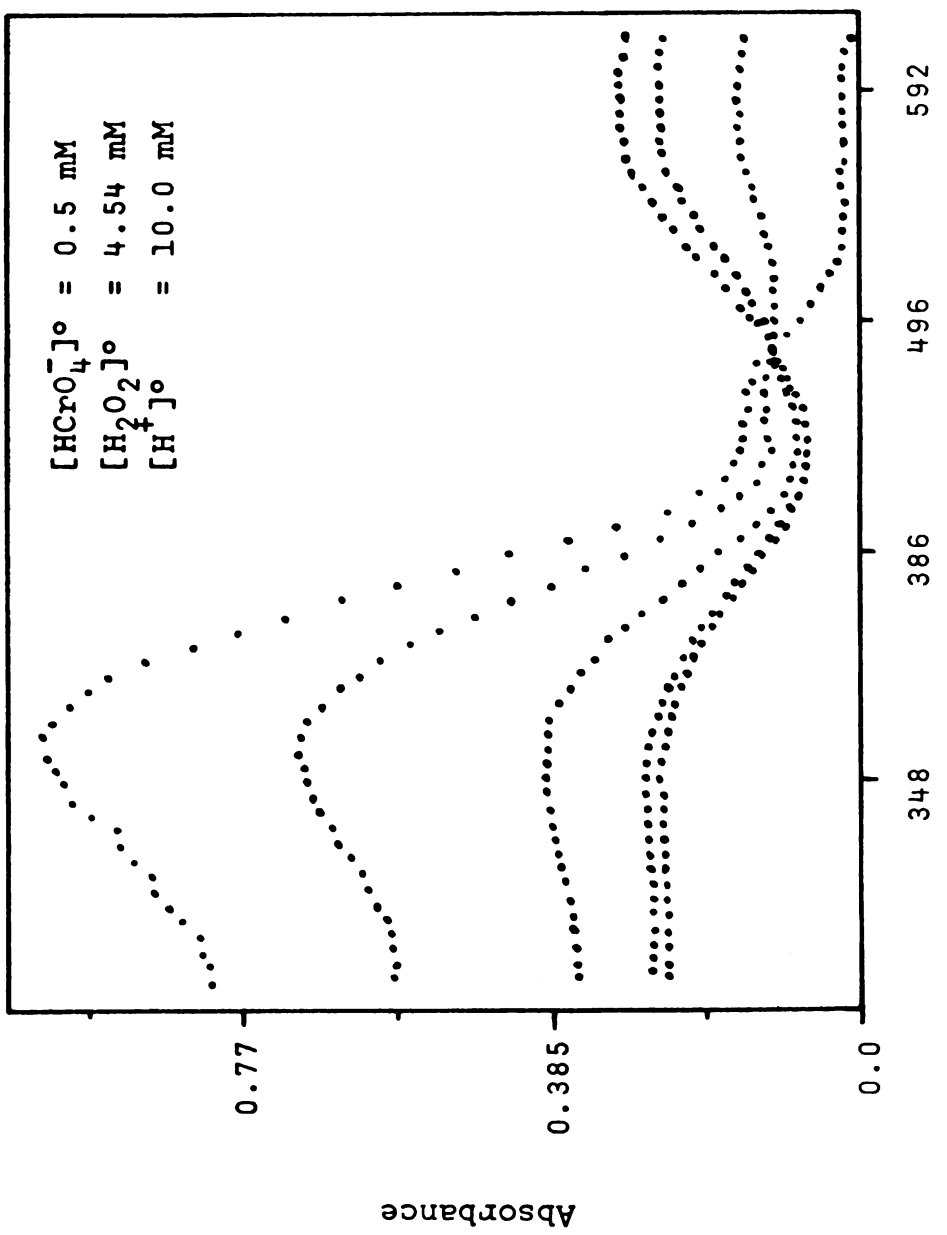

Figure 12. Characteristic spectra isolated from Figure 11. Solvent background has been subtracted.

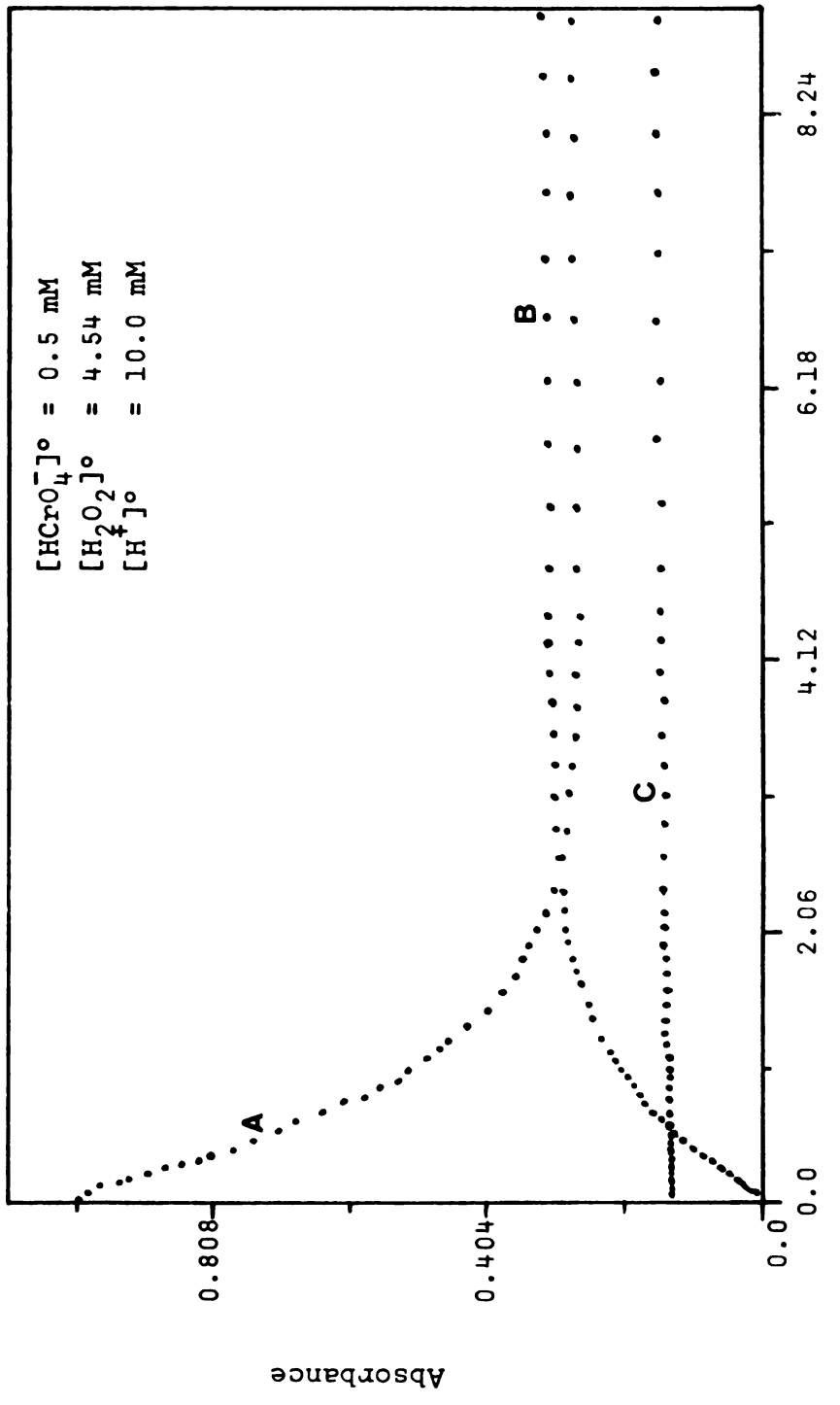

Figure 13. Time cuts for the formation of peroxychromic acid. A - 354 nm, B - 600 nm, C - 480 nm.

correspond to the maximum of the decay, the isosbestic point and the maximum of the growth.

When the initial concentrations of the reactants are changed to the values:

$$[HCrO_4^-]^\circ = 1.0 \text{ mM}$$
$$[H_2O_2]^\circ = 1.817 \text{ mM}$$
$$[H^+]^\circ = 52.0 \text{ mM}$$

the reaction reaches equilibrium, then the decomposition of peroxychromic acid starts and both peaks decay. Time developments from these data for a total of 90 seconds are shown in Figure 14. We can observe the fast growth (or decay), followed by the slow decomposition process. In Figure 15 is shown the first 2.1 seconds of the reaction which displays a small anomaly for the decay. This was also observed by Wilkins et al.[65] who attributed it to small amounts of $Cr_2O_7^{2-}$ in the solutions.

A simple test for an "uncomplicated" reaction in which both reactant and product absorb, can be made by plotting $\ell n|A(t) - A(t_\infty)|$ vs time at different wavelengths. If the reaction is "uncomplicated" these plots must be wavelength independent (see Appendix A). In Figure 16 we see such plots from data corresponding to the experimental conditions given for Figure 11. It is evident that under these conditions the reaction which gives peroxychromic acid is "uncomplicated".

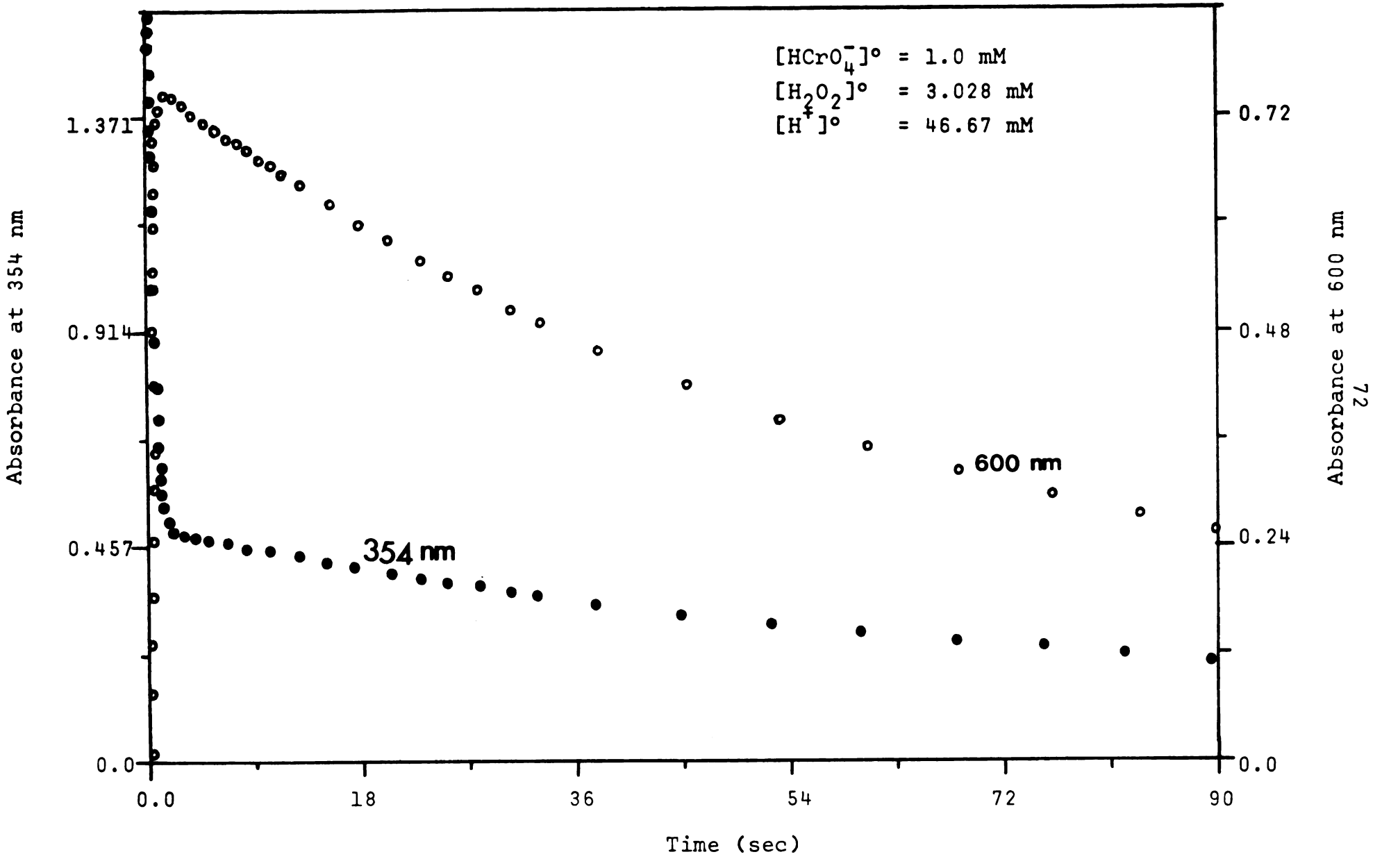

Figure 14. Time cuts for the formation of peroxychromic acid, showing the slow decomposition process.

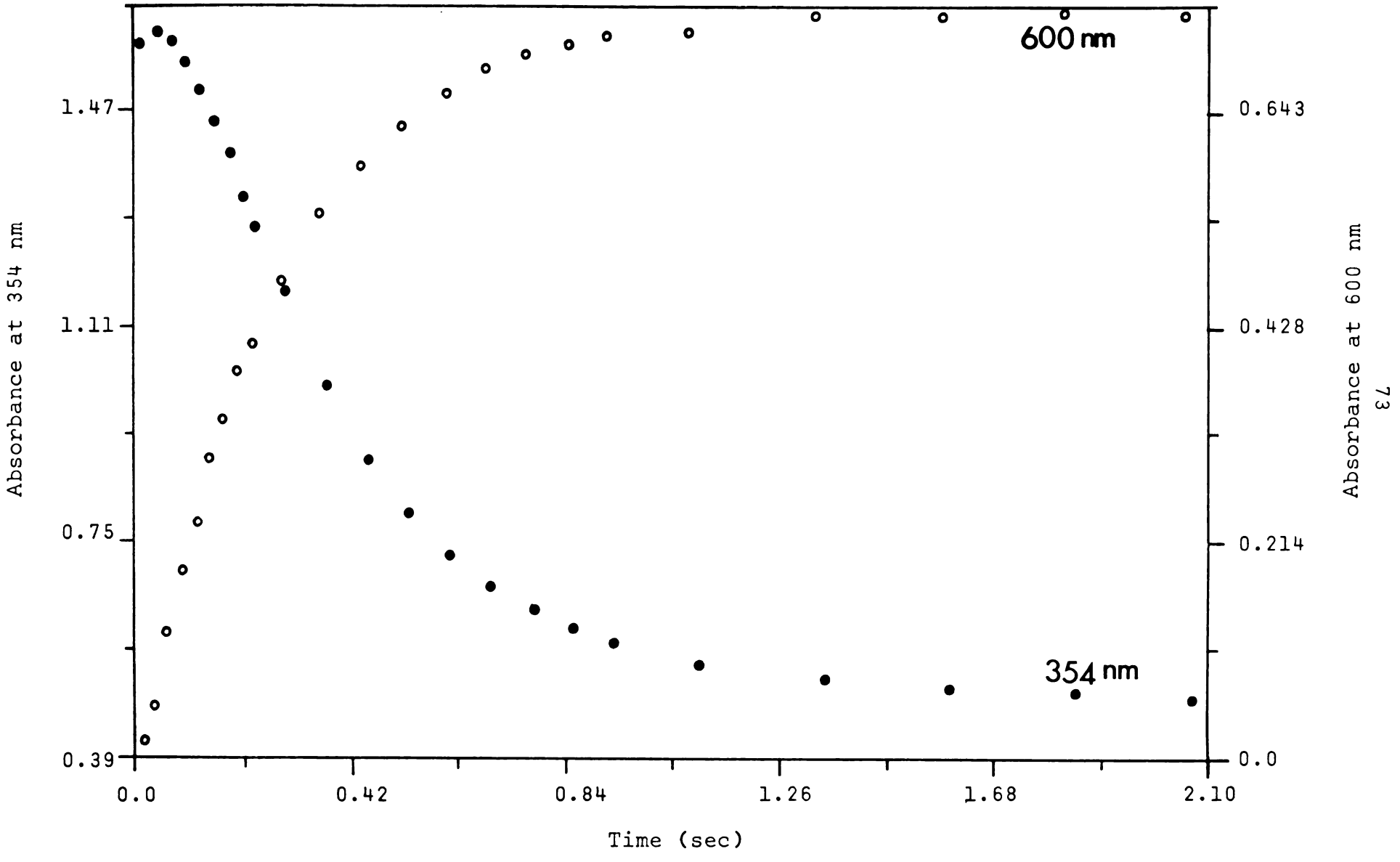

Figure 15. Time developments during the first 2.1 seconds from Figure 14.

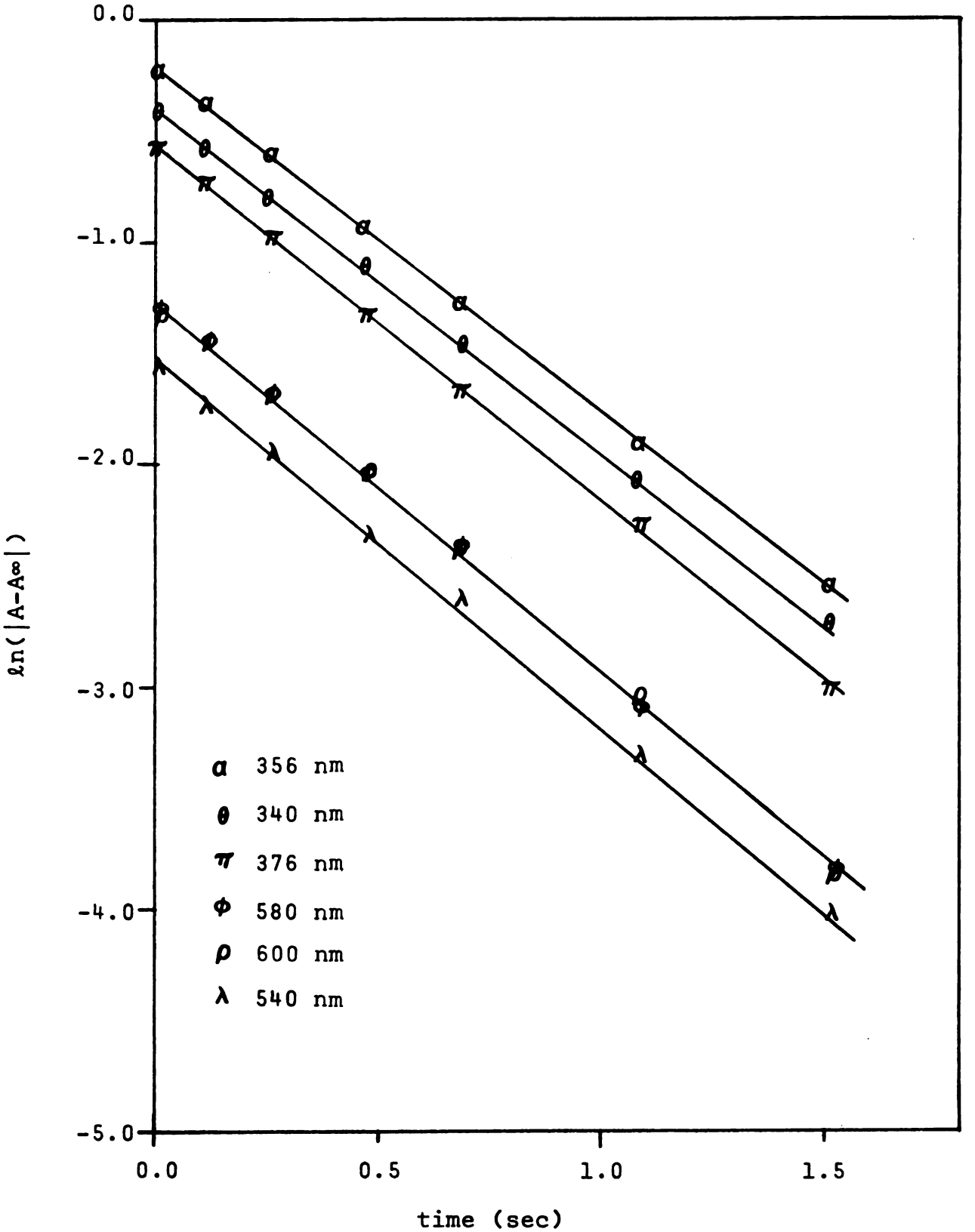

Figure 16. Plots of $\ln(|A-A_\infty|)$ vs time at various wavelengths for the formation of peroxychromic acid. $[HCrO_4^-]^\circ$ = 0.5 mM, $[H_2O_2]^\circ$ = 4.54 mM $[H^+]^\circ$ = 10.0 mM, α,θ,π are decays while φ, ρ, λ are growths.

IV.4.4. Flow Cell Performance, Fixed Wavelength

IV.4.4.1. Dead Time

The dead time of a stopped-flow apparatus is the time required to transfer the solutions from the mixing chamber to the observation point and bring them to a complete stop. The dead time therefore depends upon the mixing efficiency and the stopping time of the apparatus as well as the flow velocity obtained for a particular experiment. If the stopping time has been found to be very small and the mixing is very efficient, then the dead time can be estimated from the equation: $t = V/U$[36], where V = dead volume = volume from the point of mixing to the end of the observation window, and U = average flow velocity in ml/sec.

For our mixing and observation cell we have:

(1) V_1 = volume from the first to the second mixer $\sim$0.015 ml

V_2 = volume of the second mixer $\sim$0.024 ml

V_3 = volume from the second mixer to the end of the short path length window $\sim$0.009 ml.

So: $V = V_1 + V_2 + V_3 \sim 0.048$ ml

Our typical flow velocity was $\sim$18 ml/sec and resulted in a calculated dead time for the short path length equal to $\sim$2.66 msec.

(2) For the long path length we had the additional volume of $\sim$0.073 ml and the corresponding dead time is $\sim$6.7 msec.

The dead time was also computed from data obtained by studying the formation of peroxychromic acid at ∿600 nm, under pseudo-first order conditions (initial concentrations: $[HCrO_4^-]$ = 5 mM; $[H_2O_2]$ = 44.97 mM, $[H^+]$ = 22.5 mM). A semi-logarithmic plot of $(A(t_\infty) - A(t_o)/(A(t_\infty) - A(t))$ vs time has been made with the use of our time zero (see Figure 17). An extrapolation of the resulting straight line to the value of the absorbance that could have been observed if reaction had not occurred at time zero, gives the dead time as the difference between our time zero and the true time zero of the reaction[36]. From Figure 17 we extract 2.5 msec as the dead time of the short path length for this particular experiment. Similar plots gave a dead time for the long path length of ∿5.5 msec.

IV.4.4.2 Mixing Efficiency and Stopping Time

The mixing efficiency is good enough that we have not yet been able to measure its deviation from 100% complete mixing at the time of observation in the short path length cell (perhaps because of the double mixer we are using). We mixed equal amounts of 2×10^{-4} molar paranitrophenolate and 1×10^{-4} molar hydrochloric acid and observed the absorbance through the short path length cell at 400 nm where the p-nitrophenolate absorbs. The resultant absorbance was a flat straight line. This means that the reaction, which is diffusion controlled[30], is over by the time the mixed solutions reach the observation point. Such results could

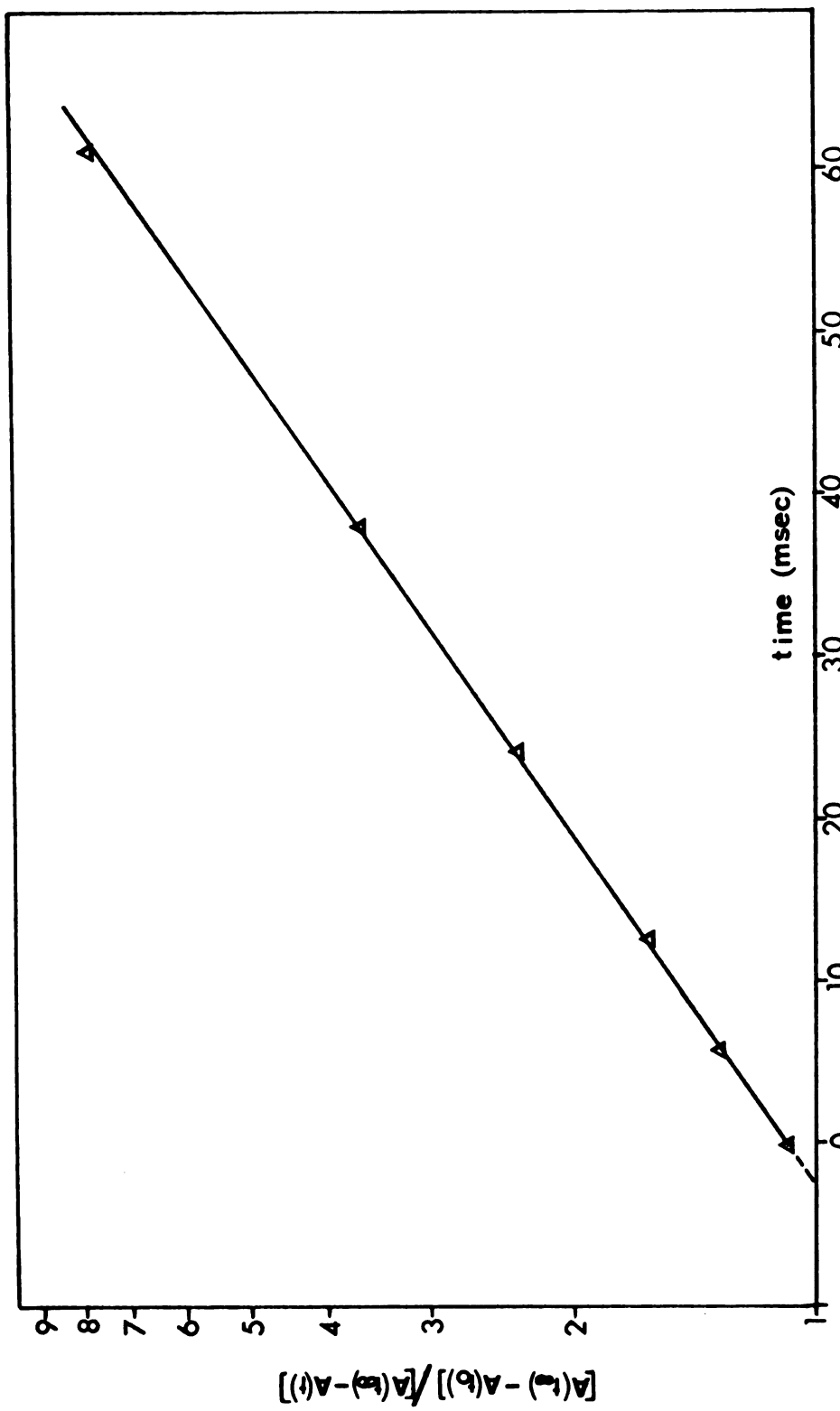

Figure 17. Semilogarithmic plot of $[A(t_\infty) - A(t_o)]/[A(t_\infty) - A(t)]$ vs. time for the dead time computation (Concentrations of the solutions: $[HCrO_4^-]$ = 5 mM, $[H_2O_2]$= 44.97 mM, $[H^+]$ = 22.5 mM).

not have been obtained unless complete mixing had occurred before the solution reached the observation window.

No mixing artifacts were detected by pushing solvent vs solvent and the absorbance during flow stays reasonably constant after the constant flow velocity has been reached. In Figure18 we see the trace from a fixed wavelength reaction of potassium anthracenide with ethanol as photographed from our display scope. In this case the data collection was triggered with the stop flag.

The stopping time was found to be reproducible and less than one millisecond. Recall that stopping time is the time required for the mixed solutions to come to complete rest, after the flow has been stopped. One of the reactions studied was the following:

$$Fe^{3+}\ (0.01M) + SCN^{-}\ (0.01M) \rightarrow FeSCN^{2+}$$

The absorbance change was followed at 455 nm. In Figure 19 we see the first 200 msec of the reaction, while in the inset is a closer look at the time of flow stop (from 10 to 14 msec after the stop flag had triggered the data collection). The rounding, which results from non-abrupt stopping of the solutions when the stopping plunger stops, seems to be very small.

IV.4.4.3. Reliability of the System

Successive pushes with the same solutions were very reproducible and we did not have to discard any of them.

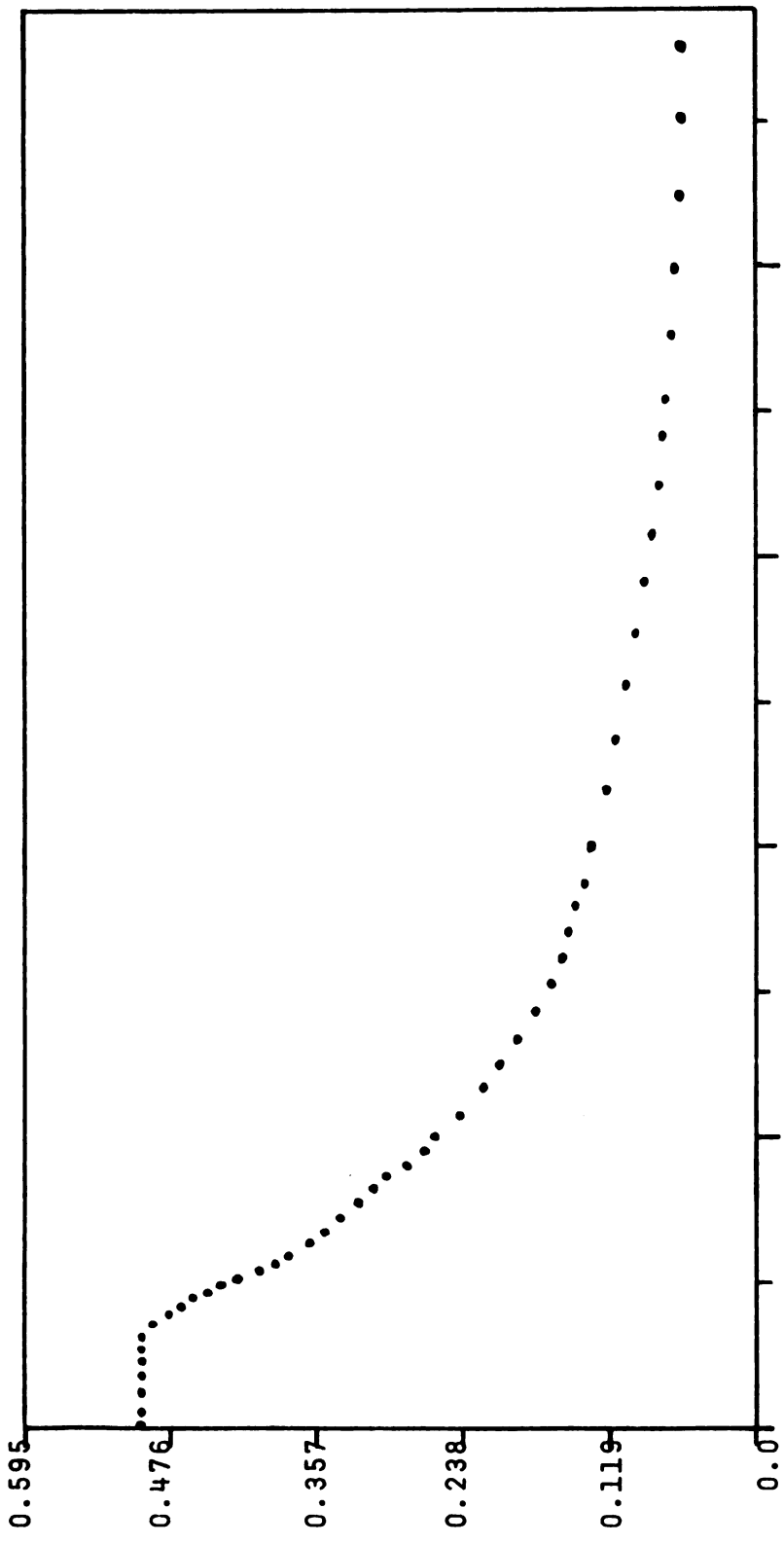

Figure 18. Decay of the 732 nm peak of K^+,An^- after mixing with Ethanol, showing the constancy of absorbance during flow (fixed wavelength technique).

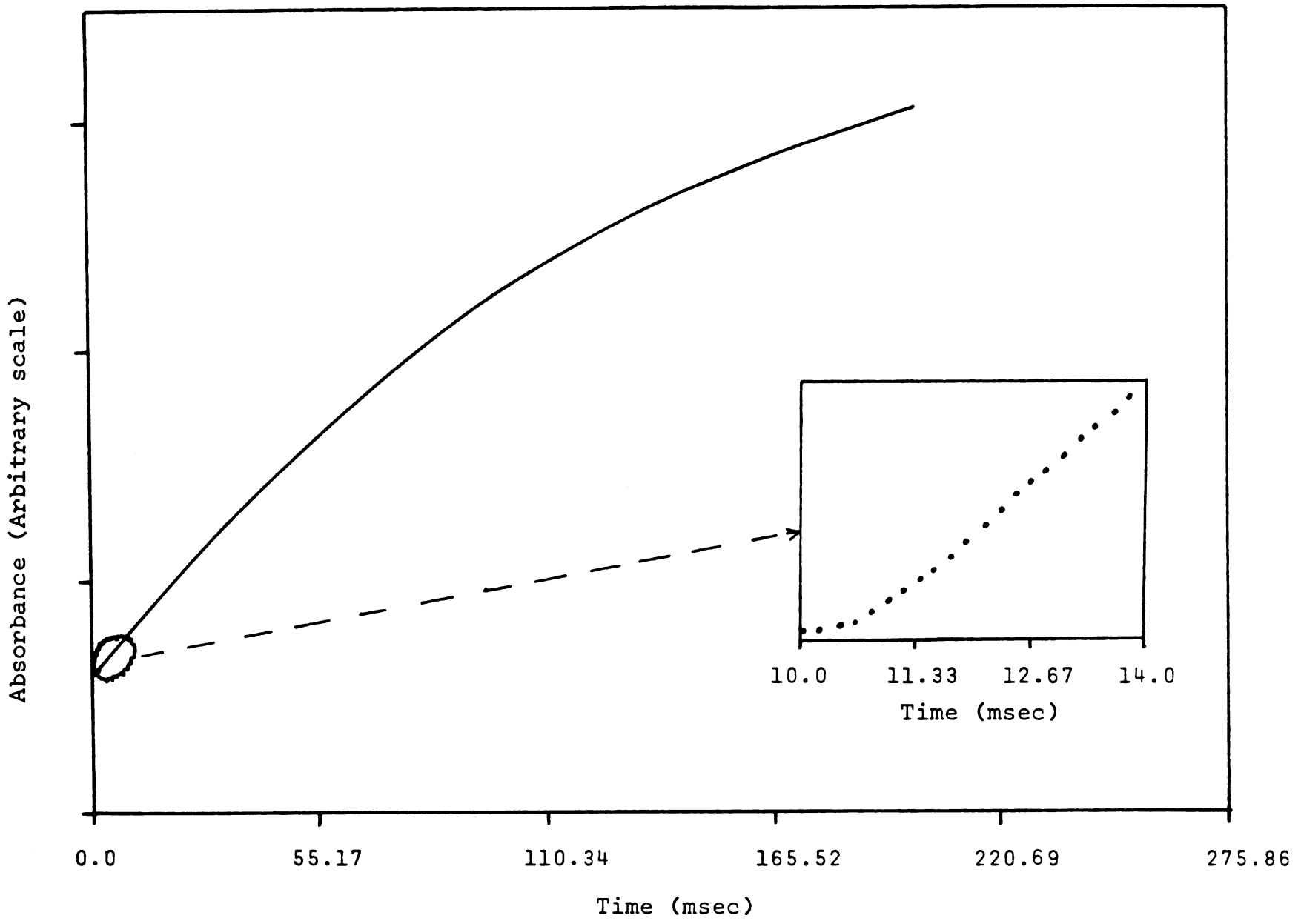

Figure 19. Growth of the $FeSCN^{2+}$ complex at 455 nm for the stopping time estimation.

No leaking problems were detected when the syringe plungers were properly adjusted. The entire system could be pumped to $p \leq 1 \times 10^{-4}$ torr, and stayed evacuated long enough for a complete run with air-sensitive materials to be made (∿12 hours). It has been used at temperatures up to 40° C with good results and no detectable thermal artifacts. Low temperature studies have not yet been made because the flow valves do not perform well at temperatures below ∿10° C (Kontes type valves with Teflon stopcocks). Special adjustable Teflon inserts can be constructed and used in the same valves for low temperature work. One such valve is ready to be tested with a push-pull type insert, similar to the syringe plungers.

One problem which remains is the relatively large hold-up volume; that is, the volume between the pushing syringes and the observation point. This is important, especially for biological applications where the volume of reactants is limited. However, the hold-up volume could be decreased with a slight modification of the present design. Also, some back diffusion from the mixing chamber occurred, depending upon the solution densities and the duration of the observation. Because of this problem we were sometimes forced to use only two pushes per filling of the syringes and to discard the middle one.

IV.4.4.4. Quantitative Measurements

The formation of blue peroxychromic acid was investigated at ∿30° C and the results are summarized in Table I.

Table I. Observed pseudo-first order rate constants and calculated third order rate constants for the reaction: $HCrO_4^- + 2H_2O_2 + H^+ \rightarrow CrO_5 + 3H_2O$.

Wave-length in nm	$[H^+]^\circ$ mM	$[H_2O_2]^\circ$ mM	$[HCrO_4^-]^\circ$ mM	Number of Pushes	k_{ps} (b) sec^{-1}	$kx10^{-4}$ M^{-2} sec^{-1}	Scan Speed	Path Length
340	10.0	4.54	0.5	2	1.605±0.080	3.535±0.176	75	1.85 cm
374	"	"	"	2	1.700±0.073	3.744±0.161	"	"
405	"	"	"	2	1.699±0.057	3.742±0.125	"	"
354	"	"	"	3	1.532±0.160	3.374±0.352	"	"
360	"	"	"	1	1.396	3.075	"	"
376	"	"	"	4	1.470±0.180	3.238±0.396	Fixed W.L.	"
376(a)	20.0	9.085	1.0	3	5.085±0.113	2.798±0.099	"	"
590	10.0	4.54	0.5	2	1.500±0.010	3.304±0.022	75	"
580	"	"	"	4	1.900±0.034	4.185±0.075	Fixed W.L.	"
540	"	"	"	2	1.763±0.130	3.883±0.286	75	"
580	"	"	"	2	1.762±0.113	3.881±0.249	75	"
608	"	"	"	2	1.742±0.129	3.837±0.284	75	"

Table I. Continued.

Wavelength in nm	$[H^+]^\circ$ mM	$[H_2O_2]^\circ$ mM	$[HCrO_4^-]^\circ$ mM	Number of Pushes	k_{ps} (b) sec^{-1}	$kx10^{-4}$ M^{-2} sec^{-1}	Scan Speed	Path Length
580	20.0	9.085	1.0	4	5.708±0.512	3.141±0.282	Fixed W.L.	1.85 cm
580	22.5	44.97	5.0	2	30.485±1.113	3.013±0.110	"	0.2 cm
580	20.0	89.94	10.0	1	42.541	2.365	"	"

(a) Not a very good fit because of the initial deviation from pseudo-first order decay.

(b) Standard deviations for successive pushes were computed from the equation:

$$\sigma = \left[\frac{1}{n-1} \sum_{i=1}^{n} (k_i - \langle k_i \rangle)^2\right]^{1/2}$$

The estimated standard deviations of k_{ps}^i obtained by fitting individual curves is generally much smaller.

(c) All experiments were carried out at an ionic strength of 0.1M adjusted with KNO_3. The H_2O_2 solutions were titrated with a standardized solution of $KMnO_4$.

Wilkins et al [65] have shown that the rate expression for this reaction is

$$\frac{d[CrO_5\ (aq.)]}{dt} = k[H^+][H_2O_2][HCrO_4^-] \qquad 11$$

so that under pseudo-first order conditions

$$\frac{d[CrO_5\ (aq.)]}{dt} = k_{ps}[HCrO_4^-] \qquad 12$$

with

$$k_{ps} = k[H^+][H_2O_2] \qquad 13$$

They also reported the following expression for the rate constant as a function of temperature:

$$k = 10^{7.6\pm0.2}\exp(-4500\pm200/RT)\ M^{-2}\ sec^{-1} \qquad 14$$

At 30° C this equation yields a third order rate constant of $2.26 \times 10^4\ M^{-2}\ sec^{-1}$ with limits of 1.5×10^4 and $3.76 \times 10^4\ M^{-2}\ sec^{-1}$.

In order to compute the rate constants included in Table I, we fitted the observed data either to a growth or a decay pseudo-first order expression. For this we utilized a non-linear least squares computer program (see Section IV.5.3.2). The third order rate constant was then calculated from Equation (13). Representative computer fittings are given in Figures 20 and 21. Also plots of the logarithm of the absorbance vs time are given in

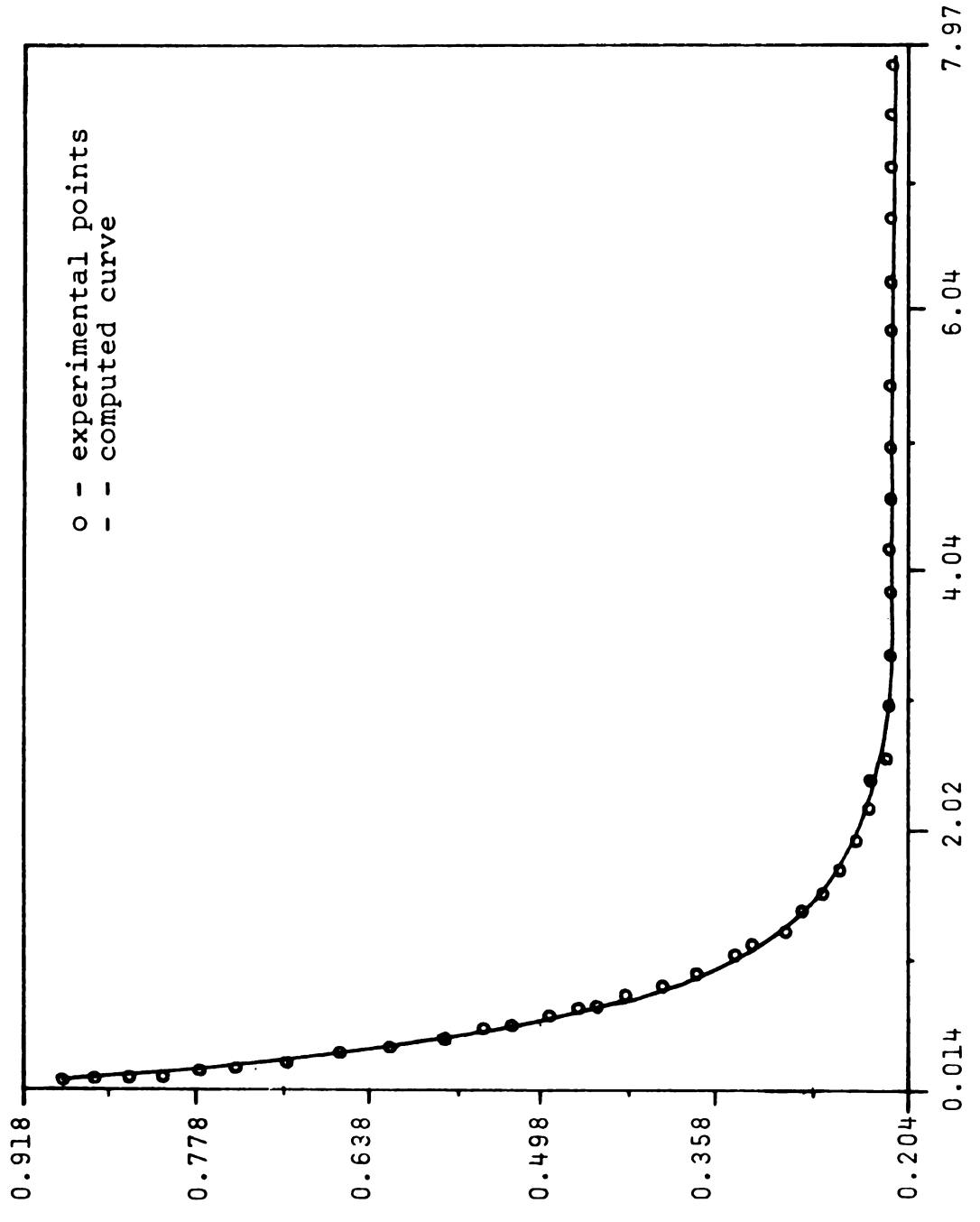

Figure 20. Decay of $HCrO_4^-$ vs time at 354 nm after mixing with H_2O_2. $[H_2O_2]^0 = 4.54$ mM, $[HCrO_4^-]^0 = 0.5$ mM $[H^+]^0 = 10.0$ mM.

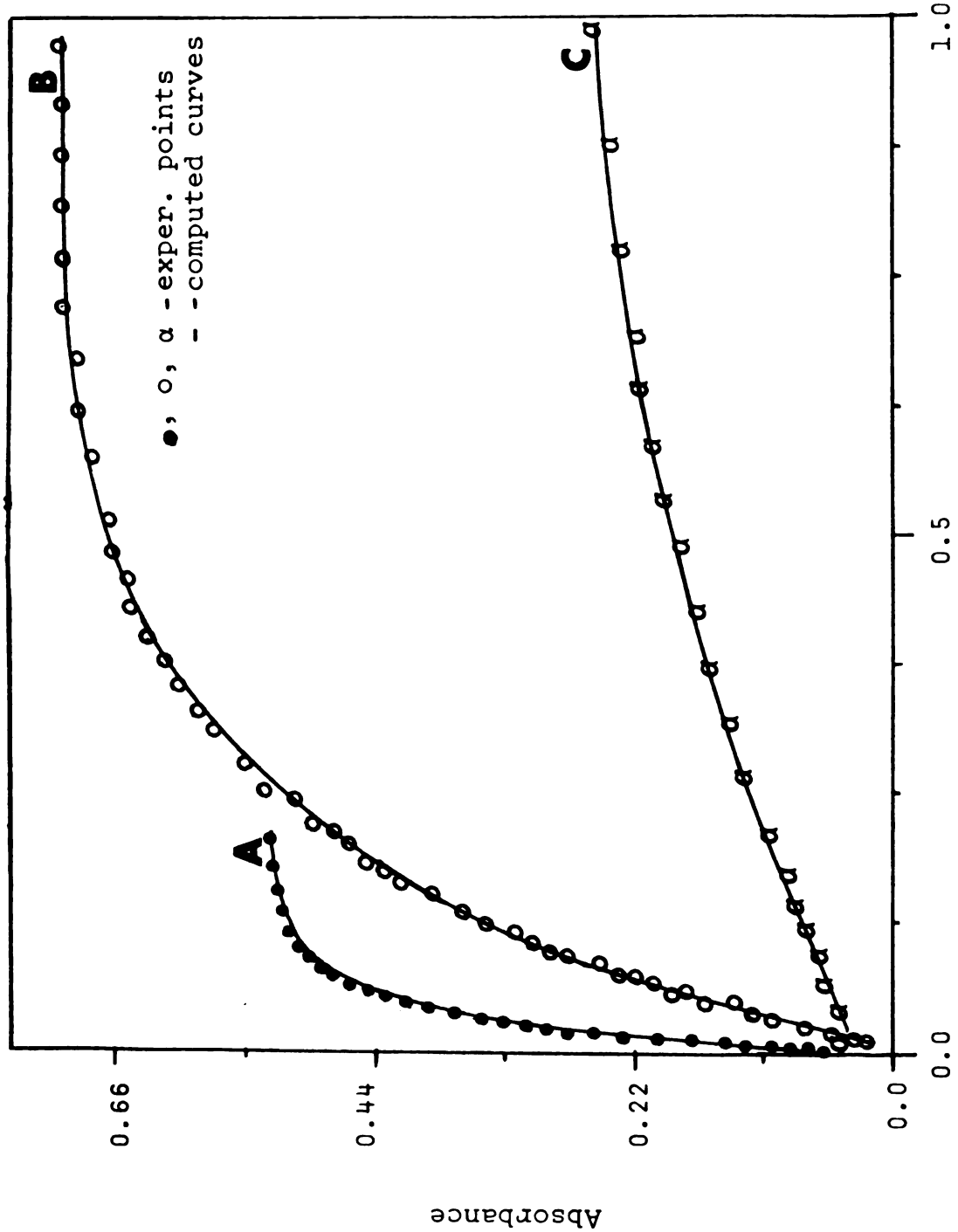

Figure 21. Growth of peroxychromic acid vs time at ∿600 nm during the reaction of $HCrO_4^-$ with H_2O_2. A - Fixed wavelength, $[HCrO_4^-]^\circ$ = 5.0 mM, $[H_2O_2]^\circ$ = 44.97 mM, $[H^+]^\circ$ = 22.5 mM. B - Fixed wavelength, $[HCrO_4^-]^\circ$ = 1.0 mM, $[H_2O_2]^\circ$ = 9.085 mM, $[H^+]^\circ$ = 20.0 mM. C - Scanning at 75 spectra/sec $[HCrO_4^-]^\circ$ = 0.5 mM, $[H_2O_2]^\circ$ = 4.54 mM, $[H^+]^\circ$ = 10.0 mM.

Figure 22.

At concentrations of $HCrO_4^-$ higher than 0.5 mM we observed the same initial deviation from pseudo-first order decay as reported elsewhere[65] (Figure 22, B).

Data from experiments with no pseudo-first order conditions were not analyzed kinetically, since our intention was to demonstrate the ability of our system and not to study extensively the formation of peroxychromic acid.

IV.5. Use of the Computer Interface

IV.5.1. General Characteristics

The only way one can really appreciate the on-line data acquisition, is to run an experiment with and without the computer. In fact, it would have been very difficult if not impossible, to obtain some of the results discussed in Chapter VI without utilizing long time averaging to improve the signal-to-noise ratio. Our averaging scheme is very versatile and the experimenter can choose how much averaging to do by setting the appropriate parameters (see Section V.1.2). However, the choice is important because we do not want to affect the rate constant(s) of the reaction by starting the averaging process too soon. The experimenter must choose the appropriate averaging parameters carefully because unaveraged data are not available after the experiment is over.

We used the reaction of aqueous NaOH with 2,4-dinitrophenyl acetate (DNPA) as an example to test the effect of

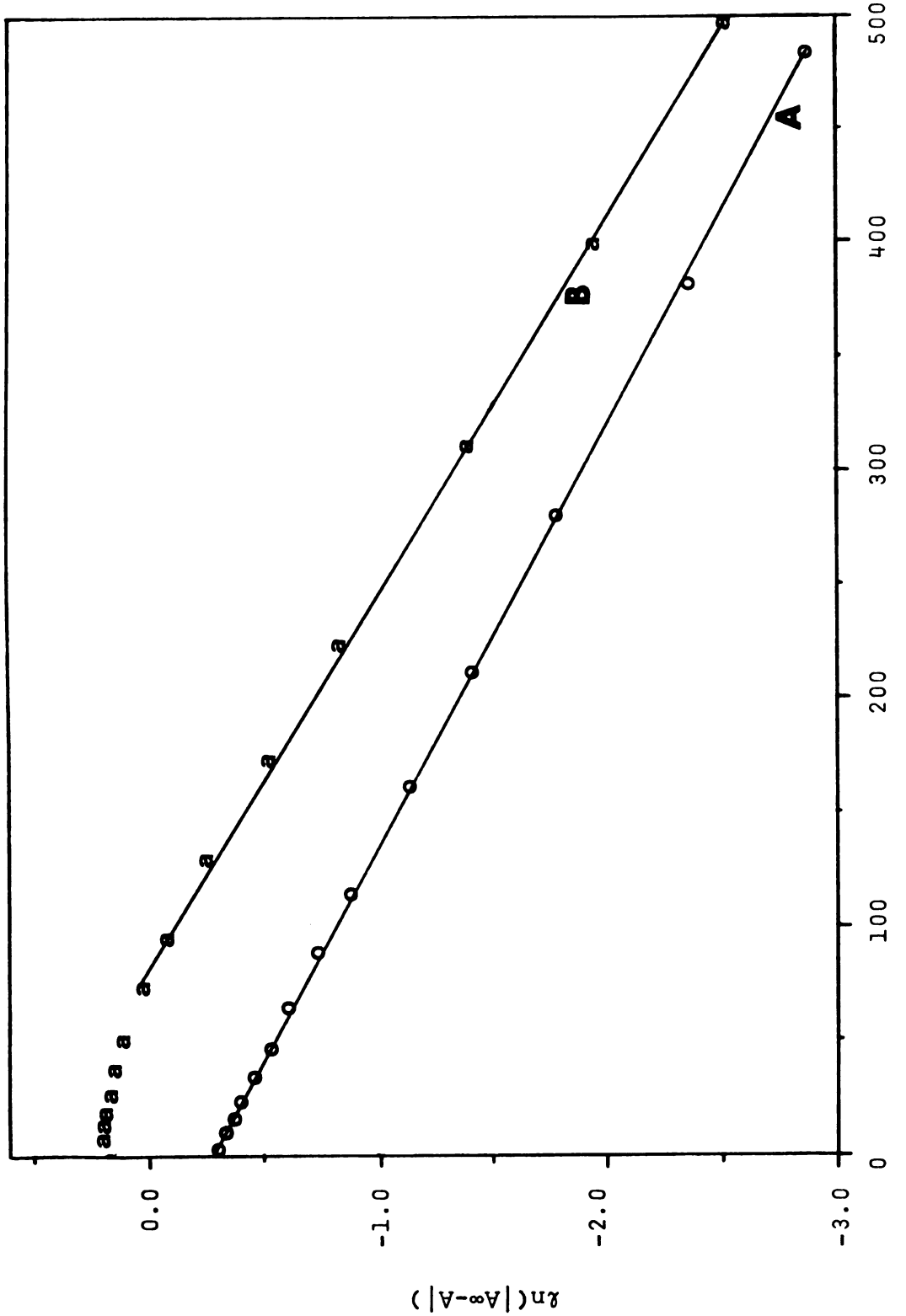

Figure 22. Plots of $\ln(|A_\infty - A|)$ vs time at 580 nm and 376 nm for the reaction of $HCrO_4^-$ and H_2O_2. A - Fixed wavelength growth at 580 nm, the line drawn has the computed slope of 5.3 sec^{-1}. B - fixed wavelength decay at 376 nm, the line drawn has a slope of 6.1 sec^{-1}. In both cases $[H_2O_2]^\circ$ = 9.085 mM, $[H^+]^\circ$ = 20.0 mM, $[HCrO_4^-]^\circ$ = 1.0 mM.

averaging on the reaction rate constant. This was a fixed-wavelength experiment at 400 nm. The parameters used and the computed pseudo-first order rate constants are given in Table II. From these results we conclude that the rate constant, at least for this fixed wavelength case, is remarkably insensitive to the averaging scheme used. However, the results obtained for a grouping factor of four might indicate an effect caused by excessive early averaging.

Generally we collect scanning data (if the reaction rate is slow enough to permit it) in order to follow the absorbance changes at various wavelengths and to check for clean stoichiometry (see Appendix A). However, the scanning mode introduces an inherent source of error; namely, vibrations of the nutating mirror. For this reason, it is probably good practice to study the kinetics at fixed wavelengths after the reaction has been proven to be "uncomplicated". As we can see from the results in Table I, there is no significant effect on the reaction rate when we go from one mode to the other.

IV.5.2. Solution Requirements

Combination of the scanning capability with the very efficient data acquisition system, reduces drastically the volume of reactants required for the complete study of a particular problem. Only about 8 milliliters of each reactant are enough to run a complete test for transient intermediates or to show clean stoichiometry. Also, of

Table II. Effect of the averaging scheme on the rate constant of a pseudo-first order reaction.

Number of Groups (a)	Samples per point for Group #1	Points Per Group	Grouping Factor (b)	k_{ps} (c)(d) sec^{-1}
8	4	10	2	18.452± 0.152
"	"	"	"	18.424± 0.113
"	"	"	"	18.744± 0.140
9	4	5	2	18.905± 0.183
"	"	"	"	19.584± 0.188
"	"	"	"	19.195± 0.159
9	2	15	2	18.612± 0.243
"	"	"	"	18.874± 0.116
"	"	"	"	19.088± 0.138
8	10	5	2	19.691± 0.176
"	"	"	"	19.134± 0.137
"	"	"	"	19.278± 0.142
5	2	15	4	(e) 19.012± 0.146

Table II. Continued.

Number of Groups (a)	Samples per point for Group #1	Points Per Group	Grouping Factor (b)	k_{ps} (c)(d) sec^{-1}
5	2	15	4	(e) 15.698 ± 0.142
"	"	"	"	(e) 15.053 ± 0.094

(a) A group is a set of points each having the same number of samples averaged per point.

(b) Determines the modulus by which the number of samples/point is increased for each successive group, according to the equation: $(SP)_G=(SP)_{G=1}(FC)^{G-1}$; where G=Group Number, FC=Grouping Factor, SP=Samples per point.

(c) Initial concentration of NaOH=0.35M.

(d) From reference 1b, pg. 97 we computed that $k_{ps} \sim 21\ sec^{-1}$, under the same conditions.

(e) The origin of this discrepancy is not known. To tell whether it is caused by the averaging scheme or by some artifact would require more data.

course, the same data can be analyzed to determine the rate constants. With the currently available averaging scheme, we can study fast initial changes followed by slower processes. This can be seen with the data for the non-pseudo-first order peroxychromic acid formation and will be analyzed more fully in Section VI.2. This ability to observe both fast and slow processes in a single push also decreases the required amounts of reactants. Also the fact that we generally find no need to discard any pushes (except when back diffusion becomes a limiting factor), increases confidence in the results obtained with only a few pushes.

In summary, the performance of the entire system shows that an experienced investigator can run a well-planned experiment and make the most efficient use of the available reactants.

IV.5.3. Calculation Schemes Used

IV.5.3.1. Program ABSTIM[66]

As mentioned already, we utilize calibrated neutral density filters in order to convert the output voltage of the logarithmic amplifier to absolute absorbance. This is done on the CDC 6500 computer with the aid of a multiple regression program (MULTREG[7]), which fits the ratio Aabs/Aobs to a polynomial in Aobs of degree up to five, keeping only the most significant terms. Aabs is the absolute absorbance and Aobs is the voltage (proportional to absorbance) as measured with our system. This fitting

is first done for the calibration filters for which absolute absorbance is known (from measurements with a CARY 15 spectrometer). Then the coefficients, which result from it, are used to fit the actual data to the same polynomial and to compute the absorbance for each data point. Note that the Aobs values are collected under the same conditions for both the calibration filters and the actual kinetics data.

After the absolute absorbance has been computed, the time corresponding to each data point is calculated from the experimental parameters with the program TIMER (Appendix B).

Finally, the time correction for actual zero of time is done and the relative variances for each data point are computed from deviations supplied by the experimenter. All the data are then printed, and data from the actual time zero and later are punched onto computer cards ready to be used for kinetics calculations (MULTREG and TIMER are included in the main program ABSTIM).

NOTE: As will be described in Section V.3.4, the raw data are automatically punched by the PDP-8I computer, together with the core-page which contains all the experimental parameters, in a format compatible with ABSTIM.

IV.5.3.2. Program KINFIT

This program was written by Dye and Nicely and has been described elsewhere[67]. The program estimates the

set of parameters which give the optimum correlation between a particular rate law and a set of data. From the information printed out, an experienced user can see how applicable the trial rate law is and decide whether to accept, modify or reject it.

A new version of the program (KINFIT2[18c]) makes it possible to determine the kind and accuracy of information required in order to be able to make decisions regarding a particular mechanism.

V. COMPUTER-ASSISTED DATA ACQUISITION AND PROCESSING

V.1. General Description

As already mentioned, an interactive on-line system was necessary for efficient acquisition and processing of the data generated by the rapid scanning stopped-flow apparatus. Because of the nature of our experiments, the following constraints had to be imposed on the system.

The absorbance data from the stopped-flow apparatus are functions of both time and wavelength and must be collected by the computer on a real-time basis without losing any of their important features. Since the chemical reactions to be studied can have duration ranging from a few msec up to several minutes, the data acquisition system had to be designed so that the information necessary to characterize a particular system, could be obtained without exceeding the available storage capacity of the computer. At the same time the signal-to-noise ratio could be improved by appropriate averaging. After collection, the data had to be stored properly for subsequent retrieval and analysis, and options for rapid computations and display were needed so that decisions could be made during the experiment. Finally, convenient editing and output options had to be available for more complex computations on a large computer.

Also, since our experiments require long preparation and data analysis times, the on-line computer was justified only on a part-time basis. Therefore it was necessary to interface our instrument with an available small computer with the features required for our experiments. A PDP8-I computer in one of Professor Enke's research labs on the fourth floor was ideally suited to our needs. However, this required transmission of data and control signals from (or to) the experiment over a long distance, since the stopped-flow apparatus is located in the basement. Parallel digital transmission of the data was found to be most efficient in our case, because it is fast and does not lead to any signal degradation.

V.1.1. Signal Enhancement in Real Time

V.1.1.1. Maximum Sampling Rate

The data sampling rate is a function of the time scale of the experiment, the computer speed and the rate of analog-to-digital conversion. The frequency at which the signal changes in a kinetics experiment depends not only upon the rate constant(s) of the reaction(s), but also upon the time elapsed since the initiation of the reaction(s). At the beginning of the reaction, the signal changes with time much faster than it does near the end. This means that a variable sampling frequency bandpass would be useful during a particular reaction as well as for different reactions. Traditionally, clock oscillators have been used to generate

a convenient sampling frequency which remains constant during a particular experiment. Programmable clocks which permit the sampling frequency to be changed during an experiment provide another solution. However, decreasing the sampling rate as a reaction proceeds, ignores useful information while permitting the computer to "idle".

One solution to this problem as emphasized by deMaeyer[83] is to sample the signal at the maximum possible rate and subsequently to reduce the necessary storage and improve the signal-to-noise ratio by appropriate digital averaging. Either intermediate storage registers to "hardware-average" the data or software averaging by the on-line computer could be used. The former is required for very fast signal changes (e.g. relaxation experiments), while the latter can be employed for stopped-flow experiments.

It was estimated that ∿40 microseconds would be required by the computer to complete the data acquisition, averaging and storage cycle. Thus, the maximum sampling frequency possible was ∿25 KHz. We also wanted to couple the sampling with the nutating mirror of the monochromator in order to correct for small changes in the rotational velocity of the monochromator. The GT-signal generated by the gear, which is attached to the nutating mirror (see Section IV.3.2), would then be used to trigger the sampling process. However, the frequency of this signal varies with the scan speed and has a maximum value of 10.2 KHz (75 revolutions/sec x 136 gear teeth/rev x 1 pulse/gear tooth = 10,200 pulses/sec).

Multiplication of the frequency of this signal was suggested by Prof. C. G. Enke and this was accomplished as described in section V.2.3. These considerations led to a nominal sampling rate of 20.4 KHz (=2 x 10.2), which has proven to give very good results in both wavelength and time resolution.

V.1.1.2. Averaging Scheme

In typical rate studies, the signal varies rapidly at first and then changes progressively more slowly as the reaction approaches completion (or equilibrium). It is therefore advantageous to use a wide bandpass at the beginning of a reaction, but to decrease it as time increases. Most instruments are designed to operate with a fixed bandpass; that is, filters are selected prior to the experiment and then not changed during the experiment. Even in these cases, one must be careful in selection of the filters, since analog filtering can distort the signal shape. In contrast to this, digital filtering (appropriate averaging or smoothing) can provide a bandpass which varies with time as needed.

As an example, consider a fixed wavelength experiment in which the absorbance varies with time. If the half-life of a fast reaction is 5 msec, then one point every 200 μsec would yield 25 points during the first half-life. Since the data acquisition time is ∿60 μsec (Section V.1.1.1), each 200 μsec "point" would actually be the average of four samples. If a slow process occurs at the same time, we

might want to continue to follow the absorbance for a total of, say, 10 sec. Continuation of the 200 μsec/point rate would give a total of 50,000 points - truly a formidable storage problem! However, after collecting the first 25 points it is a simple matter to obtain 25 additional points during the next 10 msec, each of which is an average of 8 samples at the 50 μsec rate. The next set of 25 would require 20 msec, then 40, 80, etc. Ultimately we could collect 11 sets of 25 points each. This would require only 275 storage locations. The first set of 25 points would extend out to 5 msec and each point would be the average of 4 samples. The last set of 25 points would extend out to 10.24 sec and each point would be the average of 4096 samples. If the noise were random, the signal-to-noise enhancement of the last set over the first would be 32 to 1 [$=(4096)^{1/2}/(4)^{1/2}$].

With the ability to scan wavelength during reactions, another dimension is added to the averaging problem. We have programmed the computer to provide a number of possible averaging schemes. In all cases, data collection at ~50 μsec/sample continues. But we are able to select the number of points per spectrum by averaging an appropriate number of adjacent samples, with the number chosen to avoid serious loss of spectral resolution. After this selection has been made, averaging in time according to the scheme outlined above is also done by averaging appropriate numbers of adjacent spectra together. Our scanning system produces

a forward and a back-scan on each revolution (one is the mirror image of the other). According to our data acquisition routines, averaging of adjacent spectra does not take place in the first group of collected spectra (corresponding to the first set of 25 points in the fixed wavelength example). In this way we can collect both the forward and back-scans and thus obtain a better time resolution in the early stages of the reaction. In the rest of the groups, back-scans cannot be collected, because we need that time for the spectral averaging process. If back-scans are collected in the first group they are reversed automatically in order to be used for kinetics computations.

In order to accomplish the above averaging scheme, the experimenter has to set a number of parameters which are used by the computer as counters to control the data acquisition.

V.1.1.2.1. Data Acquisition Parameters

Samples/point (SP): The number of adjacent samples which are averaged together into a single data point.

(a) Fixed-wavelength data.

A group is a set of points each having the same number of samples averaged per point.

Points/Group (PG): The number of points in the group; all groups have the same number of points.

Number of Groups (NG): The number of groups the experimenter wants to collect in order to follow the reaction up to the required time.

Grouping Factor (FC): Determines the modulus by which the number of samples/point is increased for each successive group, according to the equation: $(SP)_G=(SP)_{G=1}(FC)^{G-1}$, where G=Group number.

(b) Scanning Data.

A group is a set of spectra each being the average of N_G consecutive spectra (N_G=1 for the first group).

Spectra per group (SG): The number of spectra in each group. Determines the time length of each group, as governed by the scan speed.

Grouping factor (FC): The modulus by which the number of consecutive spectra averaged together to form one spectrum is increased for successive groups; according to the equation: $N_G=(FC)^{G-1}$ where G=Group number.

The value for each parameter depends upon the particular experiment to be performed. Their effect upon the rate constant is discussed in Section IV.5.1.

V.1.2. Control and Timing Signals

The signals generated by the scanning monochromator and the stopped-flow apparatus are used to initiate data acquisition and to synchronize the computer with the experiment. The pulses produced by the stopping plunger (Section IV.2.3.3) are used to trigger data acquisition and also as timing marks for time computations.

The BS and GT-signals of the scanning monochromator (Section IV.3.2) gave very reproducible wavelength markers

whenever scanning data were collected.

V.2. Hardware

The interfacing of our stopped-flow apparatus with a remote computer, is very complex and possesses some characteristic features. Because we scan the spectrum of absorbing species during the reaction, we had to overcome problems of timing and control which are not present in a fixed wavelength experiment. Also the location of the computer in regard to the experiment introduced the problem of transmitting and receiving information and control signals over a large distance. It was necessary to construct and assemble a large number of circuit boards, since data and control signals were handled at two locations. Only the most characteristic parts of the interface will be presented here. Details of construction are described in a "hardware manual" which is available to users of our system[72].

V.2.1. Digital Transmission Lines

The long distance between computer and experiment, combined with the noisy environmental conditions make impractical the analog transmission of data and control signals. Noise pick-up and signal degradation would result from analog transmission and decrease the quality of the experimental data. The instrumentation available at the time of construction made impossible serial digital transmission because it was too slow for our experiments ($\leq$20,000 bits per second[54b]). Parallel digital transmission

through twisted-pair cables appeared an attractive alternative. Recall that in parallel transmission each of the binary bits that make up a word is transmitted simultaneously, while serial transmission involves the output of each bit of a word, one bit at a time. In order to decrease the cost of the transmission system a "party line" structure was employed in which two or more line drivers and receivers shared a common transmission line. Line drivers and receivers from Texas Instruments Inc. were utilized because of their performance characteristics (types SN75107 and SN75109)[70]. They permit high speed transmission (<10 MHz), high sensitivity (<50 mV) at the receiver input, high common-mode rejection at the receiver input, strobe capability for the receiver and inhibit capability for the driver. The driver is composed of a stage that converts input logic levels to voltage levels that control a current switch. The current switch unbalances the voltage on the transmission lines, resulting in a voltage difference at the receiver input. The input stage of the receiver is a differential-input stage that exhibits high rejection of common-mode input signals. An intermediate stage converts the polarity of the line signal to the appropriate logic levels at the receiver output. Since the driver output is not affected by common-mode signals induced on the line, error-free transmission and recovery of data results. The driver inhibit logic is computer controlled and permits data to be transmitted to, or received from the computer via the

same lines. All drivers and receivers, required at each end of the transmission line (computer and experiment), were mounted on a single (9" x 6") circuit board which was connected to the interface with 3M type flat connection cables. The transmission line is a Belden 8769 cable (obtained from Newark Electronics), which contains 19 twisted pairs of #22 conductors. Each pair of conductors is shielded with stranded wire and foil wrapping. All of the stranded shields were connected together at one end and grounded. This prevents ground loops in the transmission cable. Each conductor is terminated at both ends with 24 ohm resistors (the characteristic impedance of each line).

V.2.2. Flag Circuits

As previously mentioned, it was necessary to utilize synchronization pulses (from the stopped-flow apparatus and the scanning monochromator) to clock the data into the computer such that the correct wavelength and time could be associated with each data point. Also, in order to output the data from the computer onto various devices (scope, plotter, cardpunch), the status of the device (ready or not ready) had to be checked by the computer before outputing any data. All of the input/output (I/O) control was achieved by a system of device flags and device codes. Each device was assigned a code number and associated with a flag circuit. In this way, the computer could recognize the device and determine its status by checking the appropriate flag.

At the appropriate time, each device must generate a "ready" pulse which triggers the corresponding flag and notifies the computer of its readiness to send or receive data, or simply to set a timing mark (Flow and BS Flags). These pulses are produced by the interruption or reflection of a light beam (see Sections IV.2.3.3, and IV.3.2) or simply by changing the state of a logic gate. The main component of each flag circuit is a J-K Master-Slave Flip-Flop (type SN7473 or SN7476), which is set by the trigger pulse of the corresponding device and cleared by the computer after the device has been serviced as well as at the initiation of the experiment[71,72].

V.2.3. Use of the Phase-locked-loop Circuit

For synchronization and automatic wavelength correction we used the GT-signal (IV.3.2) to control the data acquisition. Since the frequency of this signal is lower than the desired sampling rate (V.1.1.1) (and varies with the scan speed of the monochromator), it was necessary to construct a circuit for frequency multiplication of the fundamental GT-signal. At the suggestion of Prof. C. G. Enke, a phase-locked-loop (PLL) and divide by N circuit was constructed. With this system we maintain all sampling triggers synchronous to the experiment by integer multiplication of the GT-signal to achieve the 20.4 KHz sampling frequency. Figure 23 shows the basic principle of the circuit. The PLL (NE 565A from Signetics[73]) corrects

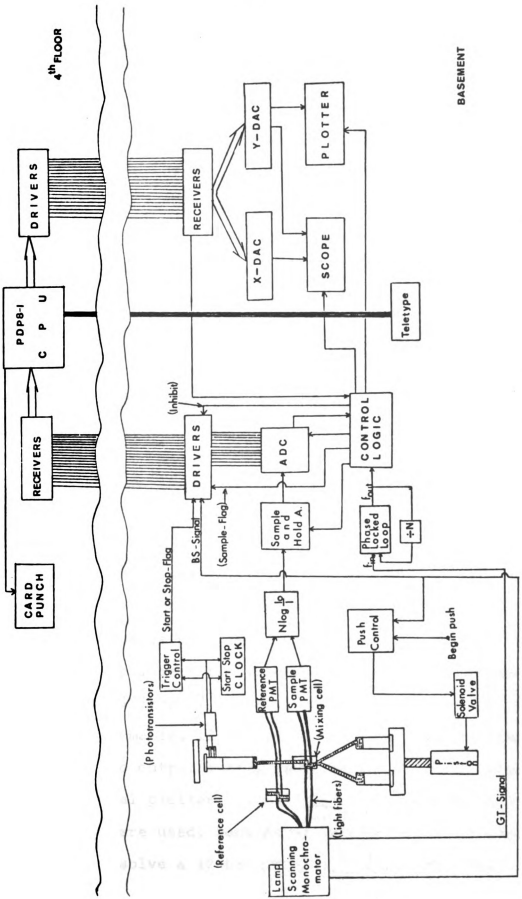

Figure 23. Block diagram of the computer interfaced scanning stopped-flow system.

its output frequency such that the two input signals are in phase and of equal frequency. Thus by changing the divide by N number (Motorola MC 4018P 7110 programmable counters), the output frequency can be made the desired multiple of the input frequency. It was necessary to "clean" the GT-signal of high frequency noise, before feeding it to the PLL circuit. For this purpose, a voltage comparator (LM311 by National Semiconductors) was used.

The above circuit was found to perform very well when properly adjusted[72] and "tracked" changes in gear speed effectively. Whenever fixed-wavelength experiments were performed, the output of a Wavetek Model 116 Signal Generator was utilized at 20.4 KHz to control the data acquisition.

V.2.4. Overall System

A block diagram of the overall system is shown in Figure 23.

Commercially available integrated circuits (IC's) were utilized to construct the control logic centers[72]. In order to sample and digitize the voltage output of the logarthmic amplifier, two interchangeable types of sample-and-hold amplifiers[74] were used in conjunction with a high speed, programmable, 12-bit Analog-to-Digital-Converter (ADC)[75]. To output analog data for the display scope or the incremental plotter, 10-bit Digital-to-Analog-Converters (DAC's)[76] were used, because of the inability of these devices to resolve a 12-bit from a 10-bit word. However,

12-bit words were punched onto computer cards for rigorous data analysis.

In order to control the devices located near the experiment, a number of control signals had to be transmitted from the computer to the devices. To do this on a one-for-one basis would have required more transmission lines than we had available. To overcome this problem, a complex Coding-Decoding system was designed and constructed from commercially available IC's. From our experience with the design and testing problems involved, we would simply install more transmission lines if we had to do it over. All circuits were constructed on standard circuit boards[77], which were then mounted in a Computer Interface Analog Digital Designer (ADD)[78].

The computer is remotely controlled by a Teletype unit and has an operating system resident on a dual magnetic tape unit (from DEC) for software and data storage. Also, the following peripherals were available for data output: An IBM 526 card punch equipped with a Varian C-1001 coupler which was modified appropriately[79] and an RCA 301 line printer[80]. Both of these peripherals are located near the computer. A Model 611 11-inch storage Display Scope[81] and a Model 6550 Omnigraphic high speed point plotter[82] are located near the stopped-flow apparatus.

V.3. Software

In order to perform the desired data acquisition, processing and output, a long and sophisticated set of

computer programs was required. Since, at the time, only 2 fields of core memory (8K or 8192 12-bit words) were available and we wanted to save field 1 (4K) for data storage, it became necessary to develop our software such that it could be loaded in the available core memory. To overcome this problem, we divided our software into two main parts:

(a) Core resident routines, which are in core memory during the entire experiment and data treatment period (these are various utility subroutines).

(b) Non-core resident routines (called Modes or Segments), which are called into core memory (from the magnetic tape) as needed and only one at a time.

A core resident routine supervises the loading of the appropriate Mode according to the experimenter's command (as controlled via the Teletype and the display scope). This has proven to be a very efficient way to utilize 4K of core memory for ∿18K of software.

V.3.1. Data Acquisition

The flow-chart for the data acquisition mode is shown in Figure 24. Only the two main options have been included in this flow chart; namely, scanning and fixed-wavelength data. In addition, data for absorbance calibration with neutral density filters, wavelength calibration with absorbing glasses, solvent background and background at infinite time (t_∞) can be easily collected. The experimenter simply sets the data collection parameters (V.1.1.2.1),

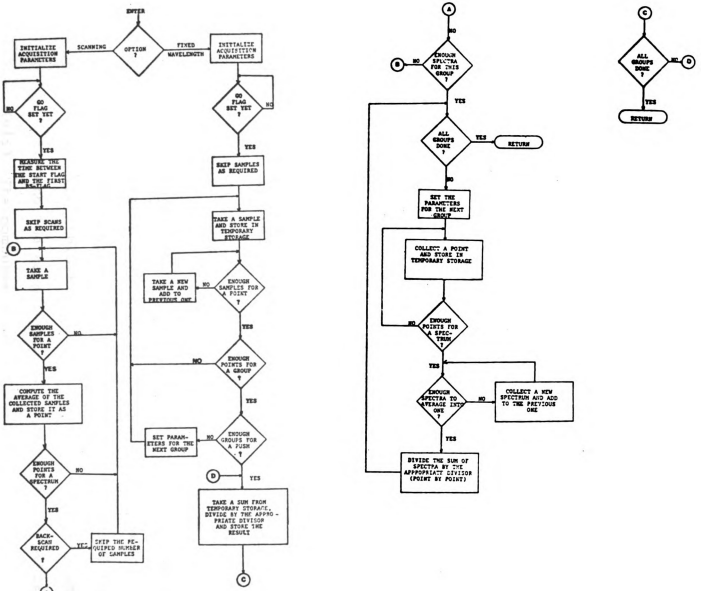

Figure 24. Flow-chart for the data acquisition routines.

or just changes any of them as required, selects the appropriate option and initiates the stopped-flow experiment (Push). The digital sample collection then takes place according to the following sequence of events:

(i) Start Flag occurs - push has begun, real time clock is started.

(ii) Data collection begins on the falling edge of the next BS-pulse, real time clock is read and stored with the experimental parameters.

(iii) The next sample trigger (from PLL) activates the HOLD mode of the sample-and-hold amplifier (SHA).

(iv) The same sample trigger is delayed $\sim$5 μsec (with a monostable multivibrator) in order to allow the SHA to "settle", and then triggers the ADC.

(v) 100 nsec before the 12 parallel digital bits are ready, the ADC generates an End of Conversion pulse. This pulse, after suitable delay through a monostable multivibrator, opens the data latch (temporary 12-bit word register) and sends a SAMPLE READY signal to the sample flag.

(vi) The computer recognizes the SAMPLE READY FLAG, the inhibit on the data line drivers is removed and the sample is clocked into the accumulator.

(vii) The computer clears the sample flag and proceeds to average and store the data.

The next sample trigger begins the process again.

Since the computer keeps track of BS-pulses, the samples are averaged and stored in the correct sequence with respect to both time and wavelength.

When the fixed-wavelength option is selected the sampling and digitization process starts with the STOP Flag and goes through steps (ii)-(vii).

The data as collected during a push are stored in field 1 (∿4K of core memory), and after the collection is over they can be stored permanently on magnetic tape. A file name is associated with each push when stored on tape. This file name consists of a date code, a run code (characterizes a set of pushes), a push code and the operator's initials to make future reference easy.

After the raw data have been stored on tape, the experimenter can ask for quick computations to be performed and examine the data before continuing the experiment. The desired data during flow can be averaged to give the absorbance at t_o, which then can be subtracted from the raw data. Solvent background and absorbance at t_∞ (if collected) can also be subtracted. After these computations, the desired wavelength or time displays can be examined, which may indicate that modifications in the experiment are required. Future options, such as logarithmic computations, can be introduced, if more core memory is available.

V.3.2. Description of Output Options

Displays of spectral growth and decay with arbitrary scale expansion and selection of particular spectral scans individually or collectively can be obtained on the storage scope. Time developments at any particular wavelength covered in the experiment, with arbitrary starting and ending times as well as scale expansions can also be examined on the scope. In this way, any desired time period, at any point from the beginning of the reaction and at any wavelength can be analyzed as soon as the push is over. Hardware and software are also available to plot on the incremental plotter whatever is displayed on the scope.

Finally, the time displays from the scope can be punched onto computer cards for more detailed data analysis. The decimal number corresponding to each data point on the time-cut is punched. The time corresponding to each point is computed on the CDC 6500 computer from the experimental parameters, which are also punched for each data file (IV.5.3.1). An option for punching entire spectra can be easily added, such that spectral shapes could be analyzed on a large computer.

The performance of the interface has been tested together with the stopped-flow apparatus and the results are discussed in Section IV.4.

VI. RESULTS

VI.1. Dissociation of Na^- in Ethylenediamine (EDA)

Based upon the equilibrium constant and the reverse rate constant from pulse radiolysis studies[26], the forward rate of the reaction

$$Na^- \rightleftarrows Na^+ + 2e^-_{solv} \qquad 15$$

in EDA should be slow enough to permit its study by stopped-flow methods. We hoped to be able to examine the disappearance of the optical band of Na^- and the appearance of that of e^-_{solv} by mixing a solution of Na in EDA with a solution of ammonia in EDA. Small amounts of ammonia should shift the equilibrium to the right. Another method of shifting the equilibrium to the right is the addition of small concentrations of "2,2,2 Crypt"[16]. This would have the advantage that it would not alter the solvent properties as drastically as would the addition of large amounts of ammonia.

VI.1.1. Equilibrium Studies of the Effect of Ammonia Addition

Solutions of Na in EDA were prepared in a cell which consisted of a 2.0 mm quartz optical cell and two quartz side vessels. Sodium was distilled into one side vessel and EDA into the other. A solution of the appropriate concentration was then made by dissolving the required amount of metal in EDA. Various amounts of ammonia were added to

this metal solution and its effect upon equilibrium (15) was studied by recording the optical spectra at room temperature with a Beckman DK-2 spectrophotometer.

The following results were obtained: The solution without any ammonia had only one absorption band at ∿660 nm corresponding to Na^-[18]. When about 1.7 weight % ammonia was added, a second band started growing in at ∿1300 nm corresponding to e^-_{solv}[18]. As the concentration of ammonia was increased (up to ∿9.3 weight %) the absorbance of the e^-_{solv} band continued to increase. Equilibrium constants for reaction (15) were computed from the equation:

$$K = \frac{[Na^+]x[e^-_{solv}]^2}{[Na^-]} \times \frac{\gamma_{Na^+} x\ \gamma^2_{e^-_{solv}}}{\gamma_{Na^-}} \qquad 16$$

Conservation of charge gives:

$$[Na^+] = [Na^-] + [e^-_{solv}]$$

Thus equation (16) becomes (for $\gamma_{Na^-} = \gamma_{Na^+} = \gamma_{e^-_{solv}} = 1.0$):

$$K = \frac{\{[Na^-]+[e^-_{solv}]\}x[e^-_{solv}]^2}{[Na^-]} \qquad 17$$

The concentrations of Na^- and e^-_{solv} were calculated from the absorbance measurements at ∿660 nm and ∿1300 nm respectively. The corresponding molar absorptivities have been reported elsewhere[25]. The following values were obtained for the

equilibrium constant at three ammonia concentrations:

$K = 1 \times 10^{-7}\ M^2$ with ∿9.3 weight % NH_3

$K = 6 \times 10^{-8}\ M^2$ " ∿8.7 " " "

$K = 1 \times 10^{-9}\ M^2$ " ∿1.7 " " "

By extrapolating these results to 0% NH_3 we obtained K in EDA $\sim 10^{-10}\ M^2$ (from pulse radiolysis studies $K \leq 10^{-10}\ M^2$). From the above results we see that, ammonia shifts equilibrium (15) to the right as expected.

VI.1.2. Kinetics Studies

One experiment was done by mixing a solution of Na in EDA ($[Na^-] \sim 1 \times 10^{-4}$ M), with a solution of ammonia in EDA (8.9 weight % NH_3), in the stopped-flow system at room temperature. Solution stability was not good and the high vapor pressure of ammonia over the solutions (∿2.56 atm if Raoult's Law is obeyed) caused problems. The decay of the Na^- band was observed (probably due to decomposition), but no e^-_{solv} band was detected. A time cut at ∿660 nm (A) and another one at ∿1000 nm (B) is shown in Figure 25. The small growth observed during flow in B corresponds to the tail of the Na^- band. We were able to analyze kinetically, some of the decays of the Na^- band by fitting the data to a first order decay equation, namely

$$A_t = A_o\, e^{-kt} \qquad 18$$

where A_t = absorbance at time t

A_o = absorbance at time t=0

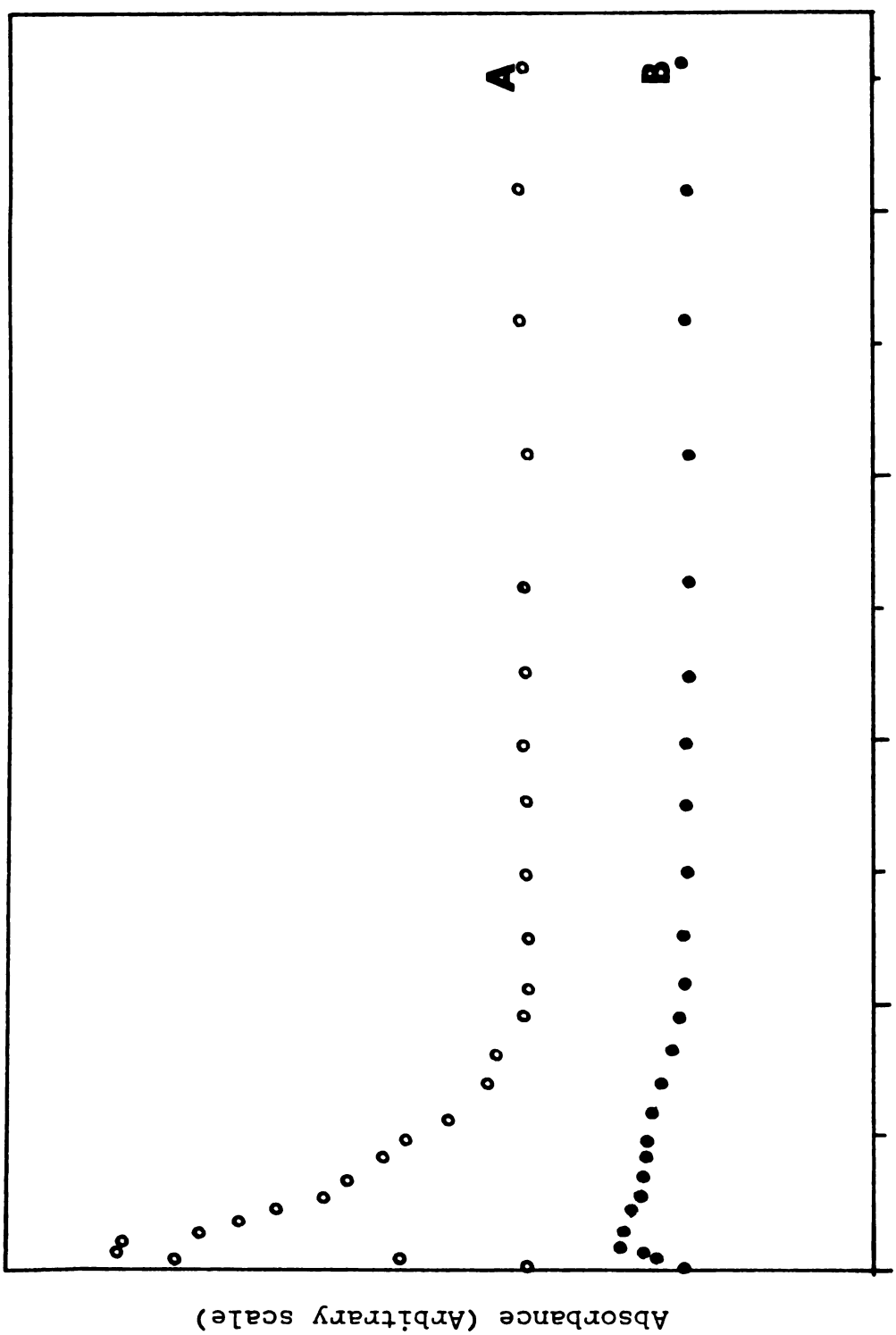

Figure 25. Time cuts from the dissociation of Na^- in EDA at A - ~660 nm and B - ~1000 nm.

A representative computer fitting is shown in Figure 26. A first order rate constant of 1.7 sec^{-1} was obtained.

It was thought at the time that small amounts of impurities in the solvent or the stopped-flow apparatus caused the decomposition of the solution. Because of the problems caused by the high ammonia vapor pressure, we decided to repeat the experiment with a solution of "2,2,2 Crypt" and with more carefully purified solvent. Also, the flow apparatus was prerinsed as described in Section III.2.3.

Two experiments were done with "2,2,2 Crypt" solutions (8.94×10^{-4} M and 8.6×10^{-4} M). Similar results were obtained in both cases as with the ammonia solution.

We were unable to find the reason for the decomposition at the time and turned to the studies with the more stable solutions of aromatic anions. However, in the first experiment with potassium-anthracenide in THF we were faced with the same decomposition problem. A systematic check of the flow apparatus, showed that the Teflon insert in one of the Fisher-Porter joints located between the mixing cell and the flow valves did not maintain a vacuum tight seal when the reacting solutions were pushed through the system. This resulted in contamination of the ammonia (or "2,2,2 Crypt") solution with oxygen or water followed by decomposition of the Na^- solution. Because of the time required to purify the EDA and to prepare the solutions, we abandoned further studies on the dissociation of Na^- in EDA.

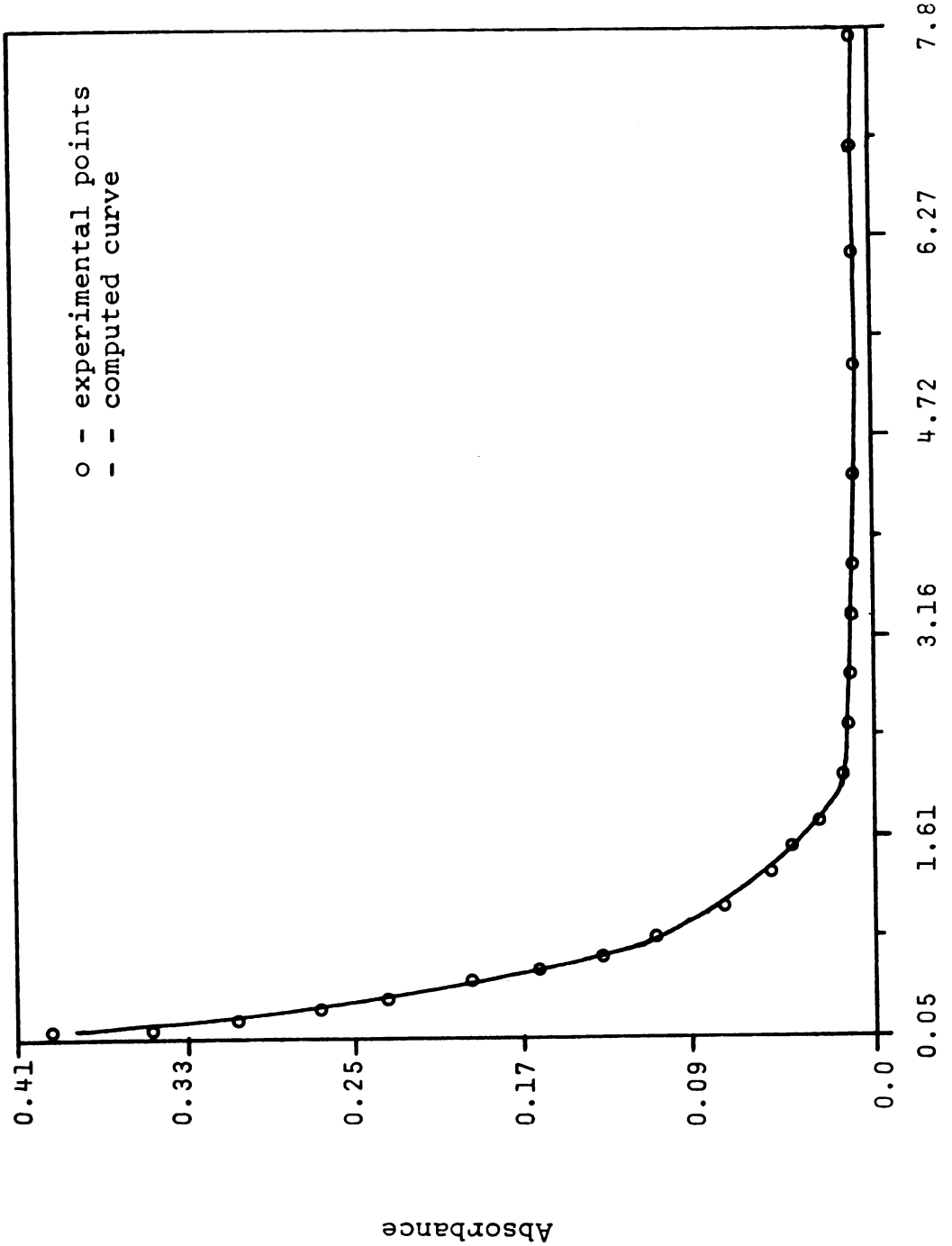

Figure 26. Typical computer fit for the decay of Na^- at ∿660 nm.

VI.2. Effect of Cation Complexing Agents on the Protonation of $K^+,An^{\cdot-}$ in THF

A number of studies[7-15,84] have shown that the protonation of aromatic radical anions in solution depends not only upon the acidity of the proton donor but also very strongly upon the state of aggregation of the ions in solution. Changes in the state of aggregation and the structure of the solvation shell of the protonated species, affect the rates and the free energies of the protonation processes. For this reason the addition of complexing agents which would destroy the contact ion pairs of the type $M^+,A^{\cdot-}$ (e.g. $K^+,An^{\cdot-}$) is expected to drastically affect the protonation rates. Two complexing agents (Figure 27), which have proven to effectively complex metal cations[18], were used in this work.

VI.2.1. Effect of "Crown" on the ESR Spectrum of $Na^+,An^{\cdot-}$ in Diethylether (Et_2O)

The ESR spectra of alkali salts of many aromatic radical anions show hyperfine splitting by the alkali cation, presumably because of contact pair formation[85,86]. Complexation of the cation should be able to prevent such contact pair formation. To demonstrate this effect the ESR spectrum of Na^+, $An^{\cdot-}$ in Et_2O was recorded at -70° C without and with "Crown" present. The solution of $Na^+,An^{\cdot-}$ was prepared in a cell which consisted of a 2.4 mm i.d. ESR tube sealed to an inverted U-tube. A break-seal was attached on one arm

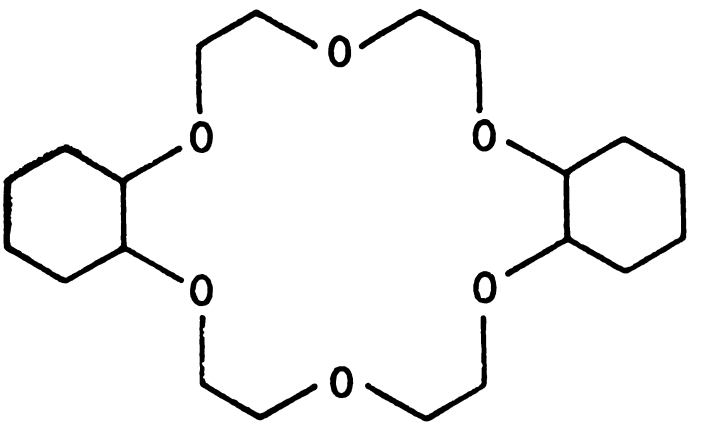

I

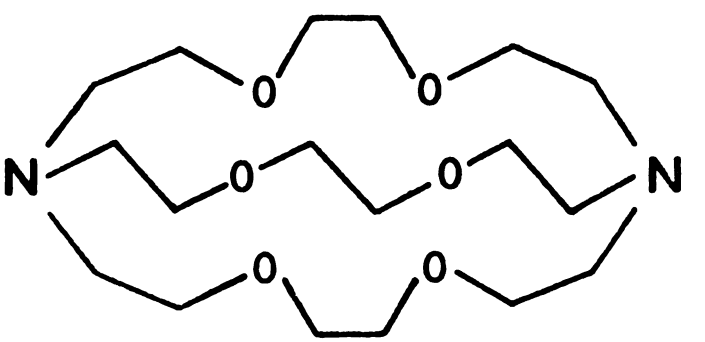

II

Figure 27. Cation complexing agents. (I) "Crown", (II) "2,2,2 Crypt".

of the U-tube, and a sidearm on the other one. First the required amount of "Crown" (always in excess) was enclosed under vacuum in the break-seal. Anthracene was then introduced into one arm of the U-tube (close to the break-seal), and the metal was vacuum-distilled through the sidearm into the other arm. After distillation of the solvent, the solution was prepared and kept away from the metal. The ESR spectrum of this solution was measured at -70° C (Figure 28a) with an X-band Varian E-4 spectrometer. The hyperfine splitting by Na^+ is in agreement with the results of Hirota[85,86]. Subsequently the break-seal was broken and the "Crown" dissolved in the above solution. The addition of "Crown" to the solution caused the disappearance of the Na^+ hyperfine splitting as shown in Figure 28b, in complete accord with expectation. These results are similar to those obtained when alkali solvating agents such as "glymes" are added to similar solutions[87].

VI.2.2. Kinetics Studies

To further investigate the effect of metal-cation complexing agents upon the protonation of aromatic radical anions in ethereal solvents[8,10], the reaction of $K^+,An^{\cdot-}$ with EtOH in THF was studied in the presence of various amounts of "Crown" or "2,2,2 Crypt". Two sets of experiments were carried out. In the first case, the concentrations of $K^+,An^{\cdot-}$ and EtOH were such that, both first and second order contributions were observed in the absence of

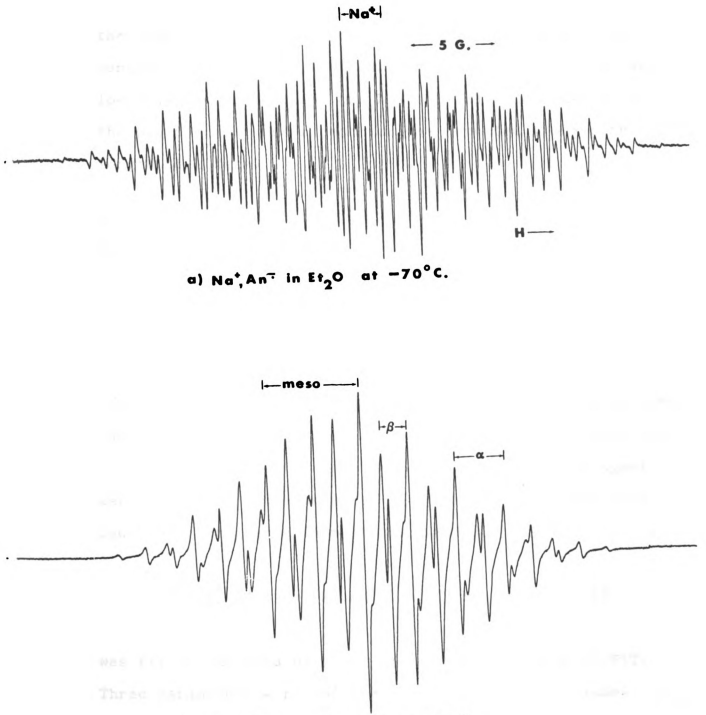

Figure 28. Effect of "Crown" on the ESR spectrum of Na^+,An^- in Et_2O.

the complexing agent (short path length cell data). In contrast the second set of experiments was carried out at low $K^+,An^{\cdot-}$ concentration and high [EtOH], such that only the pseudo-first order reaction was detected (long path length cell data).

VI.2.2.1. Short Path Length Cell Data (Path Length of the Optical Cell=2.0 mm)

First the solution of $K^+,An^{\cdot-}$, as diluted by various amounts with THF, was allowed to react with EtOH in the flow system. An example of the spectrum of $K^+,An^{\cdot-}$ taken from the observed decays is shown in Figure 29. Subsequently, the same dilutions of the $K^+,An^{\cdot-}$ solution were prepared with each complexing agent present and allowed to react with EtOH.

The data collected in the absence of complexing agent were fit to a pseudo-parallel first and second order rate law. The integrated form of the equation

$$-\frac{d[K^+,An^{\cdot-}]}{dt} = k_{ps}[K^+,An^{\cdot-}]^2 + k'_{ps}[K^+,An^{\cdot-}] \qquad 19$$

was fit to the data by using the computer program KINFIT. Three parameters were adjusted: $[K^+,An^{\cdot-}]^\circ$, the pseudo-second order rate constant (k_{ps}) and the pseudo-first order rate constant (k'_{ps}). Representative fits are shown in Figure 30, and the results obtained are listed in Table III.

The data obtained in the presence of complexing agent were

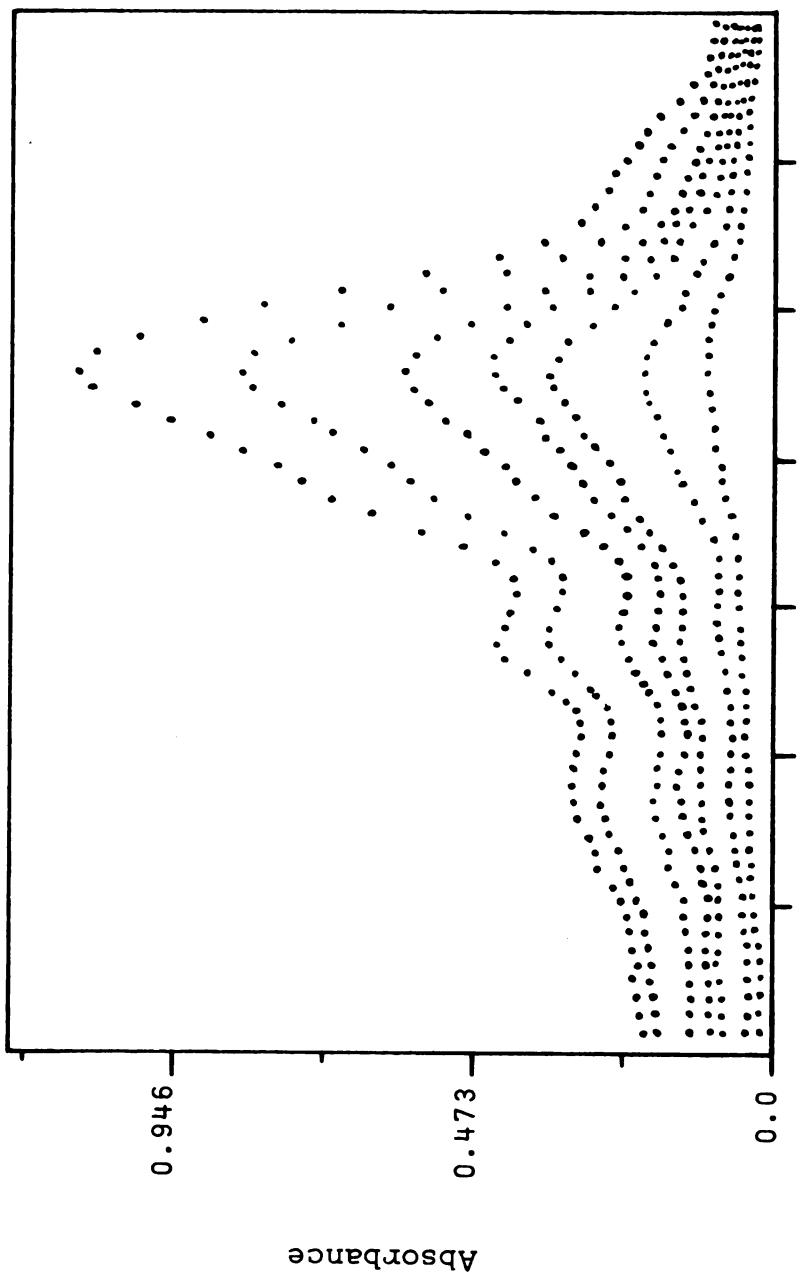

Figure 29. Time development of the spectrum of K^+,An^- during reaction with 0.083 M EtOH in THF.

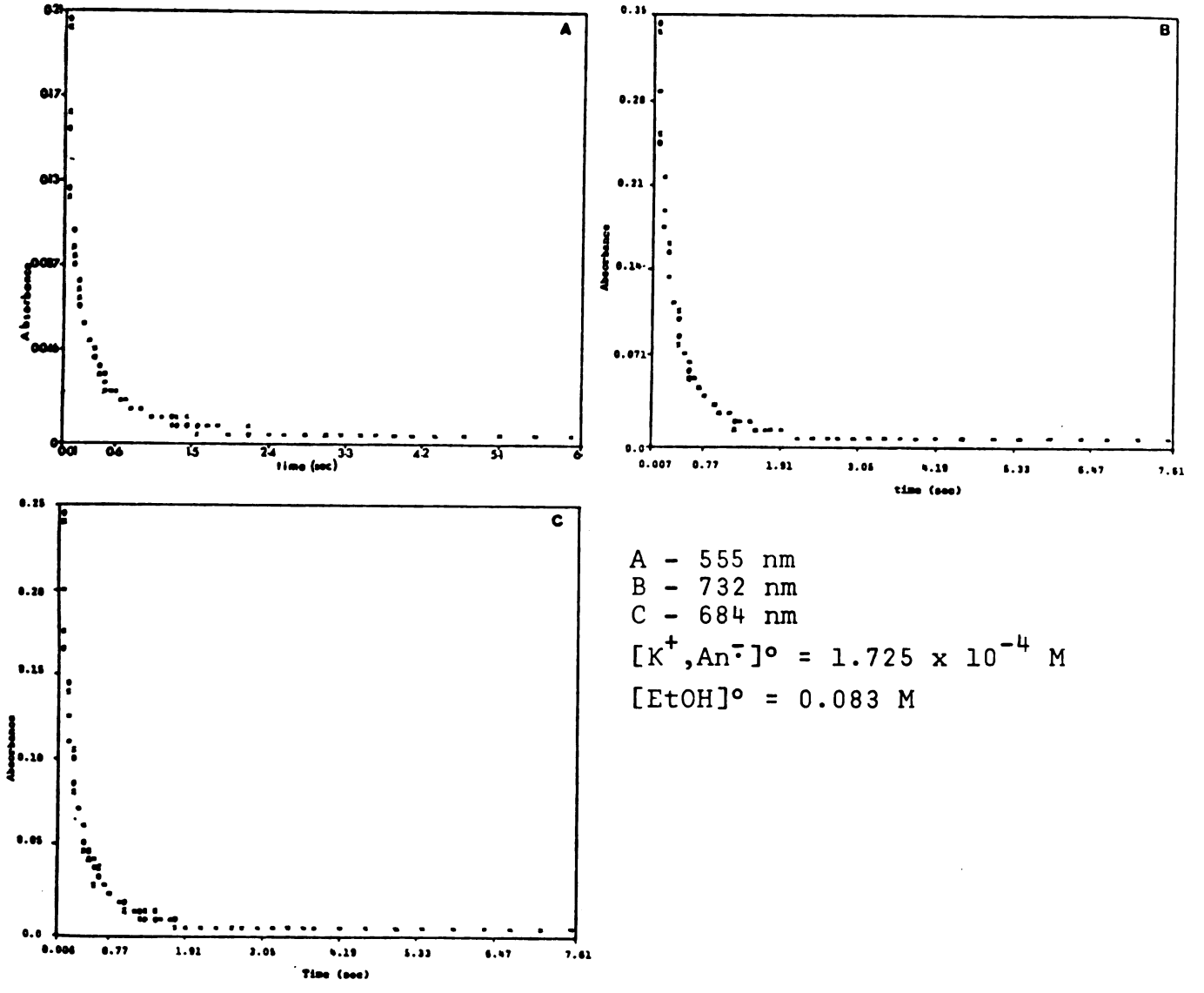

A - 555 nm
B - 732 nm
C - 684 nm
$[K^+,An^{\cdot-}]^\circ = 1.725 \times 10^{-4}$ M
$[EtOH]^\circ = 0.083$ M

Figure 30. Computer fits for the reaction of $K^+,An^{\cdot-}$ with EtOH in THF in the absence of complexing agent. For all computer fits x - experimental point, o - calculated point, = - experimental and calculated are the same.

Table III. Rate constants computed by fitting the data obtained in the absence of complexing agent to Equation (19).

Identification (File name)	Wavelength in nm	$[K^+,An^-]_o$ x10^4M	$[An]_o$ x10^4M	$[EtOH]_o$M	k_{ps}x10^{-4} $M^{-1}sec^{-1}$	k'_{ps} sec^{-1}
AQAPAI.NP	555	5.75	6.1	0.083	3.668±0.556[b]	0.752±0.121
"	604	"	"	"	4.701±0.326[b]	0.506±0.074
"	684	"	"	"	4.170±0.131[b]	0.601±0.053
"	732	"	"	"	3.636±0.051	0.602±0.032
AQAPAJ.NP	732	"	"	"	3.525±0.044	0.707±0.030
AQAPAK.NP	732	"	"	"	3.730±0.056	0.679±0.035
AQAPAM.NP	732	"	"	"	3.519±0.045	0.874±0.036
AQAPAN.NP	732	"	"	"	3.698±0.062	0.851±0.041[c]
					$<k_{ps}>$=3.622±0.097[c]	$<k'_{ps}>$=0.755±0.100[c]
AQAPAO.NP	732	4.6	4.88	0.083	3.604±0.058	0.914±0.042
AQAPAP.NP	"	"	"	"	3.698±0.036	0.933±0.030
AQAPAQ.NP	"	"	"	"	3.707±0.034	0.905±0.031
AQAPAR.NP	"	"	"	"	3.690±0.074	0.973±0.044[c]
					$<k_{ps}>$=3.675±0.048[c]	$<k'_{ps}>$=0.931±0.030[c]
AQAPAT.NP	732	3.74	3.96	0.083	3.561±0.073	0.760±0.038
AQAPAU.NP	"	"	"	"	3.772±0.088	0.603±0.039
AQAPAW.NP	"	"	"	"	3.633±0.104	0.906±0.053
AQAPAZ.NP	"	"	"	"	3.857±0.053	1.118±0.041[c]
					$<k_{ps}>$=3.706±0.134[c]	$<k'_{ps}>$=0.847±0.219[c]
AQAPBB.NP	732	2.875	3.05	0.083	3.684±0.060	1.348±0.046
AQAPBD.NP	"	"	"	"	3.717±0.069	1.411±0.052
AQAPBE.NP	"	"	"	"	3.953±0.100	1.308±0.058
AQAPBF.NP	"	"	"	"	3.776±0.073	1.419±0.054
					$<k_{ps}>$=3.783±0.120[c]	$<k'_{ps}>$=1.372±0.053[c]

Table III - Continued

Identification (File name)	Wavelength in nm	$[K^+,An^-]_o$ x10^4M	$[An]_o$ x10^4M	$[EtOH)_oM$	k_{ps}x10^{-4} $M^{-1}sec^{-1}$	k'_{ps} sec^{-1}
AQAPBK.NP	732	1.725	1.83	0.083	3.332±0.151[b]	1.275±0.072
AQAPBM.NP	599	"	"	"	4.372±0.835[b]	0.919±0.155
"	684	"	"	"	4.388±0.341[b]	1.183±0.112
"	732	"	"	"	3.506±0.174	1.122±0.082
AQAPBP.NP	732	"	"	"	3.249±0.166[c]	1.305±0.067[c]
					$<k_{ps}>$=3.362±0.131[c]	$<k'_{ps}>$=1.234±0.098[c]

Notes:

(a) A molar absorptivity of 1 x 10^4 $M^{-1}cm^{-1}$ was used at 732 nm[88].

(b) Values computed by using the molar absorptivity at 732 nm and then corrected by the appropriate factor[88].

(c) The average values of the rate constants were calculated from the results at 732 nm. The corresponding standard deviations were computed from the equation

$$\sigma = \left[\frac{1}{n-1} \times \sum_{i=1}^{n} (k_i - \langle k_i \rangle)^2\right]^{1/2}$$

analyzed as follows:

The equilibrium

$$K^+,An^{\cdot-} + C \overset{K}{\rightleftarrows} K^+C,An^{\cdot-} \qquad 20$$

was assumed to exist between contact ion pairs ($K^+,An^{\cdot-}$) and complexing agent separated ion pairs (K^+ C,$An^{\cdot-}$; C = "Crown" or "2,2,2 Crypt"). Protonation of the species $K^+,An^{\cdot-}$ occurred as in the case with no complexing agent in the solution, while the ion pairs $K^+C,An^{\cdot-}$ were protonated <u>via</u> a pseudo-first order pathway. The following equations were then combined to fit the experimental data:

$$K = \frac{[K^+C,An^{\cdot-}]}{[K^+,An^{\cdot-}]x[C]} \quad \text{(from Equation (20))} \qquad 21a$$

$$[K^+C,An^{\cdot-}] + [K^+,An^{\cdot-}] = [An^{\cdot-}]_T \qquad 21b$$

$$[C] + [K^+C,An^{\cdot-}] = C_o \qquad 21c$$

$$-\frac{d[An^{\cdot-}]_T}{dt} = k_{ps}[K^+,An^{\cdot-}]^2 + k'_{ps}[K^+,An^{\cdot-}] + k''_{ps}[K^+C,An^{\cdot-}] \qquad 21d$$

where: $[An^{\cdot-}]_T$ = Total anthracenide concentration

C_o = Initial concentration of the complexing agent

For the cases with $C_o \ll [An^{\cdot-}]^o_T$, three parameters were

adjusted; namely, K, $[An^{\cdot-}]_T^o$ and the pseudo-first order rate constant for the species $K^+C,An^{\cdot-}$ (k''_{ps}). The values of k_{ps} and k'_{ps}, computed from the data without complexing agent, were introduced as constants. For alcohol concentrations higher than 0.083 M, the values of k_{ps} were calculated from data reported elsewhere[8,10], while values of k'_{ps} were computed from the long path length cell data (VI.2.2.2). The data with $C_o >> [An^{\cdot-}]_T^o$ were fit to the same equations, with K used as a constant (computed for the $C_o \leq [An^{\cdot-}]_T^o$ case), because there was not enough information to compute three parameters. Finally, for very slow reactions at which $[An^{\cdot-}]_T$ did not decay to zero within the duration of the observation, one more parameter was adjusted; namely, $[An^{\cdot-}]_T^\infty$.

Attempts to introduce the term k'''_{ps} $[K^+,An^{\cdot-}]$ x $[K^+C,An^{\cdot-}]$, into equation (21d) were abandoned because a negative value for k'''_{ps} was obtained without significant change in the fitting (see Figure 31). Even when only the portion of the data with high $[An^{\cdot-}]_T$ (data up to ∿2.3 sec) was used, the computed value for k'''_{ps} was negative.

The results obtained when "Crown" or "2,2,2 Crypt" was added to the $K^+,An^{\cdot-}$ solution prior to protonation are summarized in Table IV. Some representative computer fittings are shown in Figures 32 and 33.

VI.2.2.2. Long Path Length Cell Data (Path Length of the Optical Cell = 1.85 cm)

The potassium anthracenide solution, which was used for the work with the short path length cell, was diluted

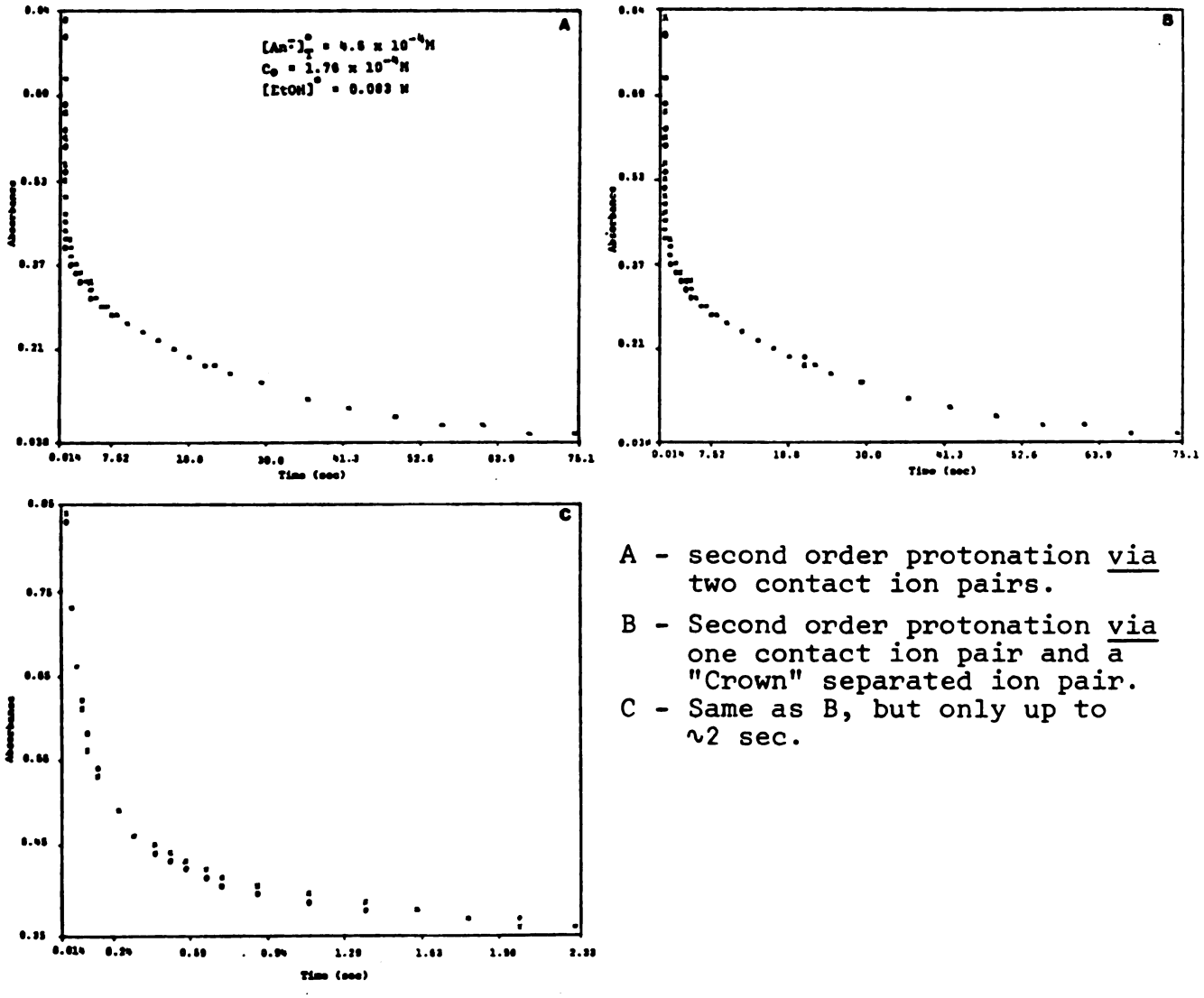

A - second order protonation via two contact ion pairs.

B - Second order protonation via one contact ion pair and a "Crown" separated ion pair.

C - Same as B, but only up to ∿2 sec.

Figure 31. Computer fits for the reaction of K^+,An^- with EtOH in the presence of "Crown". Contribution of K^+C,An^- at the second order protonation.

Table IV. Rate constants computed by fitting the data obtained in the presence of complexing agent, to Equations (21a)-(21d)

Wavelength in nm	$[An^-]_T^o$ $x10^4 M$	$[An]_T^o$ $x10^4 M$	"Crown" $C_o x10^4$ M	"2,2,2 Crypt" $C_o x10^4$ M	$[EtOH]^o$ M	$k_{ps} x10^{-4}$ $M^{-1}sec^{-1}$	k'_{ps} sec^{-1}	$k''_{ps} x10^2$ sec^{-1}	$Kx10^{-5}$ M^{-1}	Number of Pushes
732	4.6	4.88	1.76	----	0.083	3.675[a]	0.931[a]	2.452±0.615[b]	16.5 ±4.58[b]	6
752	3.74	3.96	3.08	----	0.083	3.706[a]	0.847[a]	1.203±0.063[b]	6.02±1.49[b]	6
752	2.875	3.05	4.4	----	0.083	3.783[a]	1.372[a]	1.151±0.096[b]	6.03±0.47[b]	3
555	1.725	1.83	6.16	----	0.083	3.362[a]	1.234[a]	1.227±0.013	4.0[c]	1
604	"	"	"	----	"	"	"	1.289±0.016	"	1
684	"	"	"	----	"	"	"	1.394±0.013	"	1
752	"	"	"	----	"	"	"	1.187±0.095[b]	"	4
752	"	"	"	----	0.418	9.048[d]	62.878[e]	42.0 ±9.7[b]	"	3
732	4.6	4.88	----	1.79	0.083	3.675[a]	0.931[a]	0.208±0.085[b]	46.9±30.5[b]	5
684	3.74	3.96	----	3.132	0.083	3.706[a]	0.847[a]	0.128±0.004	59.2± 1.9	1
752	"	"	----	"	"	"	"	0.131±0.004	57.1± 1.9	1
732	"	"	----	"	"	"	"	0.158±0.048[b]	71.1±21.8[b]	4
752	2.875	3.05	----	4.475	0.209	5.88[d]	15.265[e]	2.781±0.855[b]	113.7±47.0[b]	2
742	"	"	----	"	"	"	"	1.974±0.247[b]	50.1±12.2[b]	3
752	1.725	1.83	----	6.265	0.209	5.88[d]	15.265[e]	3.949±0.206[b]	50.0[c]	4
752	"	"	----	"	0.418	9.048[d]	62.878[e]	31.87 ±4.7[b]	"	4

Notes:

(a) Taken from Table III.

(b) See footnote (b) from Table I

(c) Used as constant. This value resulted in good fits.

(d) Calculated from data reported elsewhere[8,10].

(e) Taken from Table V.

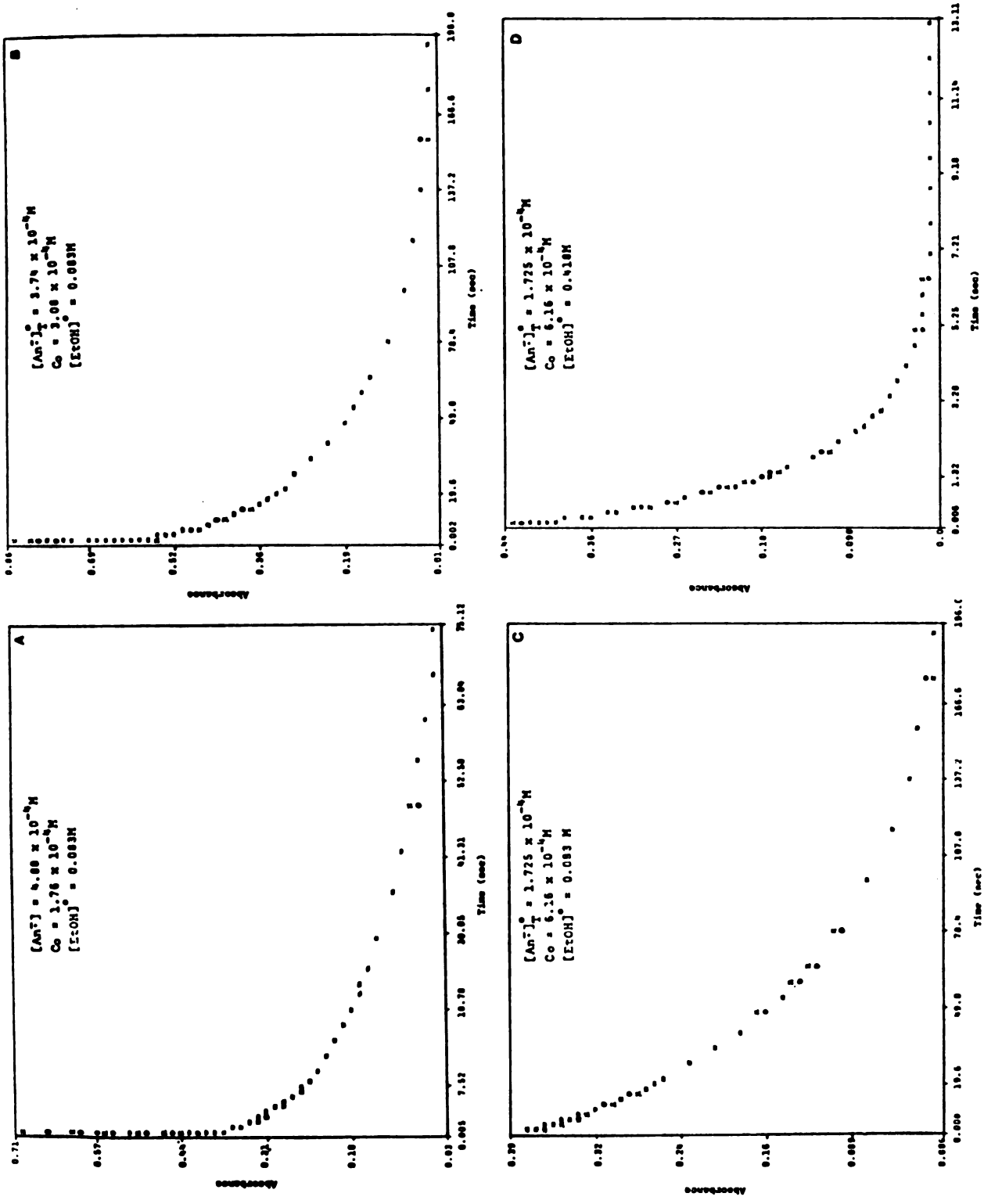

Figure 32. Representative computer fits for the reaction of K^+,An^- with EtOH in the presence of various "Crown" concentrations.

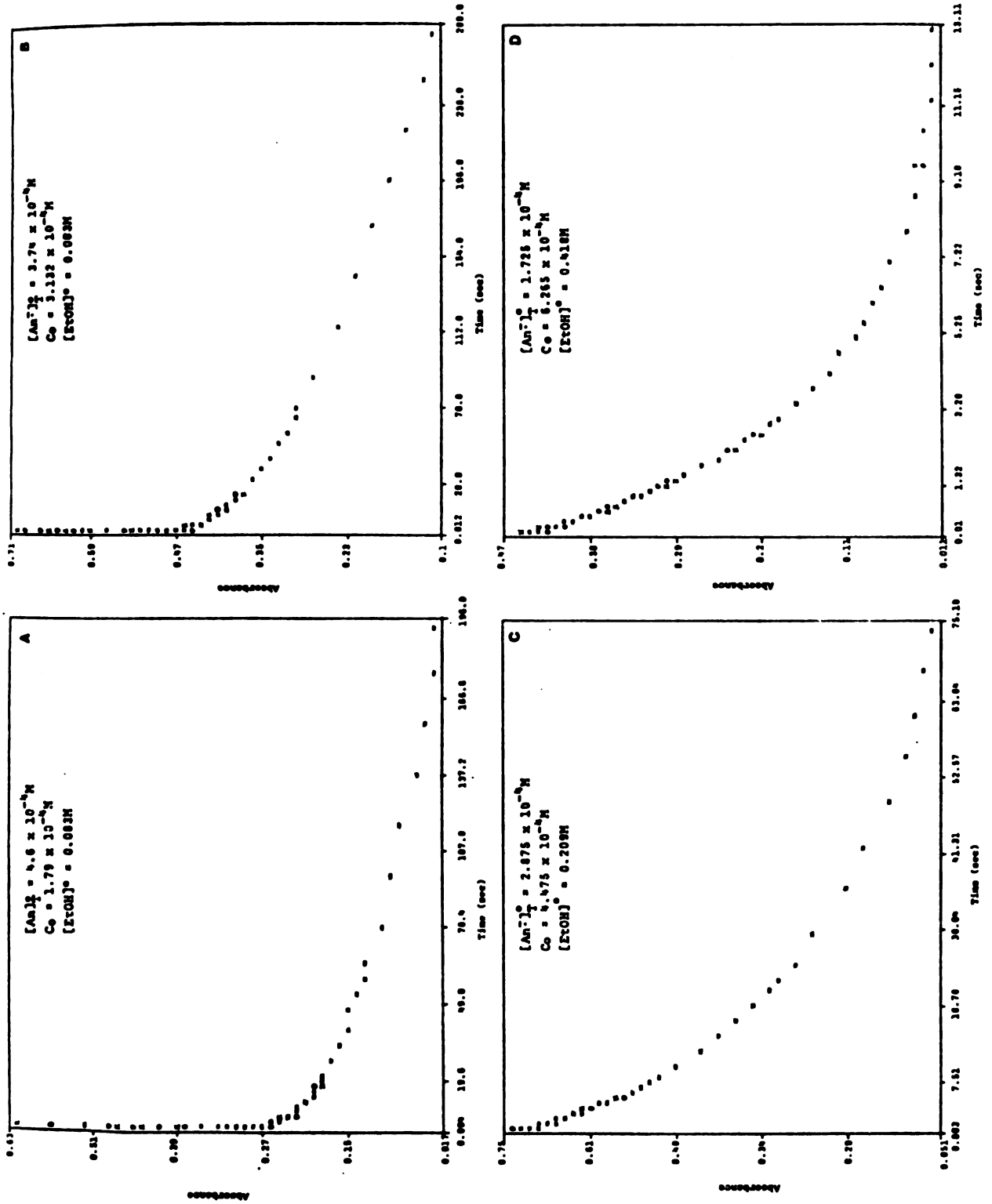

Figure 33. Representative computer fits for the reaction of K^+,An^- with EtOH in the presence of various "2,2,2 Crypt" concentrations.

by a factor of 10 in order to be utilized for the low $[K^+,An^-]$ studies (5 days after the previous work) with no significant change in absorbance.

The protonation in the absence of complexing agent was examined first with four alcohol concentrations. The data with low ethanol concentration ([EtOH] = 0.1045 M), showed a small pseudo-second order contribution, but a predominantely pseudo-first order rate law, and were fit to the integrated form of Equation (19). Two parameters were adjusted in this case; namely, $[K^+,An^-]^o$ and k'_{ps}, while k_{ps} was introduced as a constant, because the second order contribution was very small. However, the data with [EtOH] $\geq$ 0.2 M showed only a pseudo-first order dependence and were fit to the equation:

$$A = A_o e^{-k'_{ps}t} + A_\infty \qquad 22$$

where A_o = absorbance at the beginning of the reaction

A_∞ = absorbance at infinite time

Three parameters were adjusted in this case: A_o, A_∞ and k'_{ps}, the pseudo-first order rate constant. A_∞ was always $\sim 0.1\ A_o$.

The results obtained are listed in Table V. In Figure 34 $\ell n\ (A-A_\infty)$ is plotted versus time, for three alcohol concentrations.

The effect of "Crown" and "2,2,2 Crypt" was investigated at two concentrations of complexing agent, with $[EtOH]^o$=0.418 M.

Table V. Results obtained with low potassium anthracenide concentration in the absence of complexing agent.

Identification (File name)	Scan Speed (Spectra/sec)	Wavelength in nm	$[K^+,Ap^-]_o$ $\times 10^5$M	$[An]_o$ $\times 10^5$M	$[EtOH]_o$ M	$k_{ps} \times 10^{-4}$ $M^{-1}sec^{-1}$	k'_{ps} sec^{-1}
AUAPAL.NP	75	732	5.75	6.1	0.1045	4.4[a]	1.723±0.047[b]
AUAPAM.NP	"	"	"	"	"	"	1.689±0.052[b]
AUAPAO.NP	"	"	"	"	"	"	1.876±0.068[b]
AUAPAP.NP	"	"	"	"	"	"	1.824±0.073[b]
							$\langle k'_{ps} \rangle$=1.778±0.087[c]
AUAPAW.NP	Fixed W.L.	732	5.75	6.1	0.209	----	15.391±0.136[d]
AUAPAX.NP	"	"	"	"	"	----	15.216±0.147[d]
AUAPAY.NP	"	"	"	"	"	----	15.065±0.140[d]
AUAPAZ.NP	"	"	"	"	"	----	15.387±0.208[d]
							$\langle k'_{ps} \rangle$=15.265±0.156[c]
AUAPBA.NP	"	"	"	"	0.293	----	25.102±0.250[d]
AUAPBB.NP	"	"	"	"	"	----	28.207±0.370[d]
AUAPBD.NP	"	"	"	"	"	----	28.901±0.382[d]
AUAPBE.NP	"	"	"	"	"	----	28.292±0.458[d]
							$\langle k'_{ps} \rangle$=27.626±1.710[d]
AUAPBG.NP	"	"	"	"	0.418	----	58.000±1.800[c]
AUAPBI.NP	"	"	"	"	"	----	65.927±1.410[d]
AUAPBJ.NP	"	"	"	"	"	----	63.613±1.480[d]
AUAPBK.NP	"	"	"	"	"	----	60.784±2.410[d]
AUAPBL.NP	"	"	"	"	"	----	66.066±1.410[d]
							$\langle k'_{ps} \rangle$=62.878±3.471[c]

(a) Calculated from data reported elsewhere[8,10] and used as a constant.

(b) From fit of data to parallel first and second order decay (Equation 19).

(c) See footnote (b) from Table 1.

(d) From fit of data to a pseudo-first order decay (Equation (22).

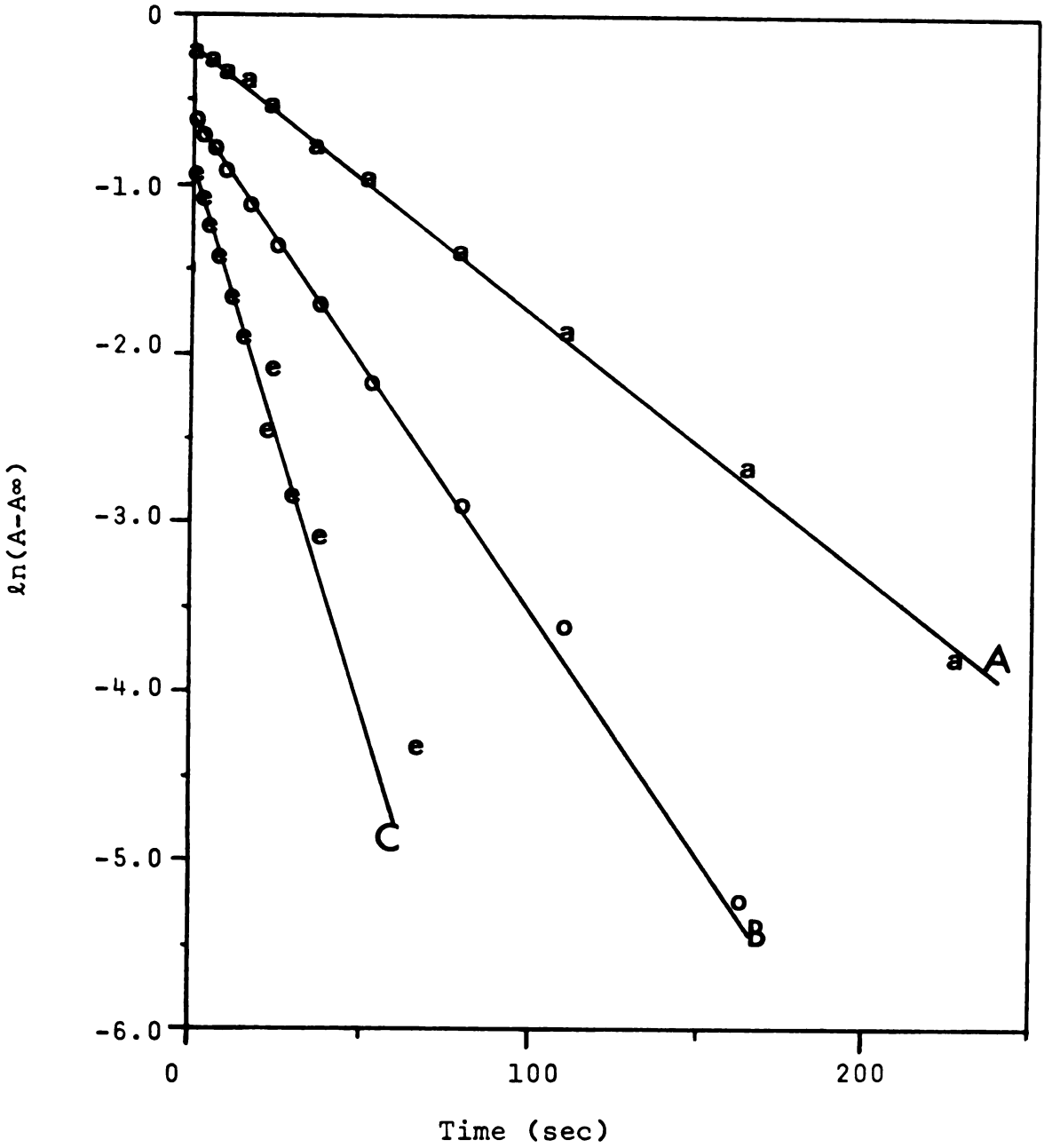

Figure 34. Plots of ℓn(A-A∞) vs time for the reaction of K^+,An^- (∿5x10^{-5} M) with EtOH in THF. A - [EtOH]°= 0.209 M, the line was drawn with the computed slope of ∿15.7 sec^{-1}. B - [EtOH]° = 0.293 M, the line was drawn with the computed slope of ∿28.9 sec^{-1}. C-[EtOH]° = 0.418 M, the line was drawn with the computed slope of ∿65 sec^{-1}.

The data obtained with ["Crown"]$^{\circ}$ $\sim$0.5 [K^+,$An^{\cdot-}$]$^{\circ}$ were fit to the Equations (21a) - (21c) and (23).

$$-\frac{d[An^{\cdot-}]_T}{dt} = k'_{ps}[K^+,An^{\cdot-}] + k''_{ps}[K^+C,An^{\cdot-}] \qquad 23$$

Three parameters were adjusted: K, $[An^{\cdot-}]^{\circ}_T$ and k''_{ps}. Also $[An^{\cdot-}]^{\infty}_T$ was introduced as a parameter whenever the absorbance had not decayed to zero. k_{ps} was used as a constant. For the data with ["2,2,2 Crypt"]$^{\circ}$ $\sim$0.5 [K^+,$An^{\cdot-}$]$^{\circ}$ it was impossible to use the same rate law as that used for the "Crown" case. However, a pseudo-first order decay of the form

$$A = A_o e^{-k''_{ps}t} \qquad 24$$

was used successfully. Two parameters were adjusted in this case: A_o, the absorbance at the beginning and k''_{ps}, the pseudo-first order rate constant for the complexing agent separated ion pair (K^+C,$An^{\cdot-}$).

Finally, the data with C_o >>> [K^+,$An^{\cdot-}$]$^{\circ}$ were fit to Equation (24) for both complexing agents.

The results are summarized in Table VI. Characteristic fits are shown in Figure 35.

Table VI. Results obtained with the long path length cell in the presence of "Crown" or "2,2,2 Crypt".

Identification (File name)	Scan Speed (Spectra/sec)	Wavelength nm	"Crown" $C_o x10^5 M$	"2,2,2 Crypt" $C_o x10^5 M$	k'_{ps} sec^{-1}	k''_{ps} sec^{-1}
AUAPBV.NP	75	760	1.76	----	62.878[b]	1.476±0.056[d]
AUAPBW.NP	"	"	"	----	"	1.327±0.081[d]
AUAPBX.NP	"	"	"	----	"	1.329±0.081[d]
AUAPBP.NP	Fixed W.L.	∿752	"	----	"	1.139±0.354[d]
AUAPBR.NP	"	"	"	----	"	1.610±0.356[d]
AUAPBS.NP	"	"	"	----	"	1.164±0.372[d]
AUAPBT.NP	"	"	"	----	"	1.009±0.384[d]
AUAPBZ.NP	75	"	79.2	----	----	0.932±0.003[e]
AUAPCA.NP	"	"	"	----	----	1.017±0.010[e]
AUAPCB.NP	"	"	"	----	----	0.965±0.003[e]
AUAPCC.NP	"	"	"	----	----	0.931±0.002[e]
AUAPCD.NP	"	"	"	----	----	0.946±0.003[e]
AUAPCJ.NP	"	"	----	1.79	----	0.886±0.004[e]
AUAPCK.NP	"	"	----	"	----	0.963±0.010[e]
AUAPCM.NP	"	"	----	"	----	0.986±0.012[e]
AUAPCN.NP	"	"	----	"	----	0.977±0.009[e]
AUAPCP.NP	"	"	----	80.55	----	0.563±0.002[e]

Table VI. Continued

Identification (File name)	Scan Speed (Spectra/sec)	Wavelength nm	"Crown" $C_o x10^5 M$	"2,2,2 Crypt" $C_o x10^5 M$	k'_{ps} sec^{-1}	k''_{ps} sec^{-1}
AUAPCQ.NP	75	~752	----	80.55	----	0.501±0.002[e]
AUAPCR.NP	"	"	----	"	----	0.593±0.003[e]
AUAPCS.NP	"	"	----	"	----	0.549±0.001[e]
AUAPCT.NP	"	"	----	"	----	0.570±0.002[e]

Notes:

(a) For all these "pushes": $[K^+,An^{\cdot-}]^o = 5.75x10^{-5}M$; $[An]^o = 6.1x10^{-5}M$; $[EtOH]^o = 0.418M$

(b) Taken from Table V.

(c) Equilibrium constant computed from files: AUAPBV.NP→AUAPBX.NP=$(1.96\pm0.28)x10^7 M^{-1}$.
Equilibrium constant computed from files: AUAPBP.NP→AUAPBT.NP=$(1.13\pm0.41)x10^7 M^{-1}$.

(d) From fit of data to Equations (21a)→(21c) and (23).

(e) From fit of data to Equation (24).

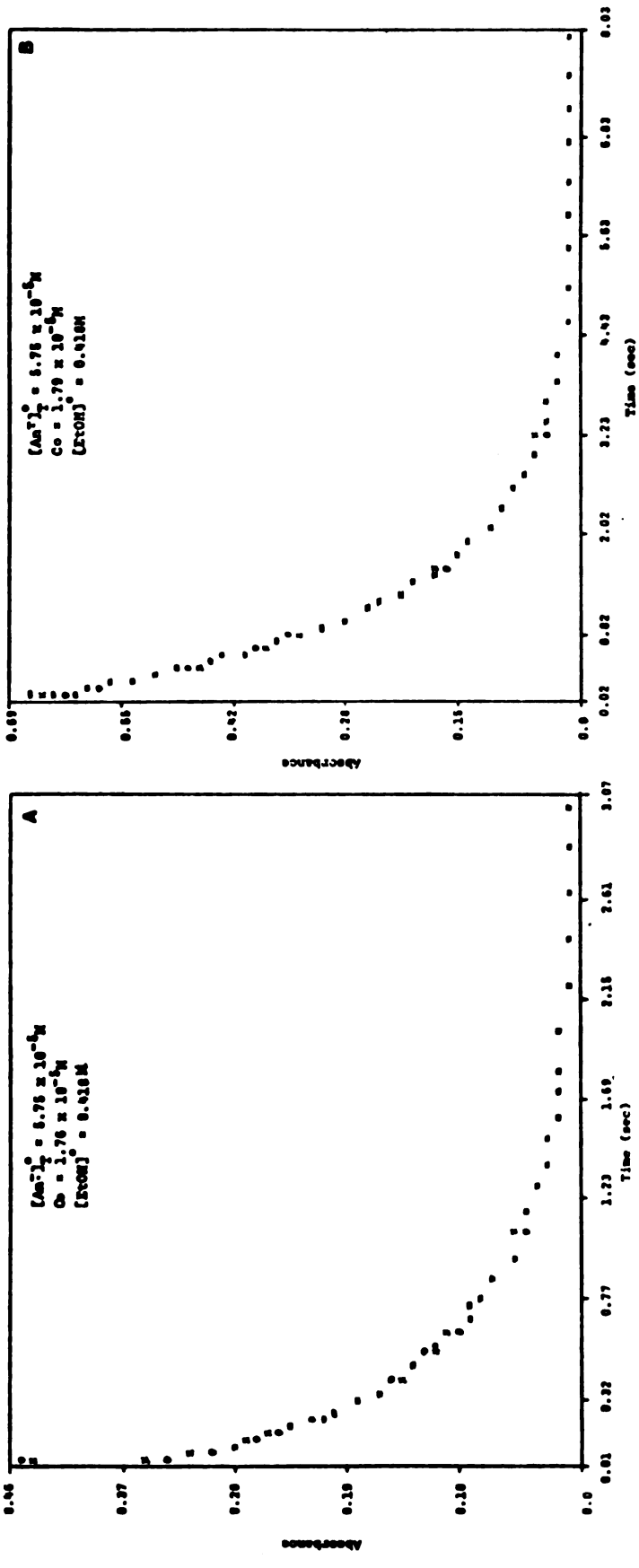

Figure 35. Representative computer fits for the reaction of K^+,An^- ($\sim$5 x 10^{-5}M) with EtOH in the presence of A - "Crown", B - "2,2,2 Cryptˮ.

VII. DISCUSSION

VII.1. Dissociation of Na^- in EDA

Since no detectable formation of e^-_{solv} occurred during the slow decomposition of the Na^- solution, its rate of production could not be measured. However, if we assume the following possible pathways for the decomposition:

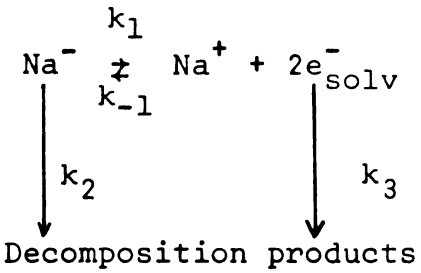

25

an estimate of the maximum value of k_1 can be calculated.

If the dissociation process had reached equilibrium, the concentration of e^-_{solv}, as computed from Equation (17) with $K=6 \times 10^{-8} M^2$ and $[Na^-] \sim 10^{-4} M$, should be:

$$[e^-_{solv}] = 1.21 \times 10^{-4} \text{ M}$$

This would result in an absorbance of $1.21 \times 10^{-4} \times 0.2 \times 1.51 \times 10^4 = 0.37$ absorbance units at ~1000 nm (the molar absorptivity of 1.51×10^4 M^{-1} cm^{-1} was computed from previously reported results[25]). Calibration experiments have shown that absorbances ≥ 0.02 should be easily measured with the instrument. This indicates that the reaction did not reach equilibrium, because no detectable absorbance changes occurred at ~1000 nm. Thus the

concentration of e^-_{solv} was:

$$[e^-_{solv}] \leq 0.02/0.2x1.51x10^4 = 6.62x10^{-6}M \qquad 26$$

for all three experiments.

The rate of decomposition of Na^- as derived from Equation (25) is:

$$\frac{d[Na^-]}{dt} = -(k_1+k_2)[Na^-] + k_{-1}[Na^+][e^-]^2 = -1.7[Na^-]$$

or

$$(k_1+k_2-1.7)[Na^-] = k_{-1}[Na^+][e^-]^2 \qquad 27$$

From pulse radiolysis studies[26] a value of $k_{-1}[Na^+]$ = $(0.132\pm0.015) \times 10^9$ M^{-1} sec^{-1} was calculated at $[Na^+]$ = 0.7×10^{-3} M. Since, in this work $[Na^+] \sim 1 \times 10^{-4}$, a good approximation for $k_{-1}[Na^+]$ is $\sim 10^8$ M^{-1} sec^{-1}.

By substitution of the known values into Equation (27), the following result is obtained:

$$k_1+k_2 = 1.7 + \frac{10^8x(6.6x10^{-6})^2}{10^{-4}} = 1.7+44 = 45.7 \text{ sec}^{-1}$$

This indicates that k_1 could be as high as ~ 50 sec^{-1} and still no formation of e^-_{solv} would be detected because of the decomposition problems.

With this information we cannot conclude whether the reaction of Na with water in EDA proceeds <u>via</u> the dissociation of Na^- or not. The performance of the stopped-flow

system as tested with the protonation of $K^+,An^{\cdot-}$ in THF, indicates that further studies on the dissociation of Na^- in EDA are possible. A solution of "2,2,2 Crypt" should be used in order to eliminate the problems caused by the high vapor pressure of ammonia, and in order not to alter drastically the properties of the solvent.

VII.2. Effect of "Crown" and "2,2,2 Crypt" on the Protonation of $K^+,An^{\cdot-}$ with EtOH in THF

It is clear from the results presented in the last chapter, that both complexing agents affect the rate of protonation of $K^+,An^{\cdot-}$ in THF in the same direction but by different amounts. The following equilibria and reaction steps should be considered to predict the species present in a solution of $K^+,An^{\cdot-}$ in THF to which a cation complexing agent (C) has been added:

$$K^+,An^{\cdot-}+C \underset{}{\overset{K_1}{\rightleftarrows}} K^+C,An^{\cdot-} \overset{K_2}{\rightleftarrows} K^+C+An^{\cdot-} \qquad 28a$$

$$2(K^+,An^{\cdot-}) \overset{K_Q}{\rightleftarrows} (An^{\cdot-},K^+)_2 \underset{k''_-}{\overset{k''_+}{\rightleftarrows}} An^{=},2K^+ + An \qquad 28b$$

$$K^+C,An^{\cdot-}+K^+,An^{\cdot-} \overset{K'_Q}{\rightleftarrows} (K^+C,An^{\cdot-};K^+,An^{\cdot-}) \underset{k'''_-}{\overset{k'''_+}{\rightleftarrows}}$$

$$An^{=},2K^+C + An \qquad 28c$$

It is assumed that dissociation of contact ion pairs $(K^+,An^{\cdot-})$ is negligible in THF[89].

If the formation of "loose" ion pairs involves only electrostatic forces, the value of the equilibrium constant K_2 can be estimated from the Fouss equation[90]

$$\frac{1}{K_2} = \frac{4\pi a^3 N \exp(b)}{3000} \qquad 29$$

$$b = \frac{e^2}{aDkT}$$

where: N = Avogadro's number

a = ionic diameter

e = charge on an electron

D = dielectric constant

k = Boltzmann's constant

The ionic diameter of the species K^+C,An^- can be computed as follows (for C = "2,2,2 Crypt"). K^+ to oxygen distance in K^+-2,2,2 Cryptate is equal to 2.79 Å[92]. Also for the ion pair K^+,An^- in THF an ionic radius of 5.7 Å has been calculated[10], while the potassium ionic radius is 1.33 Å[91]. Thus a $\sim$2.79 + 5.7 - 1.33 $\sim$ 7.16 Å for K^+C,An^-. The value of $\frac{1}{K_2} = 3.68 \times 10^4$ M^{-1} is then computed from Equation (29) at 25° C. This indicates that the dissociation of the "2,2,2 Crypt" separated ion pairs is very small ($K_2 = 2.7 \times 10^{-5}$ M). A similar dissociation constant can be expected for the "Crown" separated ion pairs.

The contribution of the equilibrium (28c) to the protonation reaction can be examined as follows. As was shown in Section VI.2.2.1 the second order term k''_{ps} $[K^+,An^-] \times [K^+C,An^-]$

did not improve the computer fits when used (together with the term $k_{ps}[K^+,An^{\cdot-}]^2$) and actually resulted in a negative value for k''_{ps}. Now we may assume two more cases. Either the second order step requires two contact ion pairs ($K^+,An^{\cdot-}$), or it requires only one $K^+,An^{\cdot-}$ and any other ion pair in the solution; either $K^+C,An^{\cdot-}$ or $K^+,An^{\cdot-}$. If we let C_o be defined by $C_o = [K^+C,An^{\cdot-}]$, then the second order protonation will be:

$$\frac{d[An^{\cdot-}]_T}{dt} = -k_{ps}([An^{\cdot-}]_T - C_o)^2 \qquad 30$$

or

$$\frac{d[An^{\cdot-}]_T}{dt} = -k_2([An^{\cdot-}]_T - C_o)x\ [An^{\cdot-}]_T \qquad 31$$

where Equation (30) requires two $K^+,An^{\cdot-}$, while Equation (31) requires only one contact ion pair. Let us now consider the limiting case $k_{ps} = k_2$, and compute the curves corresponding to Equations (30) and (31), for the case where $[An^{\cdot-}]^o_T = 4.064 \times 10^{-4}$ M, $C_o = 1.76 \times 10^{-4}$ M and $k_{ps} = 3.63 \times 10^4\ M^{-1} \times sec^{-1}$. The results are shown in Figure 36 and indicate that the second order protonation of $K^+,An^{\cdot-}$ with EtOH in THF requires two contact ion pairs.

In summary it seems justified to neglect the equilibrium (28c) and to assume that the dissociation of the species $K^+C,An^{\cdot-}$ is insignificant in THF.

Let us now propose a general mechanism in conjunction with the results reported elsewhere[10,15].

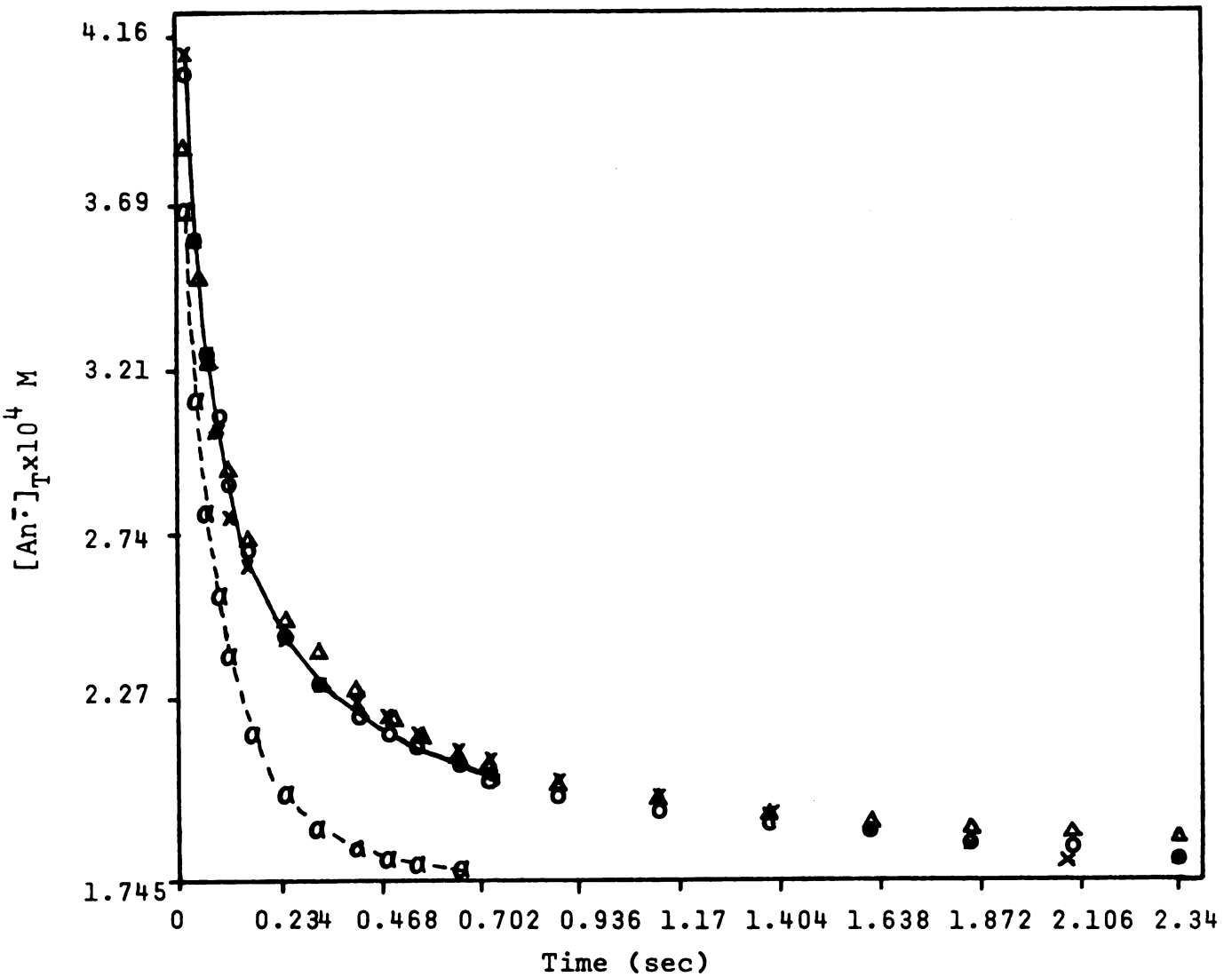

Figure 36. Effect of the complexing agent separated ion pair on the second order protonation of $K^+,An^{\cdot-}$ in THF. X-experimental points, Δ - points calculated from Equation (30), a - points calculated from Equation (31), o - points computed from Equations (21a)-(21d). Note that this is only the first 2.34 sec out of 74.0 sec required for the reaction to go to completion.

$$K^+,An^{\cdot-} + C \overset{K}{\rightleftarrows} K^+C,An^{\cdot-} \qquad 32a$$

$$2(K^+,An^{\cdot-}) \overset{K_Q}{\rightleftarrows} (An^{\cdot-},K^+)_2 \underset{k''_-}{\overset{k''_+}{\rightleftarrows}} An^{=},2K^+ + An \qquad 32b$$

$$An^{=},2K^+ + ROH \overset{k_1}{\rightarrow} K^+AnH^- + K^+RO^- \qquad 32c$$

$$(An^{\cdot-},K^+)_2 + ROH \overset{k_2}{\rightarrow} K^+AnH^- + K^+RO^- + An \qquad 32d$$

$$K^+,An^{\cdot-} + nROH \overset{k_3}{\rightarrow} AnH^{\cdot} + K^+RO^-(ROH)_{n-1} \qquad 32e^*$$

$$K^+,An^{\cdot-} + AnH^{\cdot} \overset{k_4}{\underset{fast}{\rightarrow}} K^+AnH^- + An \qquad 32f$$

$$K^+C,An^{\cdot-} + nROH \overset{k_5}{\rightarrow} K^+CRO^-(ROH)_{n-1} + AnH^{\cdot} \qquad 32g^*$$

$$K^+C,An^{\cdot-} + AnH^{\cdot} \overset{k_6}{\underset{fast}{\rightarrow}} K^+CAnH^- + An \qquad 32h$$

$$K^+CAnH^- + ROH \overset{k_7}{\underset{fast}{\rightarrow}} K^+CRO^- + AnH_2 \qquad 32i$$

$$K^+AnH^- + ROH \overset{k_8}{\underset{fast}{\rightarrow}} K^+RO^- + AnH_2 \qquad 32j$$

The above mechanism leads to the general rate law:

$$\frac{d[An^{\cdot-}]_T}{dt} = -k_{ps}[K^+,An^{\cdot-}]^2 - k'_{ps}[K^+,An^{\cdot-}] - k''_{ps}[K^+C,An^{\cdot-}] \qquad 33$$

if a steady-state concentration of the dianion $(An^{=},2K^+)$ is assumed.

The rate constant expressions are:

---

*n=1 for t-BuOH[15], while n=2 for MeOH[15] and EtOH (this work VII.2.1).

$$k_{ps} = \frac{2k''_{+} K_Q}{1+\frac{k''_{-}}{k_1}\frac{[An]}{[ROH]}} + 2k_2K_Q[ROH] \qquad 34a$$

$$k'_{ps} = k_3[ROH]^n;\ k''_{ps} = k_5[ROH]^n \qquad 34b$$

One more equilibrium must be considered during the protonation process; namely,

$$K^+RO^- + C \overset{K_{ROH}}{\rightleftarrows} K^+C+RO^- \qquad 35$$

The equilibrium constant K_{ROH} could be determined from conductance measurements. However, it can be assumed to be very small, because the dissociation equilibrium constant for K^+RO^-,

$$K^+RO^- \overset{K'_{ROH}}{\rightleftarrows} K^+ + RO^-$$

is very low. This can be justified as follows. The equilibrium constant for the formation of the ion pair $FO^{\cdot-}$, Na^+ in DMF-DME 1:1 mixture has been reported to be $1.3 \times 10^9\ M^{-1}$(93) ($FO^{\cdot-}$ is the Fluorenone radical anion, DMF = dimethylformamide, DME = dimethoxyethane). Since THF is a less polar solvent than either DMF or DME, K'_{ROH} should be $< 10^{-9}$ M.

VII.2.1. Dependence of the Pseudo-first Order Rate Constant (k'_{ps}) on [EtOH]:

The reproducibility of the results summarized in Table V and Figure 34, indicates that only the first order protonation of $K^+,An^{\cdot-}$ occurs when $[K^+,An^{\cdot-}] \sim 10^{-5}$ M and [EtOH] $\geq$ 0.2 M [The noise observed in Figure 34 is a result of the problems associated with the present fiber configuration (Section IV.4.1)]. A plot of log k'_{ps} vs log [EtOH] is shown in Figure 37. Even though we have only three points, it appears that the alcohol dependence is second order. Similar dependence was observed by Szwarc et al.[15] for the protonation of $K^+,An^{\cdot-}$ with methanol in THF.

Not enough information is available to calculate the dependence of k''_{ps} upon the ethanol concentration; however, analysis (VI.2.2.1) of the data for the short path length cell indicates a dependence similar to that of k'_{ps}.

VII.2.2. Conclusions

The reproducibility of the results reported in Table III indicates the reliability of the computer-interfaced scanning stopped-flow system (Chapters III and IV) for the study of reactions with air-sensitive solutions. The observed values for k_{ps} seem to be wavelength independent. From the concentrations given in Table III and Equation (34a), a value of 3.14×10^4 M^{-1} sec^{-1} was calculated for k_{ps}, with the use of results reported elsewhere[10]. This compares very well with the observed value of $k_{ps} = (3.63 \pm 0.16) \times 10^4$ M^{-1} sec^{-1} (overall

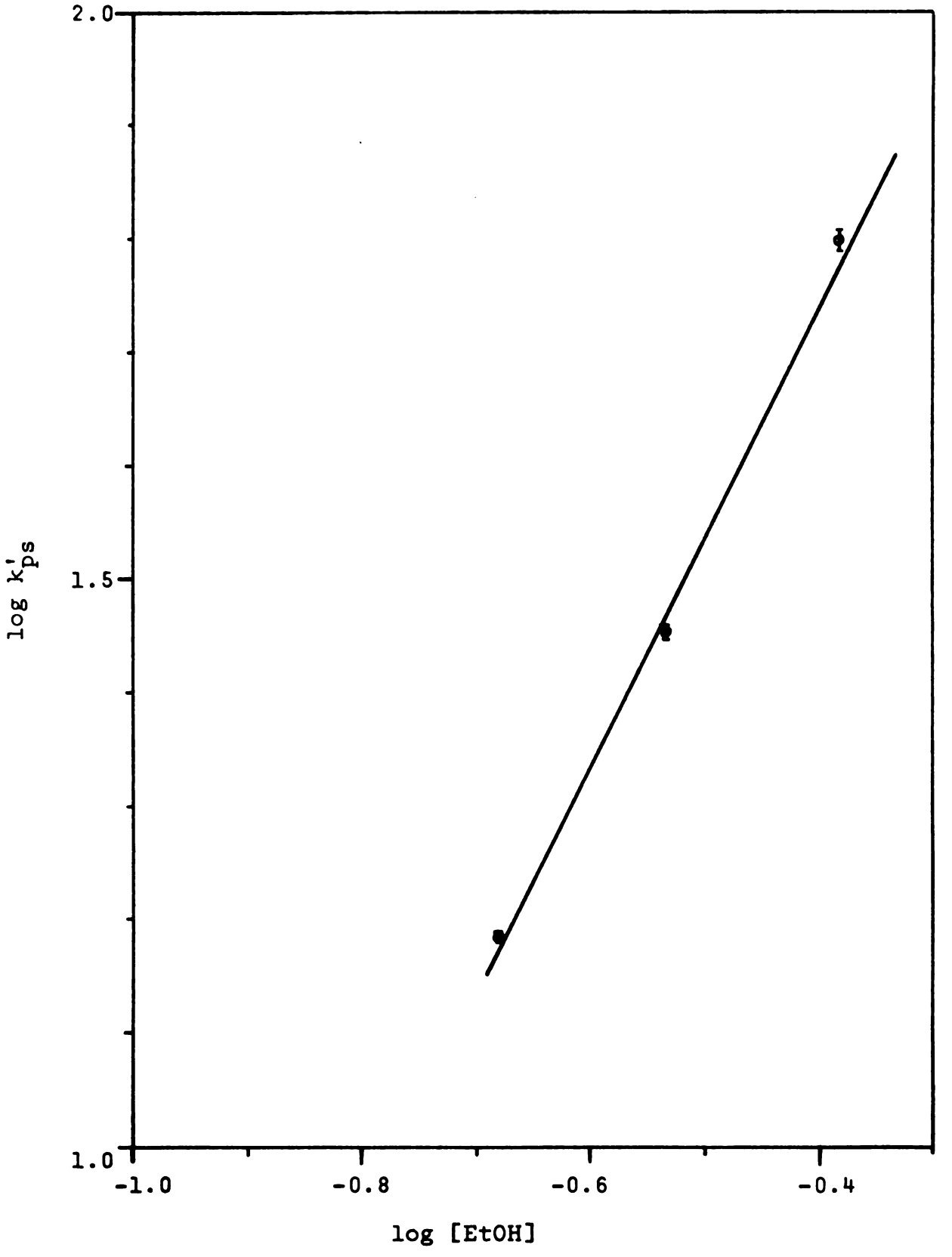

Figure 37. Dependence of the pseudo-first order rate constant (k'_{ps}) on [EtOH]. The drawn line has a slope of 2.12.

average from Table III). Note that the computation of the pseudo-first order rate constant at these low ethanol and anthracenide concentrations could not be done efficiently without the versatile computer-assisted data acquisition system.

The proposed general mechanism fits the short path length cell data reasonably well, but shows some discrepancies when the second order protonation is absent (long path length cell data). The mechanism for the pseudo-first order protonation is very important in these concentration ranges. The following mechanism might explain the inconsistency associated with the pseudo-first order data:

$$K^+,An^{\cdot-} + ROH \overset{K_1}{\rightleftharpoons} K^+,An^{\cdot-}(ROH)$$

$$K^+C,An^{\cdot-} + ROH \overset{K_m}{\rightleftharpoons} K^+,An^{\cdot-}(ROH) + C$$

$$K^+,An^{\cdot-}(ROH) + ROH \overset{k_n}{\rightleftharpoons} \text{products (}\underline{\text{via}}\text{ fast steps)}$$

Note that this is actually the "cation solvation" mechanism as introduced by Dye et al.[10] to explain the alcohol dependence of the pseudo-first order protonation step. This mechanism gives a second order dependence on ethanol, in agreement with the observed behavior (VII.2.1), and is currently under further study.

These studies have clearly shown that the second order protonation requires <u>two</u> contact ion pairs, which is an

important result. In general, the requirement of contact ion pairs for the second-order protonation is in agreement with the results obtained in solvents more polar than THF and with the cation dependence of the mechanism[10,15,84].

The computed rate constants indicate that the "Crown" separated ion pairs are protonated more rapidly than the "2,2,2 Crypt" separated ion pairs. This is expected, since the structure of "Crown" (Figure 27) allows for stronger charge localization than does "2,2,2 Crypt". The average rate constants computed from Table IV are $\sim$2.2 M^{-1} sec^{-1} for the "Crown" and $\sim$0.72 M^{-1} sec^{-1} for the "2,2,2 Crypt" separated ion pairs.

Even though specific solvent effects may alter the protonation rates significantly, the results to date (excluding those from pulse radiolysis in the pure alcohols) are consistent with an overall scheme in which the dominant factor is the degree of charge localization in the aromatic system. This is clearly shown from the rate constants listed in Table VII, since we expect the charge localization to decrease in the order:

$(An^{=},2M^{+}) > (An^{\cdot-},M^{+})_2 > (An^{\cdot-},M^{+}) > (An^{\cdot-}||M^{+}) >$ ($An^{\cdot-}$, "Crown" M^{+}) > ($An^{\cdot-}$, "2,2,2 Crypt" M^{+}) > ($An^{\cdot-}$); [($An^{\cdot-}$,$||M^{+}$) is a solvent separated ion pair].

Table VII. Summary of the protonation rate constants for various ion pairs

Ion Pair	$k\ M^{-1}\ sec^{-1}$	
$(An^{=},2M^{+})$	$\sim 1.5 \times 10^{9}$	(a)
$(An^{\cdot-},M^{+})_2$	$\sim 2.5 \times 10^{3}$	(b)
$(An^{\cdot-},M^{+})$	~ 344	(d)
$(An^{\cdot-}\|\|M^{+})$	~ 6	(c)
$(An^{\cdot-}$, "Crown" $M^{+})$	~ 2.2	(d)
$(An^{\cdot-}$, "2,2,2 Crypt" $M^{+})$	~ 0.72	(d)
$(An^{\cdot-})$	$\sim 2 \times 10^{-4}$	(e)

Notes:

(a) From reference (10).

(b) From reference (10). This could be as high as $\sim 1.7 \times 10^{10}$ depending upon the mechanism.

(c) From reference (14), if $Na^{+}An^{\cdot-}$ is assumed to exist in DME largely as the solvent separated ion pair.

(d) This work.

(e) From reference (84).

(f) Note that the rate constants depend also upon the metal cation (15).

APPENDICES

APPENDIX A

TEST FOR AN "UNCOMPLICATED" REACTION

Suppose that both the reactant (R) and the product (P) absorb and that the only other absorption is background absorption, A_B, which does not change with time. Then at any wavelength, λ, we can write

$$A(\lambda,t) = \varepsilon_R(\lambda)\cdot R(t) + \varepsilon_P(\lambda)\cdot P(t) + A_B(\lambda) \qquad (A1)$$

in which $\varepsilon_R(\lambda)$ and $\varepsilon_P(\lambda)$ are the molar absorptivities of R and P (normalized to unit path length) R(t), P(t) represent the concentrations of these species. If the stoichiometry of the overall reaction also holds during the reaction then we have

$$[P(t) - P(0)] = \nu[R(0) - R(t)] \qquad (A2)$$

in which ν is simply a ratio of balancing coefficients and P(0), R(0) represent initial concentrations. It is usually convenient to measure $A(\lambda,\infty)$, that is, the absorbance at long times. Equations (A1) and (A2) give

$$A(\lambda,t) - A(\lambda,\infty) = [\varepsilon_R(\lambda) - \nu\varepsilon_P(\lambda)][R(t) - R(\infty)] \qquad (A3)$$

Equation (A3) shows that the difference in absorbance at any time and at the end of the reaction can be written as the product of a function which depends only upon wavelength and a function which depends only upon time (for a given set of initial concentrations and

conditions). Let us re-write Equation (A3) as

$$F(\lambda,t) = G(\lambda)\cdot H(t) \qquad (A4)$$

A convenient way to test for the validity of this equation is to take logarithms of both sides to give

$$\ell n[F(\lambda,t)] = \ell n[G(\lambda)] + [\ell n H(t)] \qquad (A5)$$

Note that the absolute values of $F(\lambda,t)$ and $G(\lambda)$ must be used. This gives

$$\ell n[F(\lambda,t_2)] - \ell n[F(\lambda,t_1)] = \ell n[H(t_2)] - \ell n[H(t_1)] \qquad (A6)$$

Therefore, the difference in the logarithm of the function $A(\lambda,t) - A(\lambda,\infty)$ at two different times should be independent of wavelength. Similarly,

$$\ell n[F(\lambda_2,t)] - \ell n[F(\lambda_1,t)] = \ell n[G(\lambda_2)] - \ell n[G(\lambda_1)] \qquad (A7)$$

Therefore, the difference in the logarithm of the function $A(\lambda,t) - A(\lambda,\infty)$ at two different wavelengths should be independent of time. For a scanning system, it is easier to use Equation (A7) than Equation (A6). This is because a given scan of A vs λ takes time.

This derivation suggests a simple test for an "uncomplicated" reaction in which both a reactant and a product absorb. (The same test is valid if more than one product or more than one reactant absorb.) Plots of $\ell n(A) - \ell n(A_\infty)$ vs time are constructed at various wavelengths. Regardless of the rate law, these plots will be parallel. A very sensitive technique would be to plot the difference,

$$\ell n[A(\lambda_2,t) - A(\lambda_2,\infty)] - \ell n[A(\lambda_1,t) - A(\lambda_1,\infty)] \qquad (A8)$$

versus time. A constant value should result if the reaction is "uncomplicated". When this proves to be the case, then the logical procedure is to study the kinetics at fixed wavelength.

If the spectrum during reaction shows the presence of other absorptions, the methods of factor analysis[68] can be used to determine how many independent species are involved as well as the nature of their spectra.

APPENDIX B

SUBROUTINE TIMER

```
      SUBROUTINE TIMER (NUM,TIME,N)
      COMMON/SAVE/ISAV(128)
      DIMENSION TIME(N)
C     SUBROUTINE TO COMPUTE ELAPSED TIME IN NO. OF SAMPLES ELAPSED FOR
C     A PARTICULAR WAVELENGTH TIME CUT
C     NUM = POINT NUMBER                        ISAV(28) = SCAN SPEED
C     ISAV(5) = INITIAL SCANS SKIPPED           ISAV(6) = SMP.S SKIPD PER SCAN
C     ISAV(2) = NO. OF SMP.S PER POINT          TIME = FINAL TIMES COMPUTED
C     N = NO. OF POINTS                         ISAV(4) = BACK-SCAN FLAG
C     ISAV(3) = SPECTRA PER GROUP               ISAV(12) = GROUPING FACTOR
C     ISAV(10) = POINTS PER GROUP
C     INITIALIZE VALUES
C     SR = SMP.S PER REVOLUTION                 ES = ELAPSED SMP.S
C     APART=SMP.S SKIPPED AT BEGINNING OF EACH REVOLUTION
C     SMPOFF = SMP. OFFSET DUE TO AVERAGED SPECTRA
C     FACTOR = NO. OF SPECTRA ARERAGED PER GROUP
C     SMPIMC = SMP. INCREMENT
C     CHECK FOR SCANNING OR FIXED W.L. EXPERIMENT (ISAV(18)=1 FOR SCANNING)
      ASAV2=ISAV(2)
      ASAV5 = ISAV(5)
      ASAV6 = ISAV(6)
      ASAV12 = ISAV(12)
      ASAV28 = ISAV(28)
      IF (ISAV(18).EQ.0) GO TO 400
      SR = 40800.0/ASAV28
      ES = ASAV5*SR
      APART = ASAV6+ASAV2*(NUM-1)+ASAV2/2.0
85    SMPOFF = 0.0
      FACTOR = 1.0
      SMPINC = SR
      L = 1
      ISAV3 = ISAV(3)
```

```
C     CHECK FOR A BACK-SCAN    (ISAV(4)=2 IF BACK-SCANS COLLECTED)
      IF (ISAV(4).NE.1)  GO TO 200
C     DO LOOP ONCE FOR EACH GROUP
C     L IS THE FIRST POINT TO FORM THE NEW SMPOFF
 90   DO 100 I=L.N,ISAV3
C     COMPUTE TIME IN ONE GROUP WITHOUT BACK-SCAN
      LIM = (I+ISAV3)-1
      DO 150 K=I,LIM
      TIME(K)=ES+APART+SMPOFF
 150  ES = ES+SMPINC
C     CORRECTIONS FOR AVERAGED SPECTRA
      FACTOR = FACTOR*ASAV12
      SMPINC = SR*FACTOR
 100  SMPOFF = ((FACTOR-1.0)*SR)/2.0
      RETURN
C     COMPUTE TIMES FOR BACK-SCANS      WILL BE IN FIRST GROUP ONLY
 200  DO 300 I=1,ISAV3,2
C     COMPUTE FORWARD SCAN FIRST
      TIME(I)=ES+APART
C     NOW COMPUTE BACK-SCAN
      ES=ES+SR
300   TIME(I+1)=ES-APART
C     COMPUTE CORRECTIONS FOR AVERAGED SPECTRA
      FACTOR = FACTOR*ASAV12
      SMPINC = SP*FACTOR
      SMPOFF = ((FACTOR-1.0)*SR)/2.0
      L = 1+ISAV3
C     THE REST OF THE SCANS WILL ALL BE FORWARD
      GO TO 90
400   SR = ISAV(2)
      ES = 0.0
      APART = ASAV6+ASAV2/2.0
      ISAV(3) = ISAV(10)
      ISAV(4) = 1
      GO TO 85
      END
```

REFERENCES

1. (a) F. J. W. Roughton and B. Chance in "Technique of Organic Chemistry", edited by S. L. Friess, E. S. Lewis and A. Weissberger (Interscience Publishers Inc., New York, 1963), Vol. 8, p. 703.

(b) B. Chance et al., editors, "Rapid Mixing and Sampling Techniques in Biochemistry" (Academic Press, Inc., New York, 1964).

(c) E. F. Caldin, "Fast Reactions in Solution", John Wiley & Sons, Inc., New York, 1964, Chap. 3.

2. J. L. Dye and L. H. Feldman, Rev. Sci. Instr. 37(2), 154 (1966).

3. (a) R. E. Santini, M. J. Milano and H. L. Pardue, Anal. Chem., 45(11), 915A (1973).

(b). M. J. Milano, H. L. Pardue, T. E. Cook, R. E. Santini, D. W. Magrerum, and M. T. Raydieba, Anal. Chem. 46(3), 374 (1974).

4. B. G. Willis, J. A. Bittikofer, H. L. Pardue and D. W. Margerum, Anal. Chem., 42(12), 1340 (1970).

5. E. Ziegler, D. Henneberg and G. Schromburg, Angew. Chem. Internat. Edit. 11(5), 348 (1972).

6. S. P. Perone, Anal. Chem., 43(10), 1288 (1971). A survey with extensive list of references.

7. E. R. Minnich, Ph.D. thesis, Michigan State University (1970).

8. L. D. Long, Ph.D. thesis, Michigan State University (1973).

9. E. R. Minnich and J. L. Dye, Abstracts, 161st National Meeting of the American Chemical Society, Los Angeles, California, March 1971.

10. E. R. Minnich, L. D. Long, J. M. Ceraso and J. L. Dye, J. Amer. Chem. Soc., 95, 1061 (1973).

11. S. Bank and B. Bockrath, J. Amer. Chem. Soc., 93, 430 (1971).

12. S. Bank and B. Bockrath, J. Amer. Chem. Soc., 94, 6076 (1972).

13. G. Levin, C. Sutphen and M. Szwarc, J. Amer. Chem. Soc., 94, 2652 (1972).

14. A. Rainis, R. Tung and M. Szwarc, J. Amer. Chem. Soc., 95, 659 (1973).

15. A. A. Rainis, R. Tung and M. Szwarc, to be published in the proceedings of the Royal Society.

16. J. L. Dye, M. T. Lok, F. T. Tehan, R. B. Coolen, N. Papadakis, J. M. Ceraso and M. DeBacker, Ber. Bunsen, Gesell. Phys. Chem., 75, 659 (1971).

17. W. Weyl, Ann. Phys., 197, 601 (1863).

18. See for example:

(a) M. G. DeBacker, Ph.D. thesis, Michigan State University (1970).

(b) M. T. Lok, Ph.D. Thesis, Michigan State University (1973).

(c). F. J. Tehan, Ph.D. Thesis, Michigan State University (1973).

19. E. J. Hart and J. W. Boag, J. Amer. Chem. Soc., 84, 4090 (1962).

20. E. J. Kirschke and J. L. Jolly, Science 147, 45 (1965).

21. R. R. Dewald, Ph.D. Thesis, Michigan State University (1963).

22. L. H. Feldman, Ph.D. Thesis, Michigan State University (1966).

23. R. R. Dewald, J. L. Dye, M. Eigen and L. deMaeyer, J. Chem. Phys., 39, 2388 (1963).

24. E. M. Hansen, Ph.D. Thesis, Michigan State University (1970).

25. M. G. DeBacker, Ph.D. Thesis, Michigan State University (1970).

26. J. L. Dye, M. G. DeBacker, J. A. Eyre and L. M. Dorfman, J. Phys. Chem., 76, 839 (1972).

27. Wilhelmy, Pogg. Ann. 81, 413 (1850).

28. H. Hartridge, F. J. W. Roughton, Proc. Roy. Soc. London, A104, 376 (1923).

29. B. Chance, J. Franklin Inst., 229, 455, 613, 737 (1940).

30. T. Nakamura, J. Biochem., 70, 691 (1971).

31. R. L. Berger, B. Balko, W. Borcherdt and W. Friauf, Rev. Sci. Instr. 39(4), 486 (1968).

32. J. E. Erman and G. G. Hammes, Rev. Sci. Instr., 37(6), 746 (1966).

33. Q. H. Gibson and L. Milnes, Biochem. J., 91, 161 (1964).

34. R. R. Dewald and J. M. Brooks, Rev. Sci. Instr., 41(11), 1612 (1970).

35. R. M. Reich, Anal. Chem., 43(12), 85A (1972).

36. J. I. Morrow, Chemical Instrumentation 2(4), 375 (1970).

37. B. Chance, Rev. Sci. Instr., 22(8), 619 (1951).

38. (a) Q. H. Gibson, J. Physiol, 111, 49 (1952).

(b) Q. H. Gibson and F. J. W. Roughton, Proc. Roy. Soc. B, 143, 310 (1955).

39. M. M. Wong and Z. A. Schelly, Rev. Sci. Instr., 44(9), 1226 (1973).

40. Durrum Instrument Corporation, "Operation and Service Manual for Durrum-Gibson Stopped-flow Spectrophotometer", Palo Alto, California (1966).

41. Durrum Bulletin 60 "Durrum Multimixing Systems D-132, D-133, D-134" (1973).

42. R. K. Chattopadhyay and J. F. Coctzee, Anal. Chem., 44(12), 2117 (1972).

43. American Instrument Company "Aminco-Morrow Stopped-flow Apparatus", Cat. No. 4-8409, Silver Spring, Maryland (1971).

44. (a) Electronic Scanning Spectrometer, ITT Industrial Laboratories, Fort Wayne, Indiana.

(b) Rapid Scan Monochromator, Perkin-Elmer Corp., Norwalk, Connecticut.

(c) Millisecond Wavelength Scanning Spectrometer, Control Instrument Division, Warner & Swasey Co., Flushing, New York.

45. W. Niesel, D. W. Liibers, D. Schruwolf, J. Richter and W. Botticher, Rev. Sci. Instr., 35, 578 (1964).

46. Appl. Opt. 1 (1968).

47. P. Burke, Research/Development, April 1973, pg. 24.

48. C. R. Allen, A. J. W. Brook and E. F. Caldin, Trans. Faraday Soc., 56, 788 (1960).

49. J. M. Brooks and R. R. Dewald, J. Phys. Chem., 75, 986 (1971).

50. See references 1-9 in the article by S. P. Perone (6).

51. (a) S. J. Lindenbaum, Ann. Rev. Nucl. Sci., 16, 619 (1966).

(b) J. A. Jones, Trans. Nucl. Sci, 14, 576 (1967).

(c) B. J. Allen, T. R. Bird, At. Energy (Aust) 9, 6 (1966).

(d) J. F. Mollenauer, Trans. Nucl. Sci. 14, 611 (1967).

52. G. P. Hicks, A. A. Eggert and E. C. Toren, Jr., Anal. Chem, 42(7), 729 (1970).

53. See for example:
(a) J. W. Frazer, L. R. Carlson, A. M. Cray and M. R. Bertoglio, Anal. Chem., 43(11), 1479 (1971).

(b) S. P. Perone, J. W. Frazer and A. Kray, Anal. Chem., 43(11), 1485 (1971).

(c) S. N. Deming and H. L. Pardue, Anal. Chem., 43(2), 192 (1971).

(d) P. M. Beckwith and S. R. Crouch, Anal. Chem., 44(2), 221 (1972).

(e) R. A. Parker and H. L. Pardue, Anal. Chem., 44(9), 1622 (1972).

(f) H. V. Malmstadt, C. J. Delaney and E. A. Cordos, Anal. Chem., 44(12), 79A (1972).

54. (a) R. E. Dessy, and J. A. Titus, Anal. Chem., 45(2), 124A (1973).

(b) R. E. Dessy, and J. A. Titus, Anal. Chem., 46(3), 294A(1974).

55. V. A. Nicely, Ph.D. Thesis, Michigan State University (1969).

56. The author is grateful to Drs. M. T. Lok and F. J. Tehan for providing the required samples of "2,2,2 Crypt".

57. J. L. Dye, Accounts Chem. Res., 1, 306 (1968).

58. R. B. Coolen, forthcoming Ph.D. Thesis, Michigan State University (1974).

59. Reference 16, page 116.

60. The S. S. White Industrial Airbrasive Unit, Bulletin 6006, New York, NY (1963).

61. The author is grateful to Mr. A. E. Seer of the Michigan State University glass shop for his help in constructing the cells.

62. By Schrader, Scovill Fluid Power Division, Wake Forest, N.C.

63. By Schott Optical Glass Co., Duryea, Pennsylvania.

64. B. K. Hahn, and C. G. Enke, Anal. Chem., 45(7), 651A (1973).

65. P. Moore, S. F. A. Kettle and R. G. Wilkins, Inorg. Chem., 5(3), 466 (1966).

66. The author is indebted to Miss J. Quijano for her help in developing ABSTIM and TIMER and modifying MULTREG.

67. J. L. Dye, and V. A. Nicely, J. Chem., Ed., 48, 443 (1971).

68. J. J. Kankare, Anal. Chem., 42(12), 1322 (1970).

69. D. E. Paul, D. Lipkin, and S. I. Weissman, J. Amer. Chem. Soc., 78, 116 (1956).

70. Texas Instruments, Inc., Dallas, Texas, Bulletin CA-130.

71. For more information on device flags see any small computer handbook.

72. For more information on our particular system see "An Interactive Computer Interface for Rapid Scanning Stopped-flow Kinetics". This is a laboratory manual for our instrument.

73. SE/NE 565-Phase Locked Loop-Linear Integrated Circuits, Signetics Corporation, 1970.

74. (a) SHA 1A, Sample and Hold Module, Analog Devices Inc., Norwood, Mass.

(b) SAMPAC MP250 0.01% fast acquisition Sample and Hold, Analogic, Wakefield, Mass.

75. ADPAC MP2212 ±5V, high speed 12 bit A/D Converter, Analogic, Wakefield, Mass.

76. DACPAC MP1810-2C, high speed 10 bit D/A Converter, Analogic, Wakefield, Mass.

77. Two types were used, both from Heath Company, Benton Harbor, Michigan.

(a) Model EU-50-MG, ready to use PC boards with place for 11-16 pin IC's.

(b) Pre-sensitized single sided foils for circuit boards.

78. From Heath Company. The ADD used includes a Digital Power Module (EU-801-11), a Binary Information-Module (EU-801-12), and an Auxiliary Module (EU-801-14).

79. Modified by Mr. M. Rabb and Interfaced with help from B. Hahn, K. Caserta, R. Coolen, T. Niemczk and N. Papadakis.

80. Interfaced by Dr. Enke's group.

81. From Tektronix Inc., Beaverton, Oregon.

82. From Houston Instrument, Division of Bausch & Lomb, Bellaire, Texas.

83. Personal communication to J. L. Dye from L. deMaeyer.

84. S. Hayano and M. Fujihira, Bull. Chem. Soc. Jap., 44, 2046 (1971).

85. N. Hirota, J. Phys. Chem., 71, 127 (1967).

86. N. Hirota, J. Amer. Chem. Soc., 90, 3603 (1968).

87. M. Szwarc, Accounts Chem. Research, 2, 87 (1969).

88. From the spectrum given by P. Balk, G. J. Hoijtink and J. W. H. Schreurs in the Rev. Trav. Chim., 76, 813 (1957).

89. M. Szwarc, "Carbanions, Living Polymers and Electron-Transfer Processes" Interscience, New York, NY, 1968.

90. R. M. Fuoss, J. Amer. Chem. Soc., 80, 5059 (1958).

91. M. Szwarc "Ions and Ion Pairs in Organic Reactions", Vol. 1, Wiley-Interscience (1972).

92. B. Metz, D. Moras and R. Weiss, Chemical Communications 444 (1971).

93. K. S. Chen, S. W. Mao, K. Nakamura, N. Hirota, J. Amer. Chem. Soc., 93, 6004 (1971).

94. S. P. Perone and D. O. Jones "Digital Computers in Science Instrumentation, Applications to Chemistry" (McGraw-Hill Book Company, Inc., 1973).